SISSA
Scuola
Internazionale
Superiore di
Studi Avanzati

Neuroscience Area – PhD course in

Functional and Structural Genomics

Functions of the prion protein in neurodegeneration: a closer look to tau - PrP interaction

Candidate:

Elena De Cecco

Advisor:

Prof. Giuseppe Legname

Academic Year 2018-19

ABSTRACT

Tau protein is involved in a number of distinct neurodegenerative disorders called tauopathies, which include one of the major leading causes of death in the world, Alzheimer's disease. Over the past years, many *in vitro* and *in vivo* studies helped elucidating the main events leading to the spreading of the pathology and brain degeneration; however, the detailed molecular mechanisms underlying each step are yet to be discovered. Intracellular tau aggregates diffuse in the brain following anatomic connections, and their spreading is the result of the combination of extracellular release, uptake and seeding of the endogenous protein in receiving cells. Many molecular partners mediating tau internalization have been identified, but many others are still elusive. In particular, it would be worth investigating if different neurodegeneration-related amyloids (i.e. tau, α-synuclein, amyloid-β) might share a common pathway mediating their toxicity and cell-to-cell spreading.

In this PhD thesis, we analysed the contribution of the cellular prion protein (PrP^C) to the internalization of tau fibrils. We took advantage of the methodology extensively described in the literature to produce synthetic amyloids made of the truncated form of tau protein named K18, consisting only of the microtubule-binding domains of the protein. We compared the uptake of K18 fibrils in two mouse neuroblastoma cell lines: wild-type N2a cells and N2a cells that had been knocked-out for PrP^C (N2a KO). Our results indicate that the number of internalized amyloids is higher in N2a cells expressing PrP^C compared to their knocked-out counterpart, suggesting that the prion protein might be one of the many uptake mechanisms. Indeed, the absence of PrP^C does not block completely the entrance of tau fibrils in the cytoplasm. This phenomenon is mediated by the binding between tau fibrils and the prion protein, and configures itself as a mutual interaction: while PrP^C promotes a higher internalization of the amyloids, the presence of tau fibrils leads to an increase in the total levels of PrP^C, which accumulates on the cell membrane. Although it is not yet clear if this effect is be tau-driven or a simple side-effect, it might be responsible for a more sustained internalization rate. Subsequently, we used monoclonal antibodies directed against the different domains of PrP^C in order to evaluate their role in the uptake process. What we found is that both the targeting of the N-terminus and of the hydrophobic region negatively affect the internalization of tau K18 amyloids, while the globular domain does not seem to play a role, at least not in the specific region we considered.

As the prion protein exists also in the pathological conformation PrP^{Sc}, we analysed its interaction with K18 fibrils using prion-infected neuroblastoma cell lines (ScN2a). The exposition of ScN2a cells to K18 amyloids resulted in a strong decrease of the PK-resistant
PrP levels, independently of the type of replicating strain (RML or 22L prion strains). We hypothesize that K18 fibrils might bind either to PrP^{Sc} or, more probably, to PrP^C

and thus prevent prion replication. Indeed, neither macroautophagy nor lysosomes were found to be overactivated as a consequence of the treatment.

In conclusion, our findings point towards a role for PrP^{C} in the regulation of the cell-to-cell transfer of tau amyloids. Additionally, this study focuses on the molecular mechanisms of the relationship between tau aggregates and the pathological PrP^{Sc}. The co-presence of tau and prion pathologies has a clinical relevance, as it is a common feature of a subgroup of prion disorders characterised by a longer disease course.

LIST OF ABBREVIATIONS

3D: three-dimensional
Aß: amyloid-ß protein
AD: Alzheimer's disease
AGD: Argyrophilic grain disease
ALS: amyotrophic lateral sclerosis
APLP1: apolipoprotein 1
APOE: apolipoprotein E
APP: amyloid precursor protein
Asn: asparagine
BSE: Bovine Spongiform Encephalopathy
CBD: Corticobasal Degeneration
CDK 5: cyclin-dependent kinase 5
CJD: Creutzfeldt-Jakob Disease
CNS: Central Nervous System
CWD: Chronic Wasting Disease
CC1: charged cluster 1
CC2: charged cluster 2
Cys: cysteine
DIAD: Dominantly inherited Alzheimer's Disease
DLB: Dementia with Lewy Bodies
Dpl: Doppel
EM: Electron microscopy
ER: endoplasmic reticulum
ERAD: Endoplasmic reticulum associated protein degradation
fCJD : familial CJD
FFI: fatal familial insomnia
FRET: Fluorescence Resonance Energy Transfer
FSE: Feline Spongiform Encephalopathy
FTLD: Frontotemporal Lobar Degeneration
FTDP-17: Frontotemporal dementia with parkinsonism linked to chromosome 17
GGT: globular glial tauopathy
GGIs: globular glial inclusions
GPI anchor: glycosylphosphatidylinositol anchor.
GSK3ß: Glycogen synthase kinase 3 beta
GSS: Gerstmann-Sträussler-Scheinker disease
HPSGs: heparan sulfate proteoglycans
LAG3: Lymphocyte activation gene 3
LB: Lewy Bodies
MAPT: microtubule-associated protein tau
mGluR5: metabotropic glutamate receptor 5
MSA: Multiple System Atrophy

MT: microtubule
NCAM: neural cell adhesion molecule
NFTs: neurofibrillary tangles
NMDAR: N-methyl-D-asparthate receptor
NMR: nuclear magnetic resonance
OR: octarepeat region
ORF: Open Reading Frame
PD: Parkinson's disease
PHFs: paired helical filaments
PiD: Pick's disease
PK: proteinase K
PKA: protein kinase A
PP2A: protein phosphatase 2 A
PrP^{C} = cellular prion protein
PrP-CAA: prion protein cerebral amyloid angiopathy
PrP^{Sc} : scrapie prion protein
PSEN: presenilin
PSP: Progressive Supranuclear Palsy
PSP-CBS: Progressive Supranuclear Palsy with Corticobasal Syndrome
RPTPα: protein tyrosine phosphatase alpha
sCJD: sporadic CJD
SFs: straight filaments
SNpc: substantia nigra pars compacta
SOD-1: superoxide dismutase-1
SUMO small ubiquitine-like protein
Tau-RD: repeated domains of tau
TDP-43: TAR DNA Binding Protein 43
ThS: thioflavin S
TME: Transmissible Mink Encefalopathy
TSE: Transmissible Spongiform Encephalopathy
UPS: ubiquitine-proteasome system
vCJD: variant CJD

TABLE OF CONTENTS

INTRODUCTION

1.1. Neurodegenerative disorders

The selective degeneration of specific subsets of neurons is a common feature of a variety of different disorders grouped under the umbrella term “neurodegenerative diseases”. Although they display unique neuropathological characteristics, and are therefore considered as independent identities, emerging evidence proposes that very similar molecular pathways are involved in the progression of all these disorders, and that they are in the end all different faces of the same coin. Specifically, the aggregation and subsequent deposition of the abnormally folded proteins involved in each disease follow a common mechanism, called “prion-like” after its first identification as the behaviour of the prion protein in prion disorders. *In vitro* and *in vivo* studies showed that, to a different extent, all these proteins can act as seeds and template the aggregation of the endogenous protein into insoluble fibrils. In this section, we will give an overview of the most common neurodegenerative disorders, with a special focus on tauopathies and on their prion-like properties.

Disease	Average age of onset	Clinical symptoms	Aggregated protein
Parkinson’s Disease	~ 60 years	Movement disorder	α- synuclein
Alzheimer’s Disease	~ 65 years	Progressive dementia	Amyloid-β and tau
Amyotrophic Lateral Sclerosis	40 – 70 years average 55 years	Movement disorder	SOD-1 and TDP-43
Transmissible Spongiform Encephalopaties	45 – 65 years	Dementia, ataxia, psychiatric problems, insomnia	Prion protein

Table 1.1. Classification of the most common neurodegenerative disorders and the proteins involved in the diseases.

1.1.1. Parkinson’s disease and synucleinopathies

PD is the second most common neurodegenerative disease after AD and affects people around 65 years of age, with a higher prevalence in men [1]. Contrary to AD, PD configures mainly as a movement disorder, and dementia may be not present in all cases. Motor symptoms are caused by the progressive degeneration of dopaminergic neurons in the *substantia nigra pars compacta* (SNpc) and include bradikynesia, tremors, rigidity, postural instability. Non-motor symptoms, when present, can be observed years before the actual onset of the disease [2], suggesting that the actual pathology has a long prodromal phase that could be exploited to gather an early diagnosis and block the disease.

The etiology of PD is mainly sporadic, but it can also have genetic [3-6] and environmental origin (i.e. exposure to some environmental toxins, paraquat and the

pesticide rotenone) [7, 8]. In all cases, the major hallmark is the deposition of aggregated forms of the protein α-synuclein into structures known as Lewy Bodies (LB) [9, 10]. The pattern of spreading of LB is disease-specific and allows the discrimination between different pathologies all characterised by the presence of α-synuclein amyloids. In PD, LB localize mainly in the cell cytoplasm of the neurons in the *substantia nigra* in the form of brainstem-type LB. Pathology starts in cholinergic and monoaminergic brainstem neurons and in the olfactory system, and expands to the limbic and neocortical brain regions as disease progresses. Patients affected by Dementia with Lewy Bodies (DLB) accumulate LB in the temporal lobe, while in Multiple System Atrophy (MSA) synuclein aggregates are found in glial cells to form cytoplasmic inclusions. The localization of the amyloids, as well as their intrinsic conformations, are thought to be responsible for the different disease phenotypes. Several studies showed the ability of PD- and MSA-derived seeds to faithfully propagate their conformation in sequential passages both in cells and in mice, confirming that α-synuclein forms strains that cause distinct pathologies.

1.1.2. Tauopathies

The aberrant deposition of tau protein results in the instauration of a complex array of disorders, grouped under the name of Frontotemporal Lobar Degeneration-Tau (FTLD-Tau). FTLD is defined as the degeneration of the frontal and temporal lobes of the brain that may eventually lead to language impairment, behavioural and personality changes[11]. Non-Tau FTLD include other disorders with different aggregated proteins: FTLD-TDP, FTLD-FET and FTLD-UPS (fig). FTLD-TDP is the most common type, accounting for around 50% of total cases. FTLD-Tau is slightly less common, with a prevalence of around 40%, while FTLD-FET and FTLD-UPS are relatively rare (5-10% and 1% respectively)[12].

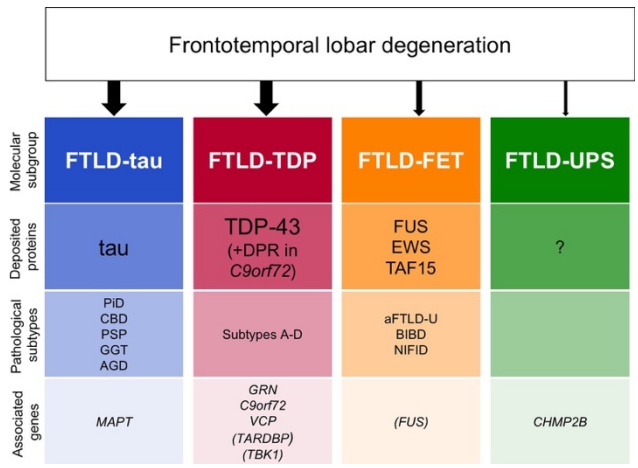

Fig. 1.1. Molecular classification of frontotemporal lobar degeneration according to the type of protein deposits [12].

FTLD associated with tau deposits comprises a variety of clinically and biochemically different disorders, collectively called tauopathies. While all these diseases have in common the accumulation of abnormal tau aggregates in the brain, many factors play a role in discriminating among neuropathological phenotypes: the involvement of different anatomical regions, the cell types affected, and the presence of distinct tau isoforms in the pathological aggregates. AD is the most common degenerative dementia showing neuronal tau pathology; however, since the accumulation of intracellular neurofibrillary tangles of tau is accompanied by the presence of extracellular deposits of Aß, AD is classified as a secondary tauopathy, as other proteins are involved in the pathogenesis. Primary tauopathies see only tau as the major player in the disease aetiology, and comprise Pick's disease (PiD), corticobasal degeneration (CBD), progressive supranuclear palsy (PSP), argyrophilic grain disease (AGD), frontotemporal dementia and parkinsonism linked to chromosome 17 (FTDP-17) and the recently characterised globular glial tauopathy (GGT) [13]

FTLD-Tau pathologies may have either a genetic or sporadic etiology. All the genetic cases go under the name of Frontotemporal Dementia with Parkinsonism linked to chromosome 17 (FTDP-17), and are due to the presence of mutations in the MAPT gene. Indeed, it was only after the discovery of FTDP-linked mutations in 1998 that the idea that tau alone could cause neurodegeneration became widely accepted [14]. To date, more than 38 mutations in the MAPT gene are associated with FTDP syndromes [15], with some genetic cases that partially or completely phenocopy the aforementioned sporadic tauopathies [16].This evidence implies that the study of tau mutations and their functional consequences can provide useful insights also in the pathogenesis of the non-genetic cases of tauopathies.

Tau protein exists in two subclasses of isoforms characterised by the presence of either 3 (3R) or 4 (4R) repeated regions constituting the microtubule-binding domain. In the physiological state, the ratio between the expression of 3R and 4R tau is around 1:1, and it is kept under strict control by regulatory mechanisms. Indeed, the dysregulation of this equilibrium and the subsequent over-representation of one of the two subclasses is the most common feature of tauopathies, both genetic and sporadic. For example, it has been shown that the MAPT locus exists in two haplotypes, either with a 900 kb inversion (H1) or non-inversion (H2) polymorphism [17].The inheritance of H1/H1 genotype is considered a risk factor for developing PSP and CBD [18], as the sequence inversion alters the splicing and results in a higher production of 4R transcripts and in an increased 4R:3R ratio.

Pathogenic mutations interest mainly the exons 9-13 of the coding region, or the splice-donor site of the intron following the alternatively spliced exon 10. Two more pathological mutations with effect on MT binding activity of tau (R5H and R5L) were identified in exon 1 [19, 20]. Those located in exons 1, exon 9, exons 11-13 affect all six tau isoforms, while those in exon 10 have their effect only on 4R- tau isoforms [15]. Tau mutations can be functionally divided into two, partially overlapping classes: mutations whose effect is at the protein level, and mutations that affect the alternative splicing of the pre-mRNA. Some mutations such as N296H, ΔN296 and ΔK280 [21, 22] have effects at both levels, and are located in exon 10 of the tau gene. No

mutations leading either to a truncated protein or the nonsense-mediated decay of the mRNA have been identified.

Type and localization of tau mutations determine, to a certain extent, the morphologies of the filaments and their isoform composition. Mutations that promote the inclusion of exon 10 lead to the formation of wide twisted ribbon-like filaments composed only by 4R-tau present in both glial and nerve cells. Missense mutations in exon 10 that do not affect splicing result in the formation of narrow twisted ribbons, composed of 4R-tau isoforms and present both in neurons and to a lesser extent in glia. Mutations that lie in the coding region outside exon 10 cause a pathology that is primarily neuronal.

Sporadic FTLD-tau pathologies might be discriminated by the type of isoform that accumulates in the brain: 3R tau, 4R tau or both classes of isoforms. (Table 1.2.) Indeed, the isoforms involved in each pathology produce specific electrophoretic profiles according to the number of repeated regions, and can be distinguished based on their molecular weight. Figure 1.2. shows the electrophoretic profiles of the three classes of tauopathies. In the next section, each sporadic tauopathy will be briefly described.

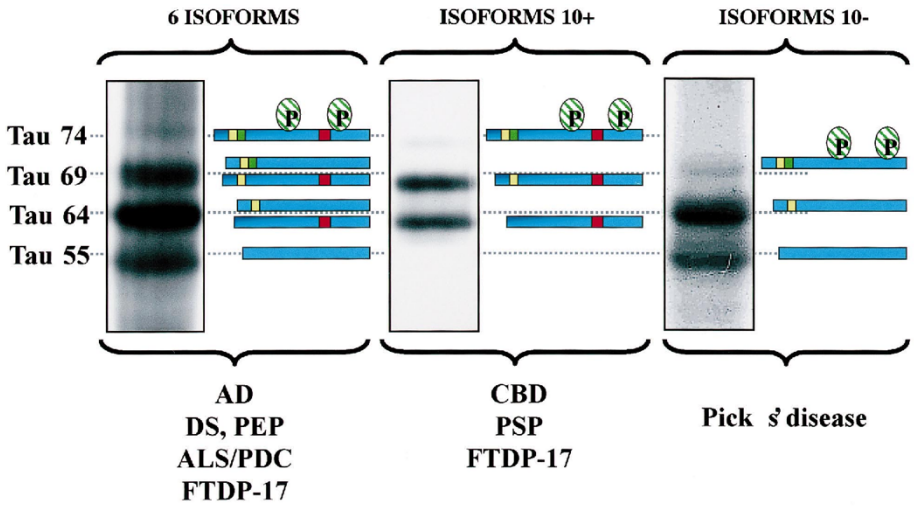

Figure 1.2. Electrophoretic profiles of pathological tau proteins with schematic representation of isoform composition [23].

Disease	Tau isoform	Affected cells	Affected brain regions	Type of aggregates
Pick's disease	3R	Neurons and glia	Frontal, temporal and parietal lobes; hippocampus	Pick bodies 
Progressive supranuclear palsy (PSP)	4R	Neurons and glia	Frontal cortices, subthalamic nucleus, brain stem	Tufted astrocytes 
Corticobasal degeneration (CBD)	4R	Neurons and glia	Frontal and parietal cortices; substantia nigra	Balooned neurons 
Globular glial tauopathy (GGT)	4R	Neurons and glia	Frontal and temporal lobes	Globular inclusions  
Argyrophilic grain disease	4R	Neurons and glia	Transentorhinal and entorhinal cortices, hippocampus	Argyrophilic grains 
Alzheimer's disease (AD)	3R and 4R	Neurons	Entorhinal cortex, hippocampus, cortex	NFTs 

Table 1.2 Neuropathological features of the tauopathies

1.1.2.1. 3R tauopathies

Pick's disease is the only member of the class of 3R tauopathies, first described by Arnold Pick in 1892 [24]. It is characterised by significant neuronal loss, gliosis and formation of round, intraneuronal inclusions called Pick bodies [24] that deposit in the hippocampus, frontal and temporal cortices [25], as well as to a lesser extent in astrocytes and glia [26]. These inclusions are made exclusively of 3R tau assembled both into straight filaments of 15-18 nm in diameter and into twisted ribbons 20-22 nm wide [27, 28]. Pick bodies are negative with the Gallyas silver stain, which instead labels neurofibrillary tangles in AD, but can be visualized by conventional Bodian staining when intracellular [29], and with methenamine-silver method when located outside the cells [30]. Clinical symptoms include changes in social behavior and personality and progressive fluent aphasia with breakdowns in the conceptual database. Variants of the disease see the prevalence of progressive nonfluent aphasia associated with left peri-Sylvian atrophy [31].

1.1.2.2. 4R tauopathies

Tauopathies with inclusions of 4R tau are more commonly observed, and include a variety of distinct disorders.

Progressive supranuclear palsy

PSP is the most common primary tauopathy and was first characterised as a clinical entity in 1964 by Steele *et al.* [32]. It is considered to be a rare disease with a peak prevalence in people around 70-74 years [33]. Tau pathology consists mainly of NFTs and intracytoplasmic inclusions called coiled bodies, both reactive with Gallyas silver stain [34]. Another hallmark of PSP are tufted astrocytes, densely packed tau fibrils which form tufts in the proximal processes around astrocytic nuclei [35]. PSP exists in a variety of clinical manifestations driven by the different localization of tau pathology in brain areas [36]. The classical phenotype for PSP is the so-called Richardson's syndrome, which combines motor (bradykinesia, unsteady gait, falls) and cognitive symptoms (bradyphenia, speech disorders, personality changes). Less common clinical presentations associate an overall PSP-like phenotype with other deficits, such as parkinsonism, progressive gait freezing, speech language, predominant cerebellar ataxia and frontotemporal dementia [37]. PSP with corticobasal syndrome (PSP-CBS) is a rare pathological condition with partial overlap between PSP and another 4R tauopathy, CBD. PSP-CBS is characterised by a variable combination of progressive motor symptoms, and can be distinguished from CBD-CBS only by autopsy.

Corticobasal degeneration

CBD was first described by Rebeiz and colleagues [38] in 1968 as a mainly motor disturb, with tremors, dystonia, rigidity and slow movements. Indeed, CBD manifestation is usually compared with atypical parkinsonism, although cognitive decline also occurs in the majority of patients [39, 40]. From a neuropathological point of view, CBD-affected brains exhibit neuronal loss and gliosis in the frontoparietal cortex as well as in the frontal and superior temporal lobes. The *substantia nigra* is also affected, with moderate to severe damages. Cortical and limbic regions show the presence of ballooned neurons positive for phosphorylated neurofilaments [41], while pre-tangle structures made of tau protein are observed in the cerebral cortex and subcortical regions [42]. On the contrary, NFTs are not common in CBD patients. Degenerating oligodendrocytes present abundance of aggregated tau in the form of coiled bodies, and in both white and grey matter there is the accumulation of argyrophilic threads, tau-positive threadlike structures located in the processes of the cells [43]. Clinical presentation of CBD often overlaps with FTD and PSP, as the all share key features like the akinetic-rigid syndrome and eye movement abnormalities. However, the presence of specific symptoms, such as the supranuclear gaze palsy typical of PSP can help the clinicians to diagnose correctly the type of disease.

Globular glial tauopathy

GGT is a recently introduced 4R tauopathy with widespread tau-positive globular glial inclusions (GGIs) in oligodendroglial and astrocytic cells [13, 44]. Tau pathology extends also to neurons in the form of diffuse cytoplasmic globular or small tangle-like inclusions [45, 46]. Specific localization of tau aggregates allows the classification of GGT cases into three main groups. Type I GGT involve mainly frontotemporal cortex and GGIs are found in the white matter. In type II, pathology extends predominantly to the motor cortex and corticospinal tract. Type III is a combination of the first two and see the presence of tau inclusions in all mentioned brain areas [13]. Emerging evidence suggest that GGT tau inclusions have a stronger seeding competency compared to other tauopathies, and compare them to GCI-type α-synuclein aggregates observed in MSA [47]. Further investigations are directed to the understanding of this peculiar behaviour, i.e. by characterizing any potential ultrastructural difference between GGT-tau and other tauopathies.

Argyrophilic grain disease

AGD is a common but still under-recognized neurodegenerative condition [48], that affects people from 65 to 100 years of age [49, 50]. The difficulty in correctly diagnosing AGD lies in the fact that it is often associated with other neurodegenerative syndromes, mainly AD but also PiD, PD, DLB, PSP, CBD, ALS [51-53], and can thus be misinterpreted as one of the phenotypical manifestations of more common disorders. Moreover, the definition of a precise clinical phenotype is still lacking, as major cognitive symptoms are highly variable and very generic. The most common sign of AGD is a slow-progressing, mild cognitive impairment [54], along with personality changes and neuropsychiatric symptoms in early and mild stages of the disease [55, 56]. However, cases have been reported in which AGD presents without cognitive deficits [57]. This vast heterogeneity is the reason why an accurate diagnosis is possible only after a *post-mortem* examination. Indeed, AGD is characterised by the deposition of small spindle-shaped aggregates (argyrophilic grains) in dendritic processes of neurons [58], positive with Gallyas staining, and pre-tangles in neurons of the limbic system [59]. Along with neurons, also oligodendrocytes accumulate tau inclusions in the form of coiled bodies and neuronal pretangles [58].

1.1.2.3. Mixed tauopathies

Alzheimer's disease

AD is classified as a secondary tauopathy due to the co-presence of amyloid-ß and tau pathologies. Amyloid-ß accumulates into insoluble plaques in the extracellular space and in the walls of blood vessels, while protein tau forms NFTs inside neurons. The two pathologies develop concomitantly and follow each one its own pattern of

progression, which is described by Braak and Braak stages [60] (Figure 1.2). In contrast to other tauopathies, one of the major clinical hallmarks of AD is a progressive dementia, which characterises the whole clinical phase of the disease (8-10 years). It is now accepted that AD starts well before the appearance of clinical symptoms, with a silent, prodromal stage that can last for over two decades [61]. The crude incidence of sporadic AD is of 1-3% with no net prevalence of specific geographic areas [62].

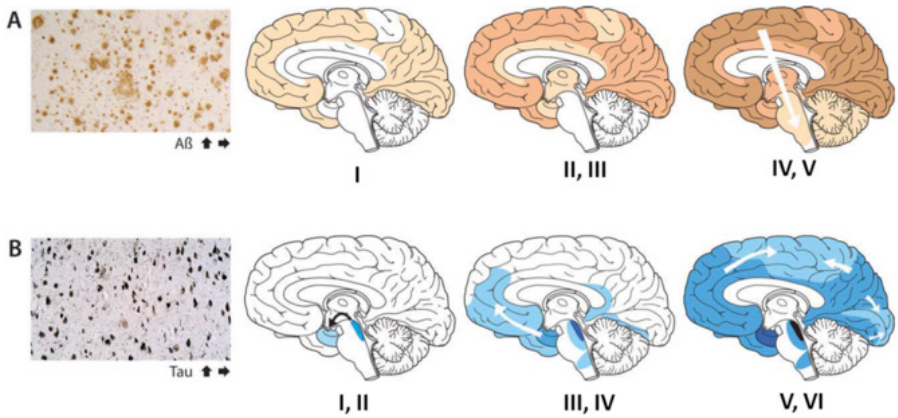

Figure 1.3. Braak and Braak staging of AD for amyloid ß (A) and tau (B) [63]. (A) Aß deposits progressively spread from the neocortex to the entorhinal area and the hippocampus, then reach the subcortical structures, the brain stem and the cerebellum. (B) NFTs made of protein tau start forming in the entorhinal cortex and then move to the hippocampus and the neocortical areas, opposite to Aß. White arrows indicate the direction of the spreading of the pathological aggregates [60, 64].

The majority of AD cases are sporadic (around 95%), affect people over the age of 75-80 years and are a result of the inability of the brain to clear Aß peptide [65]. A small portion of patients have autosomal dominant inherited AD (DIAD), which is more aggressive than its sporadic counterpart and starts to appear at around 45 years of age. In more than half of the cases of DIAD, mutations were found in one of three different genes: the amyloid precursor protein gene (APP), and the genes for presenilin-1 and presenilin-2 (PSEN1 and PSEN2) [66-69]. Most mutations in APP gene modify the APP processing and result in an increased production of the pathogenic fragment Aß-42 and in a higher ratio Aß-42: Aß-40. The same outcome is observed for the mutations affecting the presenilins, which are responsible of APP cleavage [70, 71]. For what concerns sporadic AD, potential environmental risk factors have been determined, including diabetes mellitus, mid-life hypertension, obesity and inactivity, smoking and depression [72]. Their direct association to AD pathology is not straightforward, as these lifestyle interventions provide amelioration to the overall well-being of people. A key genetic risk factor has been identified and proved certain, that is the polymorphism associated with the apolipoprotein E gene (APOE) [73, 74]. APOE exists in 3 isoforms that differ for 1 or 2 amino acids. Population studies showed that while the allele APOE2 reduces the risk for AD, having the APOE4 allele increases the probability of developing AD by three times in heterozygosity and twelve times in homozygosity [75]. Studies have shown that APOE acts only on Aß, by acting

as a chaperone and affecting its clearance and degradation, while it has no effect on tau hyperphosphorylation [76, 77].
Unlike other tauopathies, AD is characterised by the presence of all six isoforms of tau in the insoluble sarkosyl-extracts, forming the characteristic triplet of 60, 64 and 69 kDa, with additional minor bands at 72/74 kDa. This profile classifies AD as a 3R/4R, or "mixed" tauopathy. Tau aggregation seems to be initiated by the abnormal hyperphosphorylation of specific amino acidic residues [78, 79], which alters the protein's overall charge and causes its detachment from the microtubules. The increase in the amount of soluble cytoplasmic tau is the first step in the aggregation cascade. Tau aggregates mainly in the form of NFTs, but a small portion of other structures called straight filaments (SFs) is present [80-82]. NFTs are often called also paired helical filaments (PHFs) because of their appearance as helically wounding around each other. In 2017, Fitzpatrick *et al.* provided the first high-resolution (3.4-3.5 Å) map of PHFs and SFs structure using cryo-electron microscopy [83]. Despite their visible differences, PHFs and SFs share an ordered core of protofilaments spanning residues 306-378, with the C- and N- termini forming a fuzzy coat all around. The core is composed by structural motifs packed in in register, antiparallel cross-ß/ ß helical structures kept together by a mixture of hydrophobic and polar interactions. PHFs and SFs differ in their inter-protofilaments packing and are thus considered as structural polymorphs.
Aß is thought to be the trigger, or even the driver, of the whole disease process, at least in familial cases. The presence of tau pathology is mandatory for the diagnosis of AD, and although the precise interactions between the two proteins have not been fully elucidated yet, many theories have been proposed. The amyloid hypothesis postulates that tau alterations occur as downstream events of Aß deposition [84-86], while it is equally plausible that the two players proceed in parallel and enhance each other's toxicity [87].
Aß aggregates persist in the brain for many years and their amount increases over time, due to the ability of Aß to act as a template and induce aggregation [88]. Later, it was showed that the same effect can be obtained by using either brain homogenates containing Aß plaques, or synthetic aggregates made of recombinant Aß, although with a lower efficiency compared to brain material [89, 90]. This property is referred to as "prion-like seeding", and will be further discussed in a dedicated section of this work.

1.1.3. Transmissible Spongiform Encephalopathies

Prions are the causative agent of a panel of distinct neurodegenerative disorders called TSEs, which affect both humans and a wide range of animal species. Differently from all the other neurodegenerative diseases, prion disorders are the only ones for which infective transmission has been demonstrated.

1.1.3.1. Animal TSEs

Animal prion diseases include scrapie of sheep, goats and mouflons [91], bovine spongiform encephalopathy (BSE) in cows [92], transmissible mink encephalopathy (TME) in ranch-reared minks [93], feline spongiform encephalopathy (FSE) in domestic cats [94], chronic wasting disease (CWD) of cervids and spongiform encephalopathy of primates [95]. Animal TSEs are generally acquired through direct contact with contaminated urine and feces or with carcasses. Scrapie was the first animal TSE to be recognized and studied in detail. Neuropathologically, scrapie causes spongiform vacuolation in the CNS, astrogliosis and deposition of PrP^{Sc} in the form of amyloid plaques Affected animals may show signs of aggressive behaviour, ataxia and hyperactivity. The same symptoms characterise also BSE, which exists as a "classical form" (cBSE), as well as two atypical variants, H-type BSE and L-type BSE [96]. Atypical BSEs differ from cBSE in their neuropathological profile, and can be transmitted to transgenic mice and primates through intracerebral inoculation [97, 98]. The most recently discovered TSE is CWD, affecting both captive and free-ranging animals of the family of *Cervidae*. Its etiology is still unknown but might be linked to scrapie, as white-tailed deer intracerebrally inoculated with the scrapie agent developed a disease that closely resembles CWD [99]. TME and FSE are very rare disorders, with only a few cases identified.

1.1.3.2. Human TSEs

Human TSEs form a heterogeneous group of disorders with sporadic, genetic or acquired etiology, although the majority of cases are idiopathic. Acquired TSEs can be contracted from contaminated neurosurgical instruments, corneal transplantation, dura mater grafting, brain derivatives like pituitary hormone, and from consumption of prion-tainted beef products [100]. The latter is the only reported case of inter-species transmission between animals and humans, that developed a pathology with a very rapid course defined as variant Creutzfeldt-Jakob disease (vCJD). Nevertheless, letting alone this unexpected outbreak, the number of acquired TSEs cases is negligible.

Genetic TSEs account for the 10% of total cases, start to manifest at a younger age compared to sporadic disorders and have generally a more aggressive phenotype. Genetic forms include familial CJD (fCJD), Gerstmann-Sträussler-Scheinker disease (GSS) [67], fatal familial insomnia (FFI) [68] and prion protein cerebral amyloid angiopathy (PrP-CAA). More than 40 mutations in the *PRNP* gene are linked to the onset of these diseases, mainly located at the C-terminus of the protein. Among, all, the mutation Asp178Asn received particular attention because its pathogenic effects are dependent on the allele combination at codon 129. Indeed, if the mutation is coupled with the presence of a valine residue at codon 129, there is an increased risk of developing fCJD, while if there is a methionine residue, the favoured disease is FFI. In general, the M/M homozygosity is linked to an earlier onset and a shorter course of genetic prion disorders [101, 102].

sCJD is the most common human prion disorder and accounts for about 85% of cases, with an age of onset of 70 years. Symptoms develop rapidly, and affected people die within a year from the initial manifestations. sCJD is thought to result from somatic mutations of *PRNP* gene or from random structural changes in the conformation of PrP^{C}; according to epidemiologic studies, no environmental factor seems to be linked to the pathology. sCJD is characterised by phenotypic heterogeneity due to the different PrP^{Sc} deposits, linked to the type of polymorphism at codon 129. The two types of PrP^{Sc} have distinct PK-resistance, aggregation properties, transmissibility and form peculiar brain lesions, probably as a consequence of specific structural features [103].

1.1.3.3. *Prion diseases with tau pathology*

Although the main hallmark of neurodegenerative disorders is the presence of aggregates constituted exclusively of one or more specific protein, there is increasing evidence that these diseases are not as isolated and separated entities as we may think. Work from Perez *et al.* and Lopes *et al.* identified in the GSK-3ß and Cdk5-mediated pathways two points of contact between prion, tau and Aß pathologies [104, 105]. Prion protein peptides spanning the amyloidogenic region can increase the activity of GSK-3ß, which in turn hyperphosphorylates tau [104]; a similar effect is achieved when the same peptide, together with Aß 1-40, deregulates the kinase Cdk5 and cause the hyperphosphorylation of tau at Ser202/Thr205 [105].
Reports of the co-presence of prion deposits and tau pathology come mainly from inherited prion disorders, which lead to the formation of dystrophic neurites with abundant hyperphosphorylated tau specifically in the proximity of large prion plaques. Classical cases of GSS with the point mutation P102L were the most affected by concomitant tau phosphorylation, but similar findings occurred also in cases of GSS with the A117V and P105L mutations. The absence of Aß deposition hints at a PrP-induced tau phosphorylation, conversely to what is thought to happen in AD. Indeed, prion protein peptides carrying the A117V mutation were very effective in displacing tau protein and inhibiting microtubules formation, possibly leading to NFTs deposition [106]. Following these observations, bot acquired and sporadic cases of CJD were examined to further characterise this phenomenon. vCJD patients presented diffused tau pathology with a pattern of hyperphosphorylation very similar to AD, but unlike the latter, hyperphosphorylation remained limited to tau deposits near amyloid plaques and did not apply to soluble tau [107]. Only a few cases of sCJD showed also tau pathology, and specifically in association with small prion plaques [108]. The hypothesis that only plaque-forming prion disorders might be able to induce tau phosphorylation remained valid until a study of a large cohort of sCJD patients revealed that also synaptic PrP deposits that do not form plaques trigger tau aggregation and phosphorylation. More in detail, the prion protein burden is correlated with the presence of tau aggregates in the forms of rods and stubs [109]. While the co-deposition of NFTs and prion plaques is considered as a sort of side-effect in classical prion disorders, it becomes the major sign of a rare form of prion disorder

called PrP-cerebral amyloid angiopathy (PrP-CAA) [110]. This peculiar case of dementia arises from a nonsense mutation at codon 145 of PrP, and is characterised by extended PrP deposition in the walls of small and medium-size vessels, as well as in the surrounding parenchyma. Neurofibrillary tangles and neurophil threads are abundant especially in the pyramidal and granule cells of the hippocampus, and are closely associated with parenchymal amyloid plaques. However, the relationship between prion and tau pathologies remain to be further investigated.

1.1.4. Amyotrophic Lateral Sclerosis (ALS)

ALS is another neurodegenerative disease characterised mainly by motor symptoms and resulting in progressive motor weakness due to the degeneration of motor neurons in the spinal cord and cerebral cortex [111]. Two misfolded proteins are involved in the pathogenesis of ALS: superoxide dismutase 1 (SOD1) and TAR DNA-binding protein 43 (TDP-43). Mutations in SOD1 are the principal cause of familial forms of ALS, which account for around 10% of cases. More than 180 point mutations of SOD1 have been identified [112, 113], and their general effect is to lead to structural instability of the mutant, with subsequent misfolding and aggregation. The same occurs if wild-type SOD1 undergoes oxidation or post-translation modification that alter its structure. In cell-free systems, the incubation of wild-type SOD1 with its mutated counterpart alone caused aggregation of the wild-type form, pointing at the hypothesis of ALS as a prion-like disorder.
TDP-43 inclusions have been found in the majority of sporadic cases of ALS and in around 50% of cases of frontotemporal dementia [12]. In addition, TDP-43 has been found in association with other proteins in Huntington's disease and, to a minor extent, in AD. Indeed, TDP-43 is a very important regulatory protein that binds to pre-mRNA molecules and affects the splicing and the expression level of more than 500 mRNAs [114]. Usually TDP-43 is located in the nucleus, but in pathological condition translocate into the cytoplasm, becomes hyperphosphorylated and starts aggregating. Growing evidence shows that TDP-43 possesses a prion like behaviour; aggregates isolated from ALS patients were able to recruit and misfold the endogenous protein in human neuroblastoma cells, resulting in amyloid structures with strong similarities to what observed in vivo, including ubiquitination and hyperphosphorylation. To exclude any contribution from non-specified brain material, synthetic TDP-43 seeds were used to template the aggregation of the endogenous protein in human embryonic kidney cells, leading to similar results [115]. Taken together, these findings corroborate the hypothesis of a prion-like mechanism for ALS.

1.2. Proteins involved in neurodegenerative disorders

1.2.1 Tau protein

Tau proteins are members of the microtubule-associated proteins (MAP) family. In humans, they are found mainly in neurons [116], with trace amounts in peripheral tissues [117] and in non-neuronal cells, especially in pathological conditions [118]. Although people commonly refer to tau as a single protein, they are actually a small family of six isoforms, originating from the alternative splicing of the *MAPT* gene located on chromosome 17q21 [117] in humans. Given this clarification, from now on the common way of referring to tau as a single entity will be adopted wherever it is not necessary to discriminate.

1.2.1.1. *Tau structure*

MAPT gene has 16 exons, but only some of them are constitutively translated [23] (Figure 1.3). Exons 2, 3 and 10 are alternatively spliced in the adult brain, giving rise to the different isoforms, that range from 37 to 46 kDa [119]. *MAPT* exons 2 and 3 encode each for a N-terminal insertion of 29 amino acids, and exon 3 is never present without exon 2. Exon 10 encodes the second (R2) out of four highly conserved imperfect repeated regions of 31 amino acids, which constitute the microtubule-binding domain of tau proteins, the other being encoded by exons 9, 11, 12. Taken together, these splicing variations yield six tau isoforms that differ for the presence of zero, one or two N-terminal insertions (0N, 1N, 2N) and the presence of either 3 or 4 imperfect repeats (3R and 4R) in the C-terminal part of the protein. Tau proteins expression is developmentally regulated, with fetal brain expressing only 0N3R tau (also called “fetal tau”), while in adult CNS all isoforms are present, although at different levels [79]. The ratio between 3R- and 4R- tau isoforms is around 1:1 in healthy brains. Maintaining this equilibrium is crucial to avoid the onset of pathological situations, as many tau-related disorders show the prevalence of one class of isoforms over the other [120].

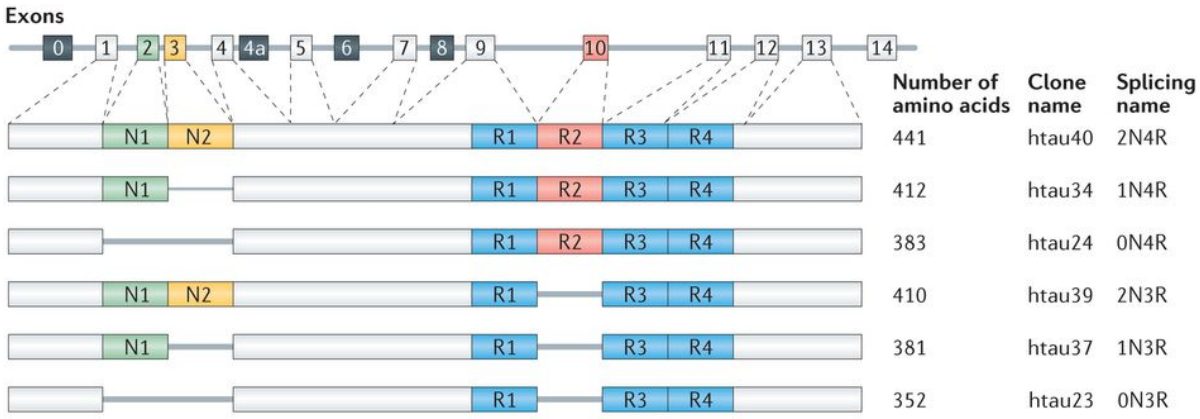

Figure 1.4. Structure of MAPT gene and of the different isoforms resulting from alternative splicing [121].

1.2.1.2. Tau functions

Tau protein functions are strictly related to its structure. Like α-synuclein, tau is a hydrophilic protein which maintains a highly flexible and unfolded conformation in solution [122]. The N-terminal part has a high content of acidic residues in the two additional insertions, followed by a proline-rich region. This segment is called the projection domain, as it projects from the microtubule surface and interacts with cytoskeletal components [123] and cytosolic organelles [124]. Moreover, the length of the projection domain is crucial in determining the axonal diameter, as it regulates the spacing between microtubules [125]. Indeed, peripheral neurons with very long and large axons usually express a longer tau isoform, called "big tau", which includes an additional N-terminal sequence encoded by the exon 4A [126].
Tau mediates also the interconnections between microtubules and neurofilaments [123] through the binding with spectrin [127] and actin [128], interacts with mitochondria [124] and with the neural plasma membrane.
The central proline-rich sequence is involved in interactions with receptor proteins, mediating many important roles in signal transduction pathways. The binding site PXXP for the SH3 domain of src-family non-receptor tyrosine kinases, such as fyn, is located in the sequence of tau spanning residues 231-237, and the two proteins were shown to colocalize beneath the plasma membrane, suggesting a role for tau in the signaling cascade modifying the cell shape [129]. A similar interaction occurs with the SH3 domain of phospholipase-C gamma isozymes [130].
The repeated regions R1-R4 located in the C-terminal part of the protein are involved in the binding of tau to the microtubules network, along with the less-conserved inter-repeat regions. In particular, they regulate tau ability to promote polymerization of tubulin into mature microtubules, inhibit the rate of depolymerization [131], and are involved in axonal transport [128, 132] [127]. The binding to microtubules is mediated by the 18-amino acid repeats through an array of weak sites. 4R isoforms are more efficient in interacting with microtubules than 3R isoforms thanks to the presence of the inter-repeat R1-R2 (peptide $_{274}$KVQIINKK$_{281}$), which increases the strength of the binding by 40 times [133, 134].
Recent data proposed that tau protein might also bind RNA through tis microtubule-binding domain [135]. Indeed, tau has been found also in the nucleus [136], and its lower solubility indicates that nuclear tau undergoes different post-translational modifications, like phosphorylation at specific sites [137]. Once in the nucleus, tau might play a role in developmental pathways, for example by binding the homeotic repressor proteins Eed.

1.2.1.3. Post-translational modifications of tau protein

Tau protein undergoes a number of post-translational modifications, including ubiquitination, glycation, acetylation, nitration and phosphorylation. As dysregulation of tau homeostasis and physiology is always a central event in tau-related

pathologies, it is of crucial importance to understand the modes of tau regulation operated by the cells.

Phosphorylation

Phosphorylation is the most common post-translational modification of tau protein. More than 80 phosphorylation sites have been identified along the amino acidic sequence (Figure 1.4) [23], suggesting that this modification has deep impacts on tau physiological functions. The addition of phosphate groups on specific residues of tau is essential to modulate its binding affinity for the microtubules [138]: higher the number of phosphate groups, lower the ability to interact with tubulin. In particular, phosphorylation at S262, S293, S324 and S356, which are located in the KXGS repeats of R1, R2, R3 and R4 domains, is known to decrease tau binding to the microtubules [138, 139].

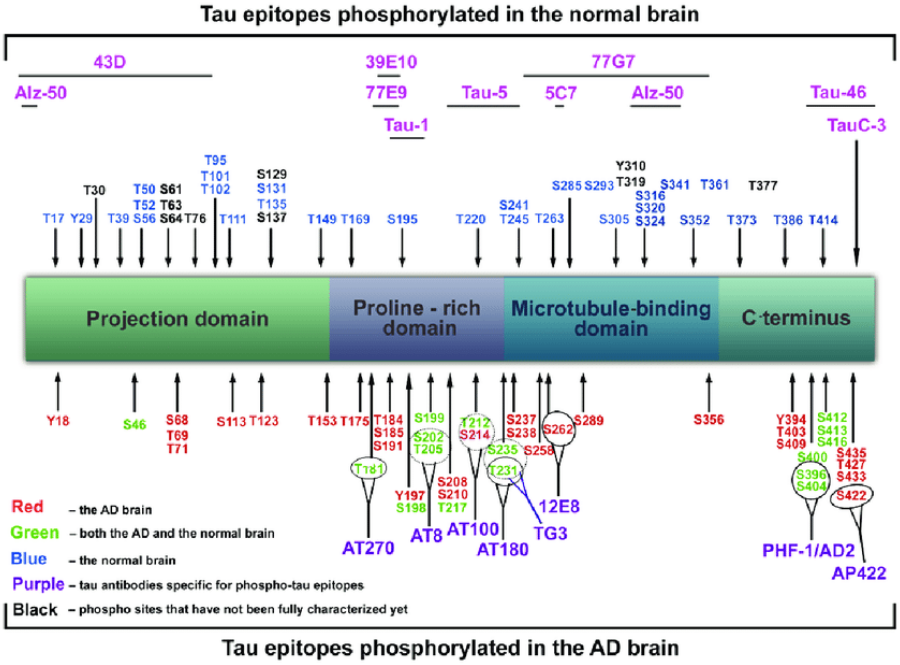

Figure 1.5. Phosphorylation pattern on human full-length tau protein in both normal and diseased brains [140]. Phosphorylation sites are indicated with different colors according to their physiological (blue) or pathological nature (red). Some sites are phosphorylated both in normal and AD brains (green), while other sites have not been fully characterised yet (black). While phosphorylation is almost equally distributed along the protein in healthy brains, AD-associated sites are concentrated in the microtubule-binding domain and in the C-terminal part. In purple are listed the antibodies that recognize specific phosphorylated epitopes.

Tau hyperphosphorylation on the proline-rich region [141] and the C-terminus [142] induce self-aggregation of the cytosolic protein, which forms first oligomeric species and then insoluble fibrils. Several lines of research indicate that abnormal tau phosphorylation might promote neurodegeneration also by compromising axonal integrity and synaptic functions [143], and by protecting it from degradation by the proteasome system [139]. Multiple kinases and phosphatases take part in the

regulation of tau phosphorylation, often with more than one protein taking care of a single phosphorylation site [144-146]. Three classes of kinases phosphorylate tau (PDPK kinases, non-PDPK kinases and kinases specific for tyrosines), while more than 70% of the dephosphorylation activity is carried out by PP2A alone. Alterations in the levels of GSK3ß have been reported in patients with AD [147-149], along with reduced activity of PP2A [150, 151]; inhibition of GSK3ß in transgenic mice reduced neurodegeneration, blocked NFTs formation and rescued neuronal loss, pointing at this kinase as a promising therapeutic target [152-154]. In 2018, Gandini et al. developed a multitarget directed ligand that simultaneously inhibits GSK3ß and the tau aggregation process, therefore triggering a synergistic response and eliminating any possible compensatory pathway [154].

Glycosylation

Glycans can be added to proteins on the amine group of Asn (N-glycosylation) or on the hydroxylic group of Ser and Thr (O-glycosylation). Tau protein from AD brains was found to be abnormally glycosylated, and in some cases also completely devoid of sugars [155, 156]. Indeed, O-glycosylation with the addition of N-acetyl glucosamine seems to compete with phosphorylation operated by GSK3ß, PKA and CDK5 on specific sites such as S356 [157, 158]. This is suggested also by the fact that impaired glucose metabolism plays a role in the onset of AD, promoting NFTs formation through reduction of O-glycosylation and GSK3ß over-activation [159]. Moreover, in vitro deglycosylation of tau aggregates disrupts the amyloid-like structure and restores tau ability to interact with microtubules [156]. These observations all suggest an important role for tau glycosylation in protecting from pathological aggregation.

Truncation

Tau undergoes truncation at D13, E391 and D421 in AD, and this modification is correlated with disease progression [160, 161]. Truncation is mediated by caspase 3 at position D421, while calpains might cut either at positions 45 or 231, generating a 17 kDa fragment [162]. Truncated forms of tau are enriched in PHFs and totally absent in control brains, which is consistent with their role in promoting aggregation and apoptosis [163]. It is now widely accepted that truncation occurs after pathological hyperphosphorylation of tau, but before the formation of NFTs [164-166]. Phosphorylation at S422 protects tau from caspase-mediated cleavage at D421, corroborating the hypothesis of tau truncation as a later event in disease progression [167].

Nitration

Nitration consist in the addition of nitrogen dioxyide to Tyr residues of proteins. Tau nitration occurs on 4 sites and involves both soluble tau and PHF-tau [168, 169], but its role in aggregation is not yet clear. Nitration at site Y18 is not related to pathology,

as is found both in AD and control brains [170], whereas nitration at Y197 and Y394 lead to *in vitro* tau polymerization but not aggregation [171].

Ubiquitination and SUMOlation

As the majority of proteins, tau is ubiquitinated on residues K254, K311 and K353 in order to be degraded by the UPS[172, 173]. Increasing tau ubiquitination leads to a reduction of tau lesions in transgenic mice overexpressing tau [174], but its role in the pathology is only secondary. Tau can also be SUMOlated at K340 by SUMO1, SUMO2 and SUMO3 [175]. SUMO1 colocalizes with tau aggregates only in APP transgenic mice, suggesting that Aß pathology is required for tau SUMOlation [176].

1.2.1.4. Truncated constructs of tau

All the six isoforms of tau show propensity to in vitro aggregation, although to a different extent according to their amino acidic composition. As a general rule, it has been observed that 4R tau isoforms aggregate more readily than their 3R counterparts, and this is due to the presence of the extra repeated region R2 in the microtubule-binding domain. Indeed, structural studies of tau filaments REF revealed that the core of the aggregates is composed by the repeated regions, while the rest of the protein forms a fuzzy coat all around it. Specifically, solid state NMR showed that only some residues (from 306 to 324) formed actual β-sheets [177], while the rest of the microtubule-binding domain remained relatively dynamic and the N- and C-termini (amino acids 1-212, 399-441) were highly mobile[178]. As full-length forms of tau have low tendency to in vitro polymerization, two truncated constructs have been developed that include only the repeated regions, either in its 4R version (K18) and 3R version (K19) (Fig. 1.6).

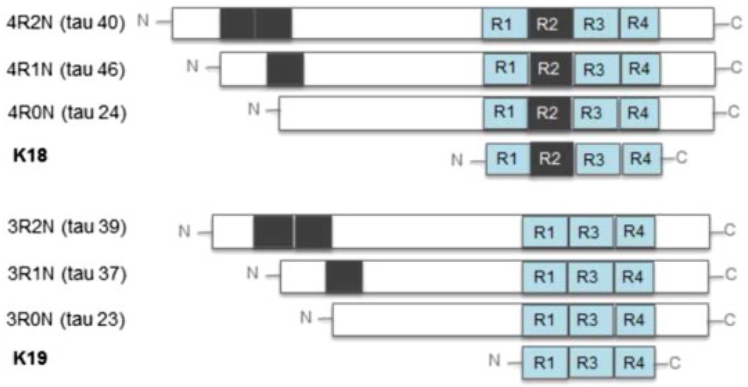

Fig 1.6. Schematic representation of the two subclasses of human tau isoforms (4R and 3R) and of the truncated fragments K18 and K19 [179]. The two constructs are often used as model systems to mimick the properties of the respective subclass of isoforms.

K18 and K19 aggregate much faster and in a reproducible way in the presence of anionic cofactors (RNA, arachidonic acid, heparin), that are needed to screen the basic charges of lysine residues. Since their first characterisation in 1994 [180], K18 and K19 fragments have been widely used to produce synthetic amyloids for cell

culture and *in vivo* studies, both in their wild-type form or with pathological mutations (i.e. P301L). Although these recombinant filaments helped in gaining insights into many aspects of tau structure and aggregation, their peculiar amino acidic sequences present some limitations that should be taken into consideration. Tau K18 and K19 represent artificial constructs not represented in nature, and are devoid of any post-translational modification that might influence their behaviour. Moreover, the use of arbitrary cofactor to promote their aggregation could result in substantial differences compared to brain-derived amyloids. This latter aspect, as well as the resolved structure of pathological tau aggregates from various tauopathies, will be discussed in section 1.3.3.1. Therefore, it remains unclear how much of the results obtained using these tau fragments is actually biologically relevant.

1.2.2. Prion protein

The cellular prion protein, denoted as PrP^{C}, is a glycosylphosphatidylinositol (GPI)-anchored protein located on the outside leaflet of the cell membrane of many cell types, with the highest concentration in the brain [181-183]. PrP^{C} is encoded by the PRNP gene (*Prnp* in other species) present as a single copy gene on chromosome 20, and its complete open reading frame (ORF) is located within a single exon [184-186]. In mouse, sheep, cattle and rat the gene has three exons with the ORF located in exon 3, while in humans, Syrian hamster and opossum the gene is composed only of two exons, and the ORF is positioned in exon 2. The other exons contain the promoter and the terminator sites. It has been shown that the physiological form PrP^{C} and the infectious protein component PrP^{Sc} share the same amino acidic sequence, and their different properties are defined only by the three-dimensional arrangement of the residues [187, 188].

1.2.2.1. Biogenesis and structural features of the cellular prion protein

PrP^{C} is transcribed first as a pre-pro-protein of 253 amino acids containing the signal sequence (first 22 amino acids) for the targeting to the endoplasmic reticulum (ER). Once in the lumen, the signal peptide is cleaved and the resulting immature protein undergoes several post-translational modifications including N-linked glycosylation on N181 and N197 (numbered according to the human protein), disulphide bond formation at positions C179 and C214, and removal of the last 23 amino acids with subsequent attachment of the GPI anchor at position 231 [189-191]. The mature form of PrP^{C} that is released from the ER has 209 amino acids [192]. In addition to this prevalent, mature PrP^{C} that is translocated to the cell surface through the exocytic pathway, two other topologically different forms are produced. ^{Ctm}PrP and ^{Ntm}PrP have both their hydrophobic domain (residues 110-134) inserted in the membrane of the ER compartment, and have respectively their C-terminal or N-terminal inside the ER lumen [193]. Their roles are not yet fully elucidated, but might be related to neurotoxicity and death, especially in the case of inherited prion diseases [194].

Once the ER-related processing is completed, mature PrP^C is sent to the Golgi apparatus, where further modifications of N-glycans to held complex sugar chains occur. PrP^C can be either non-glycosylated, mono- or diglycosylated on Asn181 and Asn197 (on human PrP^C) [195]. Glycosylation profiles vary in the different regions of the central nervous system, but the specific roles of glycosylation are not yet understood.

Mature PrP^C localizes mostly in the cholesterol- and sphingolipid-enriched domains of the plasma membrane, also called lipid rafts. This interaction seems to be important also for the preservation of the correct folding, as cholesterol depletion leads to misfolding [196].

PrP^C is constitutively internalized and recycled back to the cell surface with transit times of around 60 minutes [197]. Constitutive endocytosis of PrP^C is mediated either by "caveolae-like" domains or by chlatrin-coated vesicles [198, 199], which bind to the N-terminal positively charged motif KKRPKP. Then, PrP^C can be sent to the late endosomes and lysosomes for degradation, or routed again to the cell surface for further recycling. Other than in lysosomes, PrP^C can be degraded through the UPS-ERAD degradation pathway in the cytosol.

Bacterially expressed recombinant PrP (recPrP) is structurally equivalent to physiological PrP^C, and it has been used to gain more structural insights into the 3D organization by means of NMR and X-ray crystallography. The full-length form of PrP has a peculiar structure, conserved among different species: the N-terminal domain (amino acids 23-127) is unstructured in solution, while the C-terminus (amino acids 128-231) is folded into a globular conformation, with prevalence of alpha-helical conformation and some ß sheet structures [200, 201] (Figure 1.7).

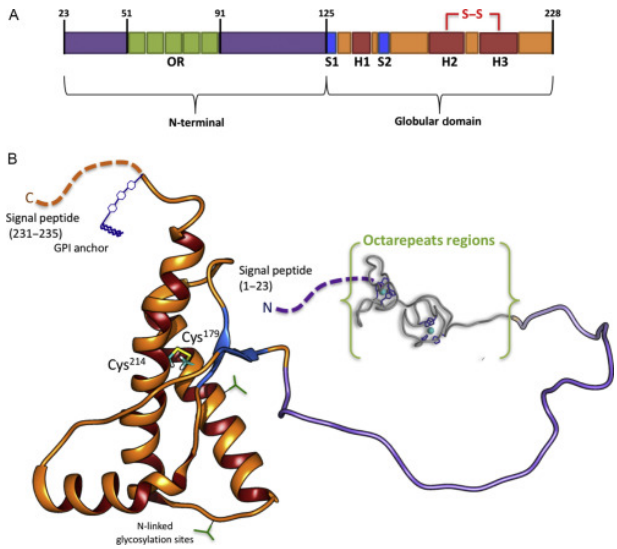

Figure 1.7. Domain organization (A) and 3D-structure (B) of the human PrP^C (23-231) [202]. (A) Schematic primary structure of the cellular prion protein showing the division in two domains and the positions of the three alpha helices and two ß-sheets. The disulphide bond between Cys179 and Cys214 is also indicated. (B) Tertiary structure of the cellular prion protein showing the structurally defined C-terminal domain and the unstructured N-terminus, with the octarepeat region in brackets. Blue dots represent metal ions that are coordinated by the OR. Both the glycosylation sites and the GPI anchor are present.

The N-terminus of PrP^C can be divided into four sub-domains, a first charge cluster (CC1), the octarepeat region (OR), a second charge cluster (CC2) and a hydrophobic region containing the conserved motif AGAAAAGA. It is considered to act as a broad molecular sensor [203] and interacts with copper ions, sulphated glycosaminoglycans and the neural cell adhesion molecule (NCAM). Moreover, the N1 fragment (amino acids 23- 110/111) generated from the alpha cleavage of PrP^C by ADAM proteases is involved in the binding with Aß oligomers which triggers the signalling cascade mediating the toxic effects of these species [204]. A similar interaction occurs also with α -synuclein fibrils, although the exact region has not been identified yet [205].
The globular domain of PrP^C is composed of three α-helices (α1, α2, α3) and two short ß-strands that form an antiparallel ß-sheet. A third ß-strand was recently identified and named ß0 [206, 207]. The α-helical regions have been shown to undergo a vast structural rearrangement into ß-sheets when PrP^C-PrP^{Sc} conversion occurs. Helices α2 and α3 constitute the core of the globular domain and are kept close by the disulphide bond between Cys179 and Cys214. Any disruption of this covalent link between the helices might be responsible for the structural modification that lead to prion formation.

1.2.2.2. Prion protein functions

The prion protein is expressed in many organs and tissues, but prevalently in neurons of the central nervous system, suggesting that it plays key roles in the brain. However, data regarding the physiological function of PrP^C are still controversial and do not offer a sufficiently clear and detailed overview on this protein.
Given that PrP^C is a highly conserved protein among mammals, it was expected that the generation of *Prnp*-ablated mice would have shed light on the still unknown functions of the protein. Nonetheless, the first two lines of PrP-null mice (*Zurich* and *Edinburgh* mice) did not show any significant phenotype, with no abnormalities in the brain or in peripheral tissues. These observations indicated that either PrP^C was not mandatory for normal development, or that other proteins were able to compensate for its absence [208, 209]. In contrast to these two lines, in which the knocking-out had been achieved simply by interrupting the ORF of *Prnp* gene with insertion cassettes, new mouse lines from which the *Prnp* gene had been completely deleted showed signs of ataxia and degeneration of Purkinje cells [210, 211]. The phenotype was rescued with the introduction of functional PrP^C. Later, it was discovered that this phenotype was due to the overexpression of the PrP paralog gene Doppel (Dpl), whose expression is overactivated by the deletion of a splice acceptor site in exon 3 of *Prnp* gene. To overcome the drawbacks of the deletion approach, Schmitt-ULM's group described the generation of PrP-knockout cell lines using the CRISPR/Cas9 approach [212]. With this innovative technology, PrP expression was ablated in N2a neuroblastoma cells, C2C12 myoblasts and NMuMG epithelial cells, revealing many potential roles of the prion protein: cellular adhesion and differentiation, receptor activity, signal transduction, metal binding, neuritogenesis.

Role of PrP^C in neuritogenesis

Inside the cells, PrP^C concentrates at the synaptic level. The accumulation of PrP^C in the synaptic terminals is in line with experiments that proved that the protein induces rapid increases of axons and dendrites [213]. In addition, the expression of PrP^C on the surface of growth cones is essential for their growth and neurite formation [214]. Indeed, soluble forms of PrP^C secreted from the membrane and released in the extracellular space behave as signalling molecules to trigger neuritogenesis, and GPI-anchored PrP^C on recipient cells acts as its receptor. The growth effect promoted by recPrP was completely abolished when either the N-terminal or the C-terminal domains were blocked with antibodies, indicating that this function is dependent on the interplay between the flexible N-terminal domain and the C-terminus. Specifically, the binding of copper ions is essential to maintain the neuritogenic function, and the elimination of the copper-binding residues resulted in neuronal toxicity [215].
Neurite outgrowth is mediated also by the NCAM-fyn signalling cascade. PrP^C and NCAM were found to co-localize in lipid rafts of neurites and growth cones [216]. PrP^C accumulates in lipid rafts enriched in p^{59}fyn non-receptor tyrosine kinase (fyn), which in turn is activated by the binding between NCAM and RPTPα. Clustering of NCAM results in its redistribution inside lipid rafts [217], where it can interact with PrP^C, be stabilized and promote neurite outgrowth.

PrP^C function in myelin homeostasis

The cellular prion protein is involved in maintaining the myelin homeostasis of peripheral neurons, and the ablation of its expression leads to a chronic demyelinating polyneuropathy affecting primarily Schwann cells. The receptor on Schwann cells that mediates PrP^C activity in myelin maintenance was identified as the G protein-coupled receptor Gpr126, which interacts with the flexible tail of PrP^C and triggers a cAMP response resulting in improved myelination[218]. Specifically, the polycationic sequence of PrP^C (KKRPKPG) is very similar to the motif of the Gpr126 agonist type-IV collagen, suggesting that the prion protein might act as an agonist of the GPCR receptor.

Modulation of NMDA receptors by PrP^C

N-methyl-D-asparthate (NMDA) receptors are a subclass of ionotropic glutamate receptors whose activation contributes to the excitatory post synaptic potential (EPSP) and long-term potentiation (LTP) [219]. The overactivation of NMDA receptors leads to an increased influx of Ca^{2+} that can greatly damage the cells. This phenomenon, called excitotoxicity, is involved in many neurodegenerative diseases, including AD [220]. Studies on PrP-null mice revealed that in the absence of PrP^C, the activity of NMDA receptors is enhanced, and postsynaptic currents have longer decay times and larger amplitude than in wild-type mice [221]. When PrP^C is

expressed, excitotoxicity is repressed through a mechanism that requires copper [222]. Specifically, copper ions bound to PrP^C facilitate the S-nitrosylation of the cysteine residues of NMDA receptors, with the consequent inhibition of their activity and a reduction of the neurotoxic effects. An interference with copper binding to PrP^C might underlie the detrimental effects of Aβ, which causes neuronal cell death by interacting with PrP^C and altering the normal activity of NMDA receptors [223].

1.2.2.3. PrP^C- PrP^{Sc} conversion

As mentioned before, the physiological form PrP^C and its pathological counterpart PrP^{Sc} share the same amino acidic sequence. The acquisition of peculiar properties (resistance to proteases, infectivity, insolubility) by PrP^{Sc} is essentially a result of the different 3D arrangement of the amino acids that alters the equilibrium between secondary structure elements by increasing the number of ß-sheets of around 40%. First hints of the idea of PrP as a "double-faced" protein came from the observation that PrP-null mice were not susceptible to PrP^{Sc} infection and transmission, which meant that the expression of PrP^C was an absolute requirement for the development of TSEs [208]. Evidence of the infectious transmissibility of scrapie to goats led first to the speculation [224] and then to the experimental demonstration [225, 226] that a protein alone could be the infectious moiety responsible for the onset and transmission of a disease. Indeed, the term "prion" coined by Prusiner is the short for "PRoteinaceous Infectious ONly particle" and refers to the unique properties of this unusual infectious agent.
The "protein-only hypothesis" proposes that the central event in prion diseases onset and progression is the self-propagating conversion of PrP^C to PrP^{Sc}. The *in vitro* generation of infectious prions starting only from synthetic proteins [227-230], in the absence of genetic material, corroborated this hypothesis that is now widely accepted. From a molecular point of view, PrP^{Sc} is thought to first recruit the monomeric PrP^C through direct interaction, then act as a template to imprint its own aberrant conformation and finally incorporate the newly formed PrP^{Sc} moiety into the growing polymers that in the end will result into insoluble plaques depositing in the CNS. The accumulation of PrP^{Sc} increases exponentially over time, as big aggregates are broken into smaller pieces which behave each one as independent seeds [231].
Two mechanisms have been proposed for the autocatalytic conversion of PrP^C into PrP^{Sc}. The nucleation-polymerization model postulates that PrP^C and PrP^{Sc} both exist in the cell at an equilibrium that is greatly shifted towards the cellular form, which is more stable. Only when an oligomeric nucleus manages to form, PrP^{Sc} is stabilized and the equilibrium moves towards the scrapie form, allowing the conversion to take place. The lag phase observed is explained by the necessity to form the stable nucleus. Addition of exogenous PrP^{Sc} seeds overcomes the rate-limiting step and greatly accelerates the polymerization. The nucleation-polymerization model might describe well the initial formation of PrP^{Sc} polymers, while the template-assisted model might explain the mechanism of fibrils elongation.

PrP^{Sc} as infectious entity has an oligomeric nature [232], and there is no experimental evidence indicating the existence of a stable monomeric unit [201]. Due to its insolubility in non-denaturing detergents, the structure of PrP^{Sc} has been only approximately determined. The use of many biochemical and biophysical techniques (spectroscopy, EM, X-rays fiber diffraction, surface reactivity measurements) along with molecular dynamics simulations allowed the development of several 3D structural models. The ß-helical model originates from EM data on brain-purified PrP^{Sc}, and proposes that PrP^{Sc} is enriched in ß-sheet elements that are arranged to form left-handed ß-helices [233] (four rung model). The ß-spiral model derives from molecular dynamic simulations of PrP in amyloidogenic conditions. In this case, while all the α-helices are retained, the number of ß-strands increases to four and they form a spiralling structure that might involve also the unfolded N-terminus. However, this model does not consider any cross- ß structure, which are a known characteristic of fibrillar PrP^{Sc}. Recently, cryo-EM measurements on pure preparations of prions from mouse brains showed that PrP^{Sc} amyloid fibrils are arranged in a four-rung ß-solenoid architecture [234], which fits very well some known structural restraints and biochemical characteristics like the high content of ß-sheets and the resistance to protease digestion [235]. Indeed, PrP^{Sc} is only partially hydrolysed by the proteases (i.e. proteinase K) to form a small, C-terminal resistant fragment of approximately 142 amino acids, called PrP^{res} or PrP 27-30 due to its electrophoretic mobility in SDS-PAGE gels. PK-resistant PrP^{Sc} accumulates in the brain with a pattern that is clearly distinct from that of PrP^{C} [236]. More than the fibrils, oligomeric species are thought to be the true responsible of prion toxicity. It has been even hypothesized that the formation of long fibrils might be a sort of protective mechanism aiming at neutralizing the more toxic effect of small aggregates [237]. A similar behaviour has been proposed also for the other proteins that are collectively called “prion-like proteins”.

1.3. Prion-like behaviour of tau protein

Prions uncovered a completely new way of disease propagation in which stable spreading of distinct misfolded protein conformers occurs between neighbouring cells and through anatomic connections. Many other neurodegenerative diseases, including tauopathies, exhibit characteristics that are reminiscent of prion disorders, as phenotypic diversity and spreading pathology. However, in order for tauopathies to be defined ad prion-like disorders, they must meet precise requirements, specifically the evidence of cellular uptake, template seeding and intercellular transfer of the newly formed aggregates to prompt the aggregation of the endogenous protein in recipient cells (Figure 1.8). This hypothesis is now supported by strong evidence coming from cell and animal models of tauopathies. Since the majority of the experiments were first performed *in vitro* and then repeated and confirmed *in vivo*, they will be listed according to the prion-like feature they aim to demonstrate: the uptake of exogenous fibrils, the induction of aggregation, the formation of distinct strain and the release in the extracellular space of newly formed aggregates.

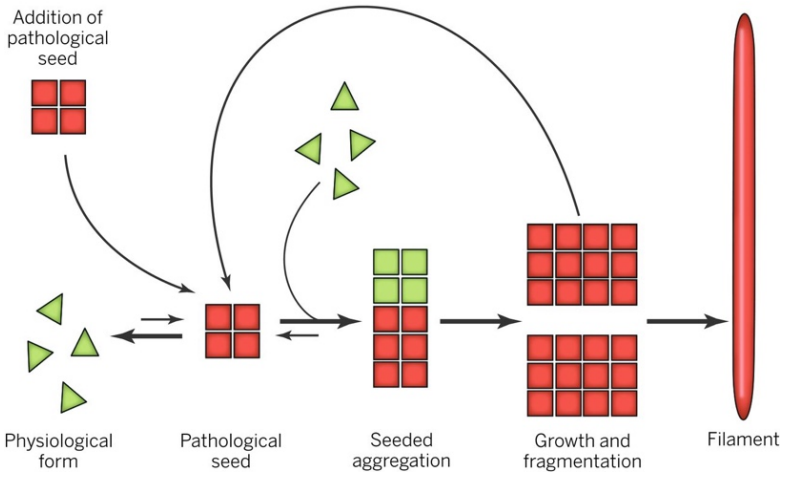

Figure 1.8. Schematic representation of the prion-like templated misfolding of the endogenous protein triggered by the addition of pathological seeds [238]. Prion-like proteins exist mainly in their physiological form (green triangles), and even if some misfolded aggregates might be present, the equilibrium is strongly shifted towards the native protein. However, when brain-derived or synthetic seeds (red squares) are added, they shift the equilibrium towards the formation of aggregates, which grow by misfolding native monomers (green squares) and incorporating them in the nascent amyloid. Big aggregates are fragmented into smaller pieces so that the number of forming amyloids grows exponentially. The resulting products are filamentous aggregates that deposit in the brain.

1.3.1. Cellular uptake of tau aggregates

In order to template the misfolding of the endogenous protein and propagate, tau seeds must first enter the cells. Figure 1.9. gives an overview of the identified mechanisms mediating tau fibrils internalization.

Murine neural precursor cells C17.2 readily internalize tau fibrils by macropinocytosis mediated by heparan sulfate proteoglycans (HSPGs) [239]. Indeed, aggregates formed only by the microtubule binding domain of tau protein (RD-tau, equivalent to K18 tau fragment) were found to co-localize with filamentous actin, that is required to form the lamellipodia-like membrane protrusions typical of macropinosomes. Inhibition of macropinocytosis with various chemicals strongly diminished tau uptake, and the same happens when HSPGs are blocked, suggesting that a direct binding between these two partners takes place. In vivo, mice treated with a heparin mimetic that blocks the HSPGs binding internalized significantly less full-length tau fibrils than control mice, meaning that this mechanism is not limited to the uptake of tau fragments and thus could be actually involved in the propagation of the disease. Smaller, low-molecular aggregated species of RD-tau (identified as dimers and trimers), but not long fibrils or monomers, exploit also bulk endocytosis to get to the cell cytoplasm of both C17.2 cells and primary neurons [240, 241]. The internalized aggregates co-localize with dextran, a marker of fluid-phase endocytosis, and with the endolysosomal compartment. Once inside the cells, tau amyloids can be transported both anterogradely and retrogradely [241].

The ability of extracellular monomeric tau to enter neurons was recently questioned by Evans et al. [242], who found that both monomeric and aggregated tau easily enter stem cells-derived neurons by overlapping but distinct mechanisms both related to

regulated endocytosis. Monomeric full-length wild-type and P301S tau are internalized first by rapid dynamin-dependent endocytosis and then by a slower, actin-dependent mechanism consistent with bulk endocytosis. Conversely to what had been observed previously [239], perturbation of actin polymerization had little effect on the number of aggregates taken up by these neurons, while dynamin inhibitors greatly reduced tau aggregates entry with a stronger effect than on monomeric tau. These findings are consistent with a classical endocytic mechanism for tau amyloids. The discrepancy of their data with previous reports is addressed by the authors as related to the type of cells, claiming that human neurons might internalize fibrils via different mechanisms compared to the murine primary neurons and non-neuronal cells used by Holmes. The question of which molecules mediate the endocytic processes is still open, as no receptors or carriers except for HSPGs have been identified yet.

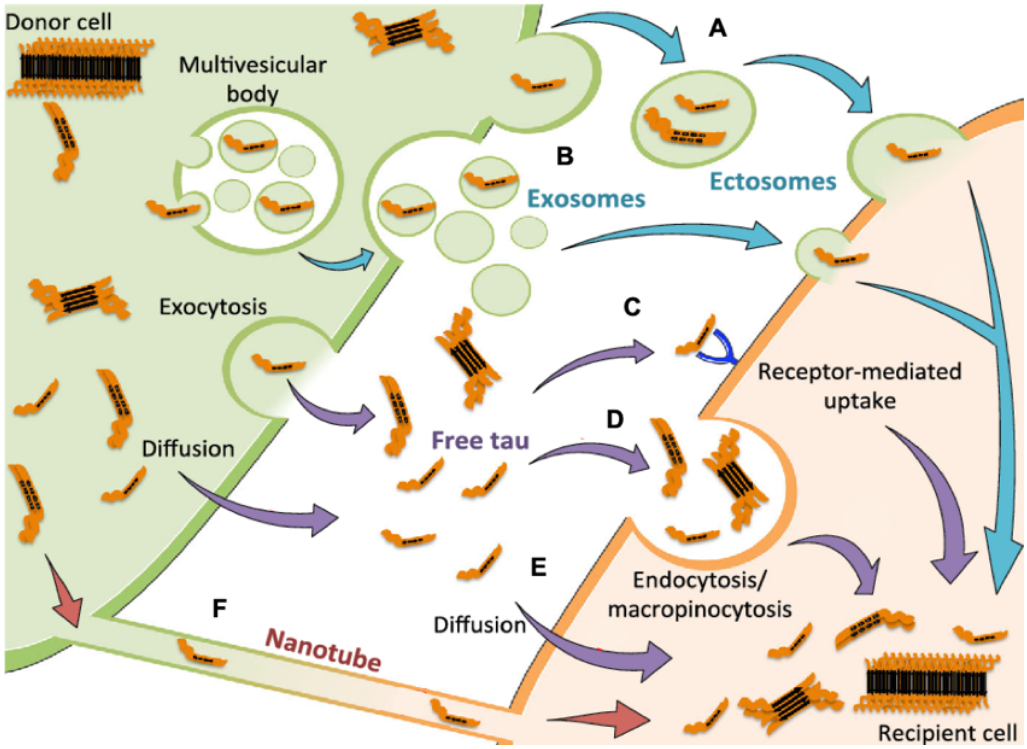

Figure 1.9. Potential mechanisms mediating the uptake of tau aggregates between cells (modified from [243]). Tau fibrils can be transferred from donor cells (green) to recipient cells (orange) through many pathways. Blue and purple arrows indicate pathways experimentally proved; red arrows indicate hypothesized mechanisms. Tau aggregates can be transferred through extracellular vesicles like ectosomes (A) or exosomes (B) that fuse with the plasma membrane and release their content in the cytoplasm. Free and aggregated tau released from donor cells in the extracellular space can bind to specific membrane proteins and be internalized by receptor-mediated endocytosis (C) or macropinocytosis (D). Monomeric tau is also able to escape from the vesicles and cross the plasma membrane simply by diffusion (E). Both tau monomers and aggregates were found inside tunnelling nanotubes connecting the cytoplasm of two cells (F).

1.3.2. Induction of aggregation

Tau aggregation propensity and induced seeding have been extensively studied and characterised in cell and animal models. It is believed that tau aggregation in pathological situations is initiated by hyperphosphorylation, followed by detachment from the microtubules and formation of a compact structure called “Alz50 state”[244]. From this point on, tau begins to aggregate into mature fibrils and undergoes several truncations. To reconstruct the steps leading to the generation of NFTs, several trials were done to reconstitute tau assembly *in vitro*. Aggregation of soluble tau as a consequence of its overexpression was observed by Thioflavin S (ThS) staining both in bacterial systems [245] and in neuro2a cells expressing tau under the control of an inducible promoter [246]. TauRD has been employed as substrate, and it is still one of the most common models in the field of tau aggregation. An in vitro study went deeper into this issue, identifying aggregates composed at least of three protein monomers as the minimal propagation unit necessary for internalization and induction of seeding in HEK293 cell line[247]. Specifically, the aggregation-competent portion of tau protein must include the microtubule binding domains, as the formation of fibrils is strictly dependent on the presence of at least one of the two hexapeptide motifs PHF6 and PHF6*, located respectively at the beginning of the third (R3) and of the second (R2) repeated regions [248].

Exogenous tau seeds to template the aggregation of the intracellular protein derive from brain homogenates of tauopathy patients, transgenic mice showing pathology, lysates and conditioned media from transfected cells bearing tau amyloids, and from synthetic fibrils generated *in vitro*. Formation of aggregates was monitored with an array of techniques including FRET-based aggregation sensor cells [179], fluorescence assays [249], biochemical insolubility assays [250] and immunohistochemical detection of pathological inclusions [251-253].

As it is expectable, tau seeds purified from patients’ brains display a higher seeding activity compared to fibrils generated *in vitro*. Nevertheless, incubation of wild-type or P301L-tau expressing cells with small amounts of synthetic preformed fibrils resulted in a consistent production of insoluble aggregates that resembled NFTs and exhibited a high degree of phosphorylation [254]. The effect of mutated tau was more pronounced, consistently with the highly aggressive phenotype of the FTDP-17 syndrome related to this mutation. Nonaka et al. [255] speculated that a cross-seeding barrier exists between 3R and 4R tau, since they observed the formation of aggregates only when 3R- and 4R- expressing cells were treated with seeds belonging to the same subclass of isoforms. Kinetic analysis of K18 and K19 aggregation revealed that this barrier is asymmetric, with K19 being able to seed both 3R and 4R tau while K18 seeds only 4R tau. The explanation is mainly structural; the repeat R3 is the preferred site for the binding between the monomeric protein and the growing fibril, but when R2 is also present, the interaction with the monomer is hampered if the monomer itself does not have R2, while is favoured if another R2 is present. When the fibrils are made only of 3R tau and R2 is not represented, the interaction can occur with both 3R and 4R isoforms indiscriminately. The presence of

R2 makes the whole structure more disordered than 3R tau, reducing the extension of the structural core and thus impairing the interaction with different isoforms[256]. However, Margittai's group claimed that the existence of such barrier is nothing more than an artefact due to the use of K18 fragment as seed. Indeed, recombinant fibrils made of the longest human tau isoform (huTau40) could easily recruit 3R tau substrate in in vitro aggregation assays, while K18 aggregates could not[257]. Assuming that the presence of ordered regions in the fibrils are required for the interaction with monomers, the difference in the seeding activity between K18 and huTau40 could be due to the fact that the last region of R4 segment is highly disordered in the former and well organized in the latter thanks to the longer amino acidic sequence. The reduce contact surface of K18 might explain why 3R monomers are not able to bind, whereas the presence of both the N- and the C- termini of the protein makes full-length forms of tau better templates for misfolding [257].

To be sure that this is the way tau pathology proceeds in human brains, many researchers took up the challenge to study the behaviour of brain-derived tau amyloids when injected into cultured cells and mice. Inoculation of brain homogenates from patients with various tauopathies into transgenic mice expressing the longest human tau isoform led to the formation of *de novo* inclusions that recapitulated the basic features of the initial pathology and that could be faithfully propagated to the next generations[252]. Previously, the same group had already shown that brain extracts from P301S expressing mice were capable of inducing the assembly of wild type tau in wild-type expressing mice, with subsequent spreading of the pathology to the neighbouring regions[251]. Over time, the pathology moves further and further, consistently with neuroanatomical transport and induction of pathology along these routes. A number of mouse models were created in which tau transgene expression was restricted to the entorhinal cortex, in order to follow brain propagation[258, 259].These studied support the hypothesis of a trans-synaptic movement of tau amyloids, as human tau was found in brain areas near the entorhinal cortex where the transgene was not expressed (i.e. dentate gyrus, CA fields of the hippocampus, cingulate cortex) [258]. The appearance of pathological tau species in brain areas around the injection site is often accompanied by the selective loss of neurons in those regions. The reliability of such systems has been questioned after the observation that the expression of transgenes under the control of the EC-specific promoter for neuropsin was not really limited to that region, but could be found in other cortical regions[260]. However, the general pattern of spreading was clear enough to convince that tau pathology proceeds through trans-synaptic spreading between cells.

Not all tau seeds seem to be able to induce pathology in transgenic mouse models; while showing a robust seeding activity in vitro, K18 seeds injected in the hippocampus caused only limited aggregation of tau, and peripheral injection did not lead to any pathology in the CNS of human-P301L tau expressing mice [261].

On the contrary, brain extracts from tauopathy patients could trigger pathology also in wild-type non-transgenic mice, promoting the aggregation of the endogenous murine

protein[252, 262]. This very strong seeding activity firmly supports the prion-like behaviour of tau amyloids in tauopathies.

1.3.3. Tau strains

Many of the studies listed above also proved that seeded tau aggregation is templated, meaning that the aggregates formed retain the same conformation and biochemical characteristics of the original seeds. Different conformers that can be faithfully propagates over time are called strains, and are thought to be responsible for the phenotypic variability of tauopathies, as is the case for prion disorders. It is straightforward to think that the morphology of tau assemblies could be an important determinant in defining the type of disease that will develop. Indeed, considering the three classes of tauopathies (3R, 4R, 3R/4R), it is clear that while the protein material is the same, it must be assembled in specific conformations that end up causing distinct pathologies. Structural insights into filaments made of recombinant tau isoforms proved that at least three types of fibrils exist, each one with individual characteristics: 3R aggregates, 4R aggregates and mixed aggregates composed of both types of isoforms that co-assemble into heterogeneous amyloids182. Mutations also affect the conformational properties of the fibrils, as they interfere with the hydrophobic and long-range interactions involved in fibrils formation. Indeed, using circular dichroism and spectroscopy techniques, Frost *et al.*, showed that aggregates composed of wild-type or mutated (P301L/V337M) tau have different secondary structures and morphology187, with the mutated fibrils showing a peculiar curved morphology and lacking the twisted appearance of wild-type fibrils. One of the first conformers to be recognized as strain and characterised comes from the seeded aggregation of recombinant wild-type tau with pre-formed fibrils made of recombinant P301L/V337M tau. After some rounds of aggregation, a new conformer termed WT* was produced189. It is composed of wild-type protein, but its tertiary structure is strikingly similar to the mutated protein used as template. Other synthetic strains were obtained from the exposure of RD-tau expressing cells to synthetic fibrils produced in different chemical environments, and 2 out of 20 showed differences in inclusion morphology, aggregate size, subcellular localization, and extended also to biochemical properties, like protease sensitivity, seeding capacity and toxicity18. Concerning human tauopathies, Guo *et al.*, [190] identified striking differences in the morphological structure of AD-seeded fibrils compared to in vitro ones, which affected their seeding potency and deposition pattern. This phenomenon is not limited to AD; indeed, inoculation of mice transgenic for human wild-type tau (ALZ17) with brain extracts from patients with different tauopathies recapitulated the major features of each disease (AGD, PSP, CBD)167. AD shows the highest homogeneity in strain composition, probably correlated to the existence of a predominant strain, whereas other diseases had strong interpatient variations, with at least two individual strains identified (PSP, AGD). As seen before, strain propagation occurs also in non-transgenic mice. When brain extracts from patients with 4R and mixed tauopathies (AD, PSP, CBD) were inoculated in non-transgenic mice, specific inclusions formed

in different subcellular localization according to the type of biological sample. AD-tau induced a thread-like pathology mainly in axons and triggered the aggregation of both 3R and 4R endogenous tau, while CBD seeds induced frequent perykarial pathology made predominantly of 4R tau. Among PSP strains, one in particular that came from the frontal cortex of the patient was found to be uniquely aggressive, with a very fast rate of spreading throughout the brain. Although showing variable seeding potency, all the three groups of strains, maintained cell specificity for neurons or glia as in the corresponding disease, such that only PSP and CBD samples induced astroglial and oligodendroglial pathology with coiled bodies that closely resemble their human counterparts.

1.3.3.1. Ultrastructural differences of brain-derived tau filaments

Thanks to the use of cryo-EM as a powerful technique to image protein aggregates, the structures of tau filaments from patients with AD, PiD and chronic traumatic encephalopathy were determined at the atomic level (3.5 Å) [83, 263, 264]. In all cases, the core of the filaments is made up by the repeated region and the rest of protein forms the fuzzy coat; however, the different interactions between short β elements result in distinct types of filaments packing.

Tau aggregates in AD come mainly as paired helical filaments (PHFs), but a portion of other structures called straight filaments (SFs) is present. Both 3R and 4R tau isoforms are involved in the aggregation process and form mixed fibrils equally incorporating the two subgroups of isoforms. This peculiar situation is made possible by the fact that the fibrils core is formed only by the repeats R3 and R4, while the repeat R2, which is present only in 4R tau, is not involved. PHFs and SFs share a common structure of the core, shaped like the letter C. The difference in the overall arrangement of the fibrils come from ultrastructural diversities in the way protofilaments interact with each other. In PHFs, the C-shaped subunits pair up symmetrically, whereas in SFs the interaction is asymmetric and weaker [83]. (Fig. 1.10)

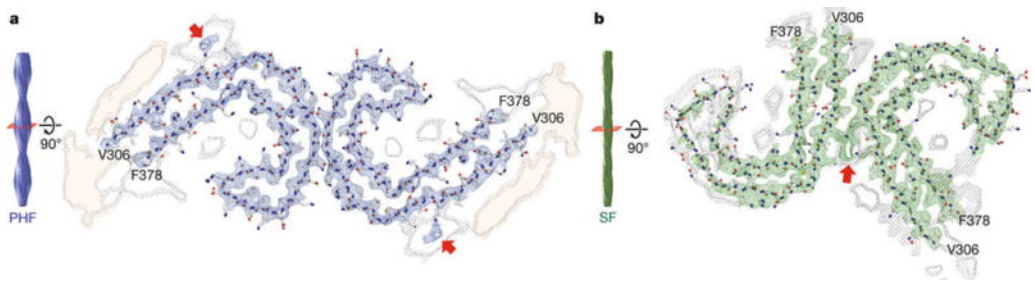

Fig. 1.10. Cryo-EM density and atomic models of the core of PHFs (a) and SFs (b) from AD patients [83].

Moreover, the comparison between PHFs and SFs from patients with either sporadic or inherited AD indicated that there is no structural difference between individuals with AD [265].
On the contrary, PiD filaments incorporate only 3R tau. The core consists of the residues 254-378, including repeats R1, R3 and R4. The β-elements of PiD filaments are arranged to form the letter J, and this particular fold is responsible for the ability of PiD aggregates to seed only 3R tau. Indeed, due to the amino acid composition, the side chains of the repeat R2 do not pack properly in this structure. When tau is folded into a J shape, Ser262 is buried in the interior of the aggregate, and cannot be phosphorylated. Indeed, in PiD no phosphorylation of Ser262 is detected. Preliminary evidence suggests also that, as for AD, also PiD patients share the same fold of the aggregates.
Falcon et al. analysed also the structure of tau aggregates found in patients with chronic traumatic encephalopathy (CTE) [264]. Differently from the other tauopathies, in CTE the aggregation of tau is most probably triggered by mechanical stimulation, such as repeated injury. All six isoforms take part to the formation of the filaments. As in AD, the residues that form the core of the fibrils assemble into two C-shaped protofilaments; however, the different arrangements of some of the β-elements create a hydrophobic cavity that is not present in AD filaments and that seems to incorporate some cofactors.
These structural data clearly show that the morphology of the aggregates vary among pathologies, although the reasons behind this phenomenon are yet to be clarified. Nevertheless, many information on tauopathies were obtained using synthetic amyloids, produced *in vitro* from either full-length or truncated tau constructs (K18, K19). When analyzing the ultrastructural details of AD fibrils, Fitzpatrick et al.[83] found that the packing of the core requires an interaction between the hexapeptide $_{306}$VQIVYK$_{311}$ and the residues 373-378. This last segment is not present in K18 and K19 constructs, which end at amino acid 372; therefore, their final assembly is different from that of PHFs and SFs from AD and should be used with caution when extrapolating *in vitro* results to tau aggregation *in vivo*. Moreover, the use of heparin as a cofactor to help the polymerization of recombinant tau *in vitro* leads to the obtainment of conformers that do not represent those found in patients [266]. Both 2N3R and 2N4R isoforms were considered. In the presence of heparin, 2N4R formed polymorphic aggregates with at least four different conformers with a common kinked hairpin fold. Heparin-induced 2N3R amyloids were more homogeneous, with an ordered core mad of the third repeats of two parallel tau monomers. Fig. 1.11 shows the schematic representations of all tau folds studied with cryo-EM. It is evident that there are strong differences between synthetic and patient-derived filaments, both in terms of the global shape of the core, and of the β-elements that interact with each other.

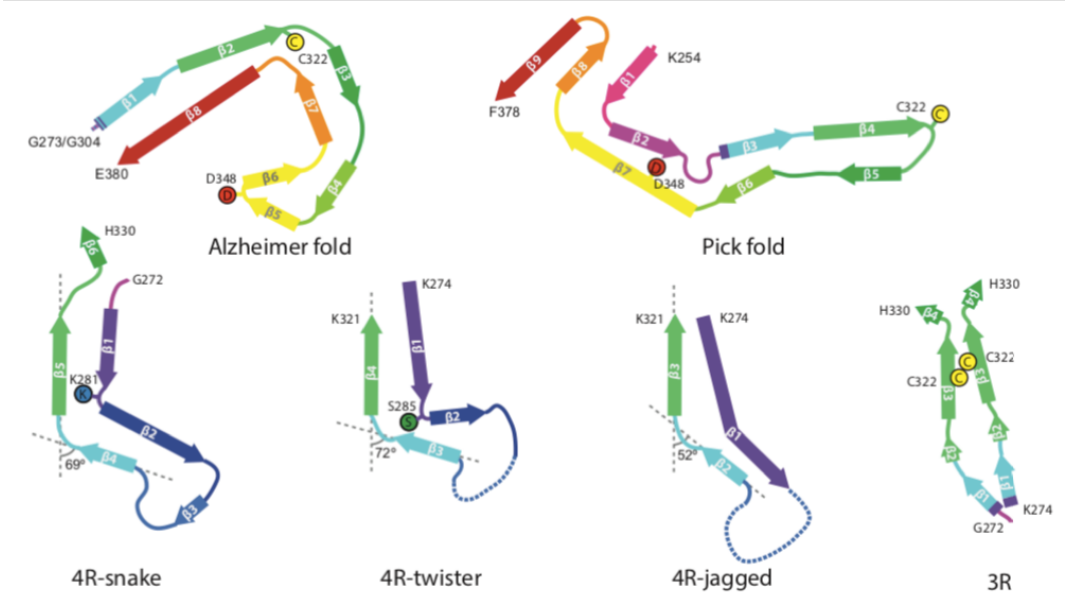

Fig. 1.11. Comparison between the structures of protofilaments from AD and PiD with those of heparin-induced filaments of 2N4R (snake, twister and jagged) and 2N3R tau [266].

Taken together, these data provide unifying neuropathological criteria to help distinguishing among tauopathies, and support the idea that the existence of distinct conformers of tau aggregates might underlie different disorders.

1.3.4. Release and cell-to-cell transfer of tau aggregates

Secretion of tau occurs in physiological conditions and independently of tau pathology. The mechanisms are still poorly understood, but there are many pathways involved. Around 90% of tau is released in a monomeric, non-phoshorylated form, often as a consequence of neuronal hyperexcitability [267]. Exosomes and ectosomes are also involved in the secretion of both soluble and fibrillar tau. Aggregates of ΔK280-RD tau were found in exosomes of overexpressing N2a cells, and they were shown to take part to the cell-to-cell spreading of the amyloids [268]. In addition, vesicles containing tau with seeding activity were found not only in brains of transgenic mice [269], but also in CSF and interstitial spinal fluids of both animal models [270] and patients [268]. In some cases, the seeded activity was limited to the acceleration of soluble oligomers formation and hyperphosphorylation rather than the induction of actual pathology [271]. Anyway, all these studies corroborate the hypothesis that extracellular vesicles are in some ways implied in prion-like propagation of tau pathology.

Other mechanisms require direct contact between cell cytoplasm through membranous connections called tunnelling nanotubes. Although their existence has been called into question, mainly because of the lack of specific markers that identify them as independent structures, their role in transferring tau amyloids seems to be definitively assessed [272, 273]. Besides having been found inside TNTs, tau fibrils promote the formation of new nanotubes, as if they were boosting their own

transcellular spreading between neurons. Monomeric tau might also be a component of the nanotubes themselves, since immunofluorescence analysis revealed that tau appears besides filaments of actin and myosin in these structures.

1.4. Cellular prion protein as a receptor for amyloids

Among the functions of PrP^C that have been discovered so far, one of the most intriguing is the ability of the cellular prion protein to act as a receptor and signal transducer for a variety of disease-related proteins [274-276]. Strikingly, all of them show an enrichment in ß-sheet elements as a common feature. The first protein for which this mechanism proved valid is indeed the counterpart of the cellular prion protein, its pathogenic conformer PrP^{Sc}. Besides being a substrate for prion-templated conversion, PrP^C plays an active role in mediating the toxic signalling of PrP^{Sc} without changing its conformation. The interaction between the two partners does not involve specific sequences, but rather macroscopic structures, as for example secondary structure elements like ß-sheets. This is clearly deducible from the fact that PrP^C from different animal species (hamster, human, bovine, cervid) transduced the toxic signalling of mouse PrP^{Sc} as efficiently as mouse PrP^C, meaning that the interplay is independent of the primary sequences [274]. Actually, the binding partner of PrP^C can be also a completely different protein, as long as ß-sheets are present; indeed, in the same paper the authors reported that oligomeric Aß was able to induce apoptosis through a signalling cascade activated by PrP^C, and that this effect could be blocked by targeting the amyloids with an oligomer-specific antibody (A11). Another way of impairing the Aß-induced apoptosis was to use truncated PrP^C forms, missing either the N-terminal segment (amino acids 27-89) or the C-terminal GPI-anchor. Moreover, when fusion peptides composed of the N-terminus of PrP^C and the Fc portion of human IgG were added to the plates, Aß bound to them and the toxic effect was abrogated. Taken together, these findings suggest that the actual binding between PrP^C and ß-sheet rich proteins occur through the N-terminal portion of the protein, while the GPI anchor is needed to activate the signalling cascade responsible for the toxic phenotype. Several studies focused on the identification of the specific regions mediating the interaction with Aß oligomers, and came up with slightly different results, that see the cluster of basic residues (amino acids 23-31, and specifically the KKRPK sequence) and the segment from amino acids 95/98 to 110 as the proper binding site [204, 277]. A third segment spanning residues 136-158 has been also identified, although only in PrP^{Sc}-induced signalling [278, 279]. As for the identity of the molecular interactors, Aß-induced toxicity seems to require the metabotropic glutamate receptor 5 (mGluR5), the tyrosine kinase fyn, and the NR2B subunit of NMDA receptor, which becomes phosphorylated and dysregulates the receptor's functions [280, 281] (Figure 1.12). Additionally, the N-terminal domain of PrP^C can penetrate the plasma membrane exploiting the polybasic regions, and once inside the cytoplasm it acts as a protein transduction domain [282, 283].
In vivo experiments proved controversial in supporting the notion that this mechanism really occurs in diseased brains. On the one hand, Strittmatter's group showed that

PrP-knockout mice treated with Aß amyloids do not suffer from suppression of long-term potentiation (LTP) as their wild-type counterparts, and treatment with anti-PrP^C antibodies rescued the phenotype of wild-type mice [284]. On the other hand, Balducci et al. did not report any difference in long-term memory between wild-type and PrP-knockout mice, raising questions on the actual importance of PrP^C-induced signalling [285]. One possible explanation for these contrasting data is that in both cases Aß oligomers were produced form synthetic material, and preparations may vary between different laboratories [286]. It might be that only some specific conformers of Aß are able to trigger their signalling cascade through PrP^C [287]. This speculation is indeed quite plausible, given that similar divergences were found when considering the interaction of PrP^C with another ß-sheet-enriched amyloid, α-synuclein fibrils. α-synuclein is the major component of Lewy bodies, the main pathological hallmark of Parkinson's disease. Contrary to Aß, which remains extracellular, α-synuclein aggregates are internalized by neurons mainly by receptor-mediated endocytosis and exert their toxic functions from the inside of the cells. Known receptors include the transmembrane protein lymphocyte-activator gene 3 (LAG3), neurexin, amyloid ß precursor-like protein 1 (APLP1), α3NKA and HSPGs [239, 288, 289].

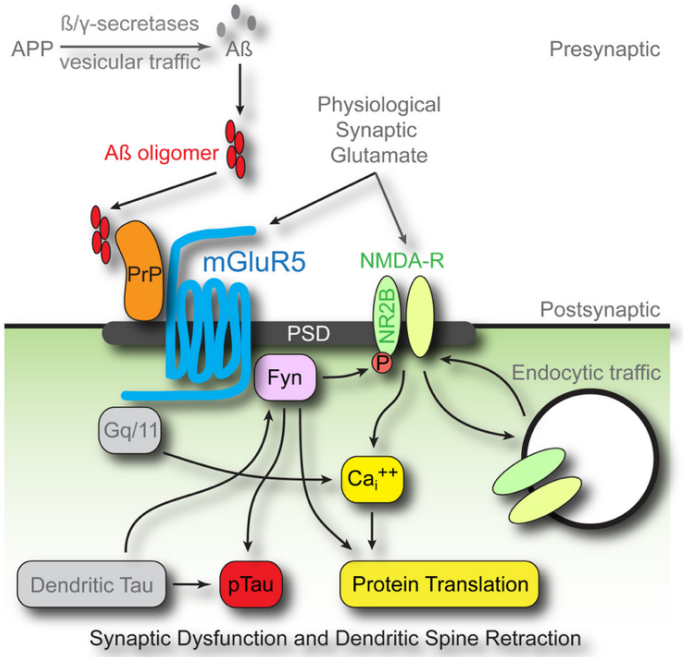

Figure 1.12. Signalling cascade activated by the binding of Aß oligomers to PrP^C [290]. Binding of Aβo to cellular prion protein (PrPC) triggers mGluR5-dependent signaling events which proceed through fyn kinase.

Recently, our group pointed at PrP^C as another putative receptor that facilitates the entrance of α-synuclein amyloids in cells [205]. In this work, a more consistent uptake of synuclein fibrils was observed in N2a cells constitutively expressing PrP^C compared to the same cell line ablated for PrP^C, and also in primary cortical neurons. SPR analysis produced two distinct constants for PrP^C-synuclein binding, which may reflect

the high disomogeneity of the fibrils preparation used. Indeed, aggregates obtained by *in vitro* fibrillization had been subjected to sonication that breaks longer fibrils randomly into smaller fragments and increases the variability of the final products. Different species, i.e. long vs. short fibrils, might show different propensities to bind to PrP^C and to exploit its activity as receptor protein to gain cell entrance. Short fibrils showed the strongest binding to PrP^C and their uptake was the most affected by the knock-out of PrP, while longer fibrils were internalized with more difficulty also in PrP-expressing cells. Short fibrillar species should not be confused with oligomers, as the former maintain the ordered ß-sheet organization typical of fibrils despite being smaller, while the latter have their own peculiar structure. Structural differences between the two species might explain why oligomeric α-synuclein was reported to not bind to PrP^C and to induce the same detrimental effects in both wild-type and PrP-null mice [291]. On the contrary, when using fibrils preparations, the role of PrP^C in the spreading of synuclein pathology is clearly assessed. Although not mandatory for the diffusion of the pathology in the brain, expression of PrP^C increases the rate of transport of the aggregates between cells and result in a higher accumulation of PK-resistant synuclein amyloids in many districts of the CNS [205, 292]. As already seen for Aß oligomers, the toxic effects of synuclein fibrils proceed through the signalling cascade initiated by mGluR5 and dependent on fyn kinase and NMDAR2B [293]; however, since Lewy bodies are intracellular, a new model was proposed in which PrP^C takes part to the endocytic pathway that brings synuclein inside the cells after a short stay in the endolysosomal compartment [205, 294].

All these findings underline that a close link exists between the prion protein functions and its role in the spreading of different neurodegenerative diseases other than TSEs. From a therapeutic point of view, the discovery of a shared mechanism underpinning the spreading of very different diseases like PD and AD is of extreme importance, as it allows the development of common therapeutics directed against PrP^C that might be able to delay the neurotoxicity of many protein aggregates and block their spreading. Given these very promising results, the question arises if other prion-like disorders like tauopathies take advantage of the prion protein to disseminate in the brain and cause degeneration, and if any treatment targeting PrP^C would in some way bring any benefits to patients.

AIM OF THE RESEARCH

One of the most intriguing challenges posed in the field of neurodegenerative diseases concerns the possibility of finding some sort of “common ground” between disorders that have been so far considered as separate entities. Several *in vitro* and *in vivo* studies showed that there is a cross-talk between neurodegeneration-related proteins, which appear to share some key features that reflect into similar disease progression. In this perspective, the identification of receptor proteins that could be involved in more than one neurodegenerative disorder would offer a completely new point of view on these pathologies, as well as interesting therapeutic targets to be used against an array of disorders.
The cellular prion protein PrP^{C} has been reported to bind to both amyloid ß and synuclein fibrils, to mediate their toxic effects and, in the case of synuclein, also to promote their entrance into the cell cytoplasm. Therefore, in this thesis we focused our attention on whether PrP^{C} might exert the same effect on tau fibrils. In particular, we evaluated two aspects of the possible interaction between the cellular prion protein and tau amyloids:

i. The ability of PrP^{C} to facilitate the internalization of tau K18 amyloids in neuroblastoma cell lines. Taking advantage of the tau truncated fragment K18, widely used as a model for the study of tauopathies, we first assessed the existence of an interaction between the cellular prion protein and the amyloids. Next, we evaluated the internalization of tau fibrils in cell lines that either express or not the prion protein on the cell surface. Potential therapeutic approaches were evaluated by targeting specific domains of PrP^{C} with antibodies.

ii. To promote PrP^{Sc} clearance in prion-infected cell lines mediated by tau K18 fibrils. As observed by Aulic *et al.* [205], synuclein amyloids promote the clearance of PrP^{Sc} in ScN2a cells, most probably through the inhibition of prion conversion. We investigated if tau fibrils show the same propensity to decrease the prion levels in prion-infected cells, and we evaluated the contribution of the cellular degradation pathways to the tau-induced PrP^{Sc} clearance.

MATERIALS AND METHODS

2.1. Tau K18 expression and purification

Expression and purification of recombinant tau K18 fragment were performed as previously described. Briefly, pET-11a expression vector containing the sequence encoding for tauK18 was transformed into *E.*coli BL21(DE3) strain (Stratagene), and protein expression was achieved according to the following protocol: an overnight culture of *E.*coli BL21(DE3) was inoculated in 2L of Luria-Bertani medium complemented with ampicillin 100µg/mL and grown at 37°C until 0.8 $O.D._{600}$, when protein expression was induced with 0.8 mM IPTG and the temperature was lowered to 30°C to minimize degradation. The cells were harvested by centrifugation after 5 hours from induction. Lysis was performed at 4°C using PandaPlus Homogenizer in the presence of protease inhibitors (Complete™ ULTRA Tablets, EDTA-free, glass vials Protease Inhibitor Cocktail, Roche) and the supernatant containing the recombinant protein was subjected to a boiling step that precipitates the majority of the proteins except for tau. The supernatant was then loaded onto a 5 mL HiTrap SP FF chromatographic column (GE Healthcare) in binding buffer (20 mM MES, 50 mM NaCl, 1 mM EDTA, 0.1 mM $MgCl_2$, 2 mM DTT, 0.1 mM PMSF, pH 6.8) and eluted with a linear gradient from 0% to 60% of elution buffer (20 mM MES, 1 M NaCl, 1 mM EDTA, 0.1 mM $MgCl_2$, 2 mM DTT, 0.1 mM PMSF, pH 6.8). Fractions were analysed on SDS-PAGE for protein content, and those containing tauK18 were pooled together, loaded onto gel filtration column (Superdex 200 26/60, GE Healthcare) and eluted with PBS pH 7.4. Purified protein was analysed by SDS-PAGE, dyalized against water and lyophilized.

2.2. Fibrillization of tauK18

All solutions were sterilized by filtration with a 0.22 µm filter prior to use. Reactions were prepared in a 96-well black plate with transparent bottom (BD Falcon) in a final volume of 200 µL per well. Fibrillization reaction was composed as follows: tauK18 0.5 mg/mL, heparin 10 µg/mL, DTT 0.1 mM, PBS 1X pH 7.4. Due to its toxicity to cultured cells, 10 µM Thioflavin T (ThT) was added only in 4 wells that were used to monitor the aggregation reaction in *real-time*. Each well contained also a 3-mm glass bead (Sigma). The plate was covered with sealing tape (Fisher Scientific) and incubated at 37°C under orbital shaking (50 seconds of shaking at 400 rpm followed by 10 seconds of rest) on FLUOstar Omega (BMG Labtech) microplate reader. Fluorescence was monitored every 30 minutes by bottom reading at 444 nm of excitation and 485 nm of emission. The reaction was stopped after 15 hours, when fluorescence reached plateau. Newly formed aggregates were pelleted by ultracentrifugation (55000 rpm for 1 hour at 4°C), resuspended in an equal volume of sterile PBS and stored at -20°C. Before use, aliquots were thawed and sonicated for 5 minutes in an ultrasonic bath (Branson 2510).

2.3. AFM analysis

AFM analysis was performed in accordance with the method previously described [435]. Ten µL of fibril solution was deposited onto a freshly cleaved piece of mica and left to adhere for 30 min. Samples were then washed with distilled water and blow-dried under a flow of nitrogen. Images were collected at a line scan rate of 0.5-2 Hz in ambient conditions. The AFM free oscillation amplitudes ranged from 25 nm to 40 nm, with characteristic set points ranging from 75% to 90% of these free oscillation amplitudes. AFM data were analysed with Gwyddion (gwyddion. net).

2.4. Cytotoxicity assay

The cytotoxic effect of tauK18 fibrils was evaluated by measuring cellular redox activity with 3-(4,5-dimethylthiazol-2-yl)-2,5-diphenyltetrazolium bromide (MTT). 30000 N2a cells/well were cultured in 96-wells plates and treated with different concentrations of tauK18 sonicated fibrils added directly in the cell culture medium. Following 72-hours incubation, the cytotoxic effect was assessed by measuring cellular redox activity, following the manufacturer's (Sigma) instructions.

2.5. In vivo experiments

Animals

Experiments were performed on 2,5-months old transgenic male and female rats (line SHR72), and on 5 months old transgenic mice (line R4m7) both expressing human truncated 4R tau protein (amino acids 151-391) consisting of the four microtubule binding domains. Animals, chosen in random, were injected unilaterally with 3µL for rats and 2 µL for mice of insoluble tau fraction (n=2), K18 sonicated (n=3) or K18 non-sonicated (n=3). All animals were housed under standard laboratory conditions with water and food ad libitum. All experiments were performed in accordance with the Slovak and European Community Guidelines, with the approval of the Institute's Ethical Committee and study has been approved by the State Veterinary and Food Administration of the Slovak Republic.

Stereotaxic surgery

Rats and mice were anesthetized with 1.5% to 2% isoflurane (Florane) and the temperature of the animals was maintained at 37°C. Then animals were fixed to stereotaxic apparatus (Kopf Instruments, California, USA) and UltraMicroPump III (UMP III) and Micro4 Controller (World Precision Instruments, Florida, USA) were used for applying of substances. UMP III uses microsyringes to dispense nanoliter/microliter sample volumes. Animals received unilaterally 3 µL (rat) or 2 µL

(mice) of sarkosyl insoluble tau (concentration 500ng/μL) or of K18 sonicated/non-sonicated fibrils (concentration 500ng/μL, 300ng/μL).
Stereotaxic coordinates for the injection were characterized using stereotaxic atlas ("The rat brain in stereotaxic coordinates", Paxinos and Watson) and also was taken into account the age and the strain of animals. Stereotaxic coordinates for the injection into hippocampus of rats were A/P: -3.6 mm, L: -2.0 mm, D/V: 2.9 (females) or -3,1 (males) mm from bregma. For mice the stereotaxic coordinates were A/P: -2.1 mm, L: -1.2 mm, D/V: -1.8 mm from bregma (Paxinos and Watson, 1996). The needle remain in place at the injection site for an additional 5 min before the cannula was removed slowly (over 2 min). The skin was sutured and the animal was returned into home-cage and monitored until fully recovered. Post-operative care included the non-steroidal anti-inflammatory drugs.

2.6. Preparation of fluorophore-labeled fibrils

TauK18 fibrils were conjugated to AlexaFluor 488 NHS Ester (Thermo Fisher) following the protocol described by Karpowicz *et al.*[295] Briefly, tauK18 fibrils were pelleted by ultracentrifugation and resuspended in carbonate buffer (0.1 M $NaHCO_3$, pH8.3). AlexaFluor 488 was added directly to the resuspended fibrils, which were then incubated for 1 hour at 25 °C under mild shaking (300 rpm). The unbound fluorophore was removed by four dialysis steps in sterile PBS using gamma-irradiated Slide-A-Lyzer dialysis cassettes with a molecular weight cut-off of 10 kDa (Thermo Fisher). Fluorescent fibrils were aliquoted and stored in the dark at -20°C.

2.7. Preparation of biotinilated fibrils

Biotinilated fibrils were produced accordingly to the manufacturer's (Sigma) instructions. TauK18 fibrils were pelleted by ultracentrifugation and resuspended in carbonate buffer pH 9.5 to a final concentration of 20 mg/mL. Biotin NHS Ester (Sigma) was added to the resuspended fibrils with gentle stirring, and the solution was incubated for 4 hours at room temperature. Unbound biotin was removed by four dialysis steps in PBS using Slide-A-Lyzer cassettes with a molecular weight cut-off of 3.5 kDa. Biotinilated fibrils were aliquoted and stored in the dark at -20°C.

2.8. Pull-down assay

Neuro2a cells were lysed in lysis buffer (0.1% NP40, 50 mM TrisHCl pH 8, 150 mM NaCl) containing one tablet of Complete™ ULTRA Tablets, EDTA-free, glass vials Protease Inhibitor Cocktail (Roche). Total protein content was quantified using bicinchoninic acid protein (BCA) quantification kit (Pierce). 1 mg of total protein content was diluted in lysis buffer to a final volume of 500 µL, then biotinylated tauK18 fibrils were added to a final concentration of 2 µM. Samples were left standing on a rotor wheel overnight at 4°C. The day after, 30 µL were collected from each sample and stored at -20°C for further analysis (input samples). 30 µL of neutravidin bead

slurry (NeutrAvidin Agarose Resins, ThermoFisher Scientific) were added to each tube, and the samples were incubated on the rotor wheel at 4°C for 4 hours. To precipitate the beads, the samples were centrifuged at 4°C for 2 minutes at 2000 rpm, the pellet was washed with three subsequent steps of resuspension in lysis buffer and centrifugation, and finally resuspended in 20 µL of Laemmli loading buffer. Samples were boiled for 10 minutes and centrifuged at 13000 rpm for 1 minutes to detach and pellet the beads, respectively. The supernatants were collected and stored at -20°C.

2.9. Cell lines

Mouse neuroblastoma cells N2a were kindly provided by Prof. Chiara Zurzolo (Unité de traffic membranaire et pathogenèse, Institute Pasteur, Paris, France). N2aPrP KO cells were kindly provided by professor Gerold Schmitt-Ulms (Tanz Centre for Research in Neurodegenerative Diseases, University of Toronto, Toronto, Ontario, Canada), for which they used the CRISPR-Cas9-Based Knockout system to ablate the expression of PrP protein [293]. ScN2a cells are clones persistently infected with the RML prion strain as described by Prusiner's group [437] or with the 22L prion strain. Cells were grown at 37°C and 5% CO_2, in minimal essential medium (MEM) + glutamax (Thermo Fisher Scientific Inc.), supplemented with 10% fetal bovine serum, 1% non-essential aminoacids, and 100 units/ml penicillin and 100 µg/ml streptomycin.

2.10. TauK18 fibrils infection in cell lines

2uM of tauK18 amyloids was added to the cell culture medium of N2a, N2aPrP KO and ScN2a cell lines in 10 cm plates, and incubated for a variable amount of time according to the specific experimental setting (ranging from 1 day to 6 days). For the evaluation of PrP^{Sc} clearance in ScN2a cell line, cells were split and maintained for five additional passage in fibrils-free cell culture medium. For fluorescence quantification of amyloids internalization, cells were plated in 24-wells plates on 12 mm coverslips and incubated with Alexa488-labeled fibrils for 24 – 72 hours.

2.11. Trypan blue quenching of non-internalized fibrils and imaging

30000 cells were cultured on each coverslip and treated with 2 µM Alexa488-labeled tauK18 fibrils. Before fixation, cells were washed twice with sterile PBS and incubated for 5 minutes with a sterile 1:1 solution of Trypan Blue : PBS. As shown by Karpowicz *et al.*, Trypan Blue quenches green fluorescence through an energy-transfer mechanism, but being unable to enter alive cells, only the fluorescence coming from non-internalized fibrils is quenched.
Cells were then rinsed three times with sterile PBS and fixed for 10 minutes with 4% paraformaldehyde/PBS. After three washing steps, cells were permeabilized for 5 minutes with 0.2% Triton X-100/PBS, rinsed again with PBS and incubated for 1 hour with HCS Blue Cell Mask (ThermoFisher Scientific) diluted 1:1000, a specific dye that labels the whole cell cytoplasm. Coverslips were mounted in Fluoromount-G™

(ThermoFisher Scientific) and stored at 4°C for confocal fluorescence microscopy. Images were acquired using a Nikon confocal microscope (Nikon C1).

2.12. Inhibition of tauK18 internalization using POM monoclonals

Anti-PrP^C monoclonal antibodies were kindly provided by Prof. Adriano Aguzzi (Institute of Neuropathology, University of Zürich). POM monoclonals include a series of antibodies directed against multiple epitopes distributed on the whole sequence of PrP^C [296]. For the inhibition of tauK18 fibrils uptake, three antibodies were considered: POM12, which binds a degenerative epitope within the octarepeat sequence of PrP^C; POM3, which targets the amino acids 95-100 (HNQWNK) near the centre of PrP^C; POM4, which binds a conformational epitope formed by the very C-terminal (around amino acids 220) and a middle part of the protein (amino acids 121-134). N2a cells plated on coverslips were pre-treated with each POM antibody (15 µg/mL) for 1 hour at 37°C, followed by incubation with Alexa488-labeled tauK18 fibrils for 24 hours. Coverslips were processed and mounted as described above. To check the binding of POM antibodies to membrane PrP^C, cells treated with POM antibodies for 1 hour were fixed with 4% paraformaldehyde:PBS for 10 minutes, then blocked with 2% FBS for 30 minutes and incubated with Alexa594-conjugated goat anti-mouse IgG diluted 1:200 for 1 hour.

2.13. Uptake quantification

The uptake quantification was performed in blind on more than 200 cells in three independent experiments. Random fields on each coverslip were captured at 63x magnification (zoom 3X) using Nikon confocal microscope. Images were acquired as 30 - 40 z-stacks of 0.27 µm, 526 x 526, and subsequently deconvolved with a 3D deconvolution algorithm (in blind) of the NIS Elements software. Deconvolution was applied only to the green channel, as it allows a better separation of the green dots representing the fibrils. Deconvolved images were analysed using Volocity Workstation (PerkinElmer, version 4.1) and internalized fibrils were counted using a home-made script which intersects the objects recognized in the green channel with the 3D reconstruction of the cellular volume (blue channel). To discriminate the signals corresponding to fibrils from the background, we used the volume of a single monomer of synuclein as a threshold. Synuclein is very similar to tau K18 in terms of molecular weight and unfolded structure. The volume of a monomer in its multiple conformations was obtained from Zhang et al. [297]

2.14. Membrane immunostaining of PrP^C

N2a cells seeded on coverslips were treated for 24 – 72 hours with 2 µM of tauK18 fibrils. Surface staining of PrP^C was performed as described in Stincardini et al.[298]. Cells were incubated with W226 antibody diluted 1:250 in Opti-MEM (Life Technologies) for 15 minutes at 4°C, followed by washing in PBS and fixation with

4% paraformaldehyde:PBS for 10 minutes. Coverslips were then washed three times with PBS, incubated with blocking solution (2% FBS in PBS) for 30 minutes and incubated with Alexa-594 conjugated goat anti-mouse IgG (Invitrogen) diluted 1:200 in blocking solution. Finally, nuclei were counterstained with DAPI (1:1000). Coverslips were mounted in Fluoromount-G™ (ThermoFisher Scientific) and stored at 4°C. Images were acquired with Nikon confocal (Nikon C1) at 63x magnification, both as 2D-images of medial planes and series of 30-40 z-stacks 0.27 µm, 526x526.

2.15. Quantification of membrane staining

Quantification of membrane staining was performed with Volocity Workstaton (PerkinElmer) on 2D images. Image segmentation consisted first of nuclei identification by the DAPI signal, and selection of the region of interest by the Alexa-594 signal. Mean fluorescence intensity values of Alexa594-conjugated anti-PrP antibody were measured for more than 600 objects per coverslip, and weighted averages were calculated in order to identify any difference between untreated and treated samples. To confirm that 2D quantification is representative of the situation of the whole cell membrane, the same analysis was performed on a number of 3D z-stacks from both untreated and treated samples. As an additional control, N2a cells were treated with 10 µM chlorpromazine[298], and a reduction of PrP^C membrane levels was observed both with 3D and 2D images.

2.16. Quantification of total PrP^C levels by Western Blotting

Total protein contents of N2a untreated and treated with 2 µM of tauK18 fibrils were quantified using bicinchoninic acid protein (BCA) quantification kit (Pierce). Fifty µg of total proteins were used and complemented with 5X loading buffer in a ratio 1:5. The samples were boiled at 100°C for 10 minutes, loaded onto a 12% Tris-Glycine SDS-PAGE gel and transferred onto Immobilon P PVDF membranes (Millipore) for 2 hours at 4°C. The membrane was blocked in 5% non-fat milk and incubated overnight at 4°C with human anti-PrP antibody D18 diluted 1:1000. The membrane was washed three times with TBS buffer additioned with 0.2% Triton X-100, incubated for 45 minutes at room temperature with goat anti-human IgG conjugated with horseradish peroxidase and developed with the enhanced chemiluminescent system (ECL, Amersham Biosciences). After the acquisition, the membrane was incubated for 30 minutes at room temperature with anti β-actin (1:10000, A3854 Sigma-Aldrich), which is used as a normalizer. Images were acquired with Uvitec Alliance (Cambridge) and densitometric analysis was performed using Uviband analysis software. Data are expressed as mean ± SD, and the values of the controls are adjusted to 100%.

2.17. Total RNA extraction and RT-PCR analysis

The total RNA extraction was performed using PureLink RNA MiniKit with TRIzol® Reagent (Life Technologies) following the manufacturer's instruction. Briefly, control cells and cells treated with tauK18 fibrils were washed twice with PBS 1X and lysed using the TRIzol® Reagent. Following RNA isolation, a DNase I digestion was performed using 1 unit of enzyme per µg RNA for 15 min at room temperature, and RNA clean-up was implemented using RNeasy spin columns following the instructions. RNA concentration was determined using the NanoDrop system (Thermo Scientific). First-strand cDNA was synthesized using 3 µg of total RNA in a 20 µL reverse transcription reaction (RT^+ samples) mixture following the instructor manual. For each sample a non-retrotranscribed sample was carried along as a negative control (RT^- sample).
The cDNA was diluted to 10 ng/µL final concentration prior to Real-Time PCR reactions. 1 ng of cDNA was added to the reaction mix including 2× iQ™ SYBR® Green Supermix (Bio-Rad Laboratories, Inc.), 400 nM of the corresponding forward and reverse primer (Sigma), and quantified in technical duplicates on an iQ5 Multicolor Real-Time PCR Detection System (Bio-Rad Laboratories, Inc.).
After initial denaturation for 3 min at 95°C, 45 cycles were performed at 95°C for 10 sec and 60°C for 1 min. Differential gene expression of was normalized to GAPDH expression. RT^- controls were included in the plates for each primer pair and sample. The relative expression ratio was calculated using the ΔΔCT method [299]. Significance was calculated with the unpaired student t-test ($p < 0.05$). The primers used for RTqPCR reactions are listed in Table 2.1.

Gene	Chromosome	Primer sequence	Amplicon length (bp)
GAPDH	11	F: CCTGCACCACCAACTGCTTA R: CTGTCACCTTCACCGTTCC	74
PRNP	2	F: GAGACCGATGTGAAGATGATGGA R: TAATAGGCCTGGGACTCCTTCTG	80

Table 2.1.

2.18. Proteinase K digestion

ScN2a RML and 22L cell lysates (250 µg) were treated with with 20 µg/mL of proteinase K (PK) for 1h at 37°C. The reaction of proteolysis was stopped by the addition of phenylmethyl sulphonyl fluoride (PMSF) in a final concentration of 2mM. Immediately after, the samples were centrifuged at 55000 rpm, the supernatant was discarded and the pellet was resuspended in 2x loading buffer, boiled for 10 min, and resolved by 12% SDS-PAGE. The same protocol as above was used for the blotting procedure and the acquisition of the images. The antibodies used to visualize PrP^{Sc}

signal are mouse monoclonal anti-PrP W226 (diluted 1.1000 in blocking solution) and goat anti-mouse IgG conjugated to horseradish peroxidase (DAKO, diluted 1:1000 in blocking solution).

2.19. PNGase F treatment

PNGase F treatment (New England Biolabs) was performed on control and K18-treated ScN2a cell lysates. Twenty µg of total proteins were incubated with 1 µL of Glycoprotein Denaturating Buffer (10X) and water to reach a total reaction volume of 10 µL, then the mix was heated at 100 °C for 10 minutes to denature the proteins. The solution was chilled on ice and centrifuged for 10 seconds, then complemented with 2 µl of GlycoBuffer 2 (10X), 2 µl of 10% NP-40, 6 µl of H2O and 1 µl of PNGase F. The solution was incubated overnight at 37°C. Deglycosylated proteins were then analysed by Western Blot.

2.20. 3-methyladenine treatment

3-methyladenine (Sigma) was dissolved in sterile water to a final concentration of 30 mg/mL. ScN2a were first treated with K18 for 72 hours, and 3-MA at the concentration of 10 µM was added for the last 16 hours. Control consisted of untreated cells, with or without 3-MA. Cells were collected, lysed in lysis buffer and subjected to PK digestion and Western Blot analysis.

2.21. Ammonium chloride treatment

Ammonium chloride (NH_4Cl) was dissolved in sterile PBS. ScN2a were treated with K18 and 10 mM NH_4Cl for 72 hours. Control consisted of untreated cells, with or without NH_4Cl. Cells were collected, lysed in lysis buffer and subjected to PK digestion and Western Blot analysis.

RESULTS

3.1. Preparation of human tau K18 fibrils and structural characterization

The K18 fragment of human tau protein that comprises only the microtubule-binding domain (amino acids 274-372) was produced in *E.coli* BL21(DE3) bacterial strain and purified with two subsequent chromatographic steps to yield a highly pure recombinant protein. A homology comparison of the human tau microtubule-binding domain with the same region of murine tau and rat tau (taxid: *Mus musculus* and *Rattus norvegicus*, respectively) showed that the amino acidic sequence is almost perfectly conserved among these species.
Next, we set up a protocol to produce *in vitro* synthetic fibrils as described by Barghorn et al.[300].

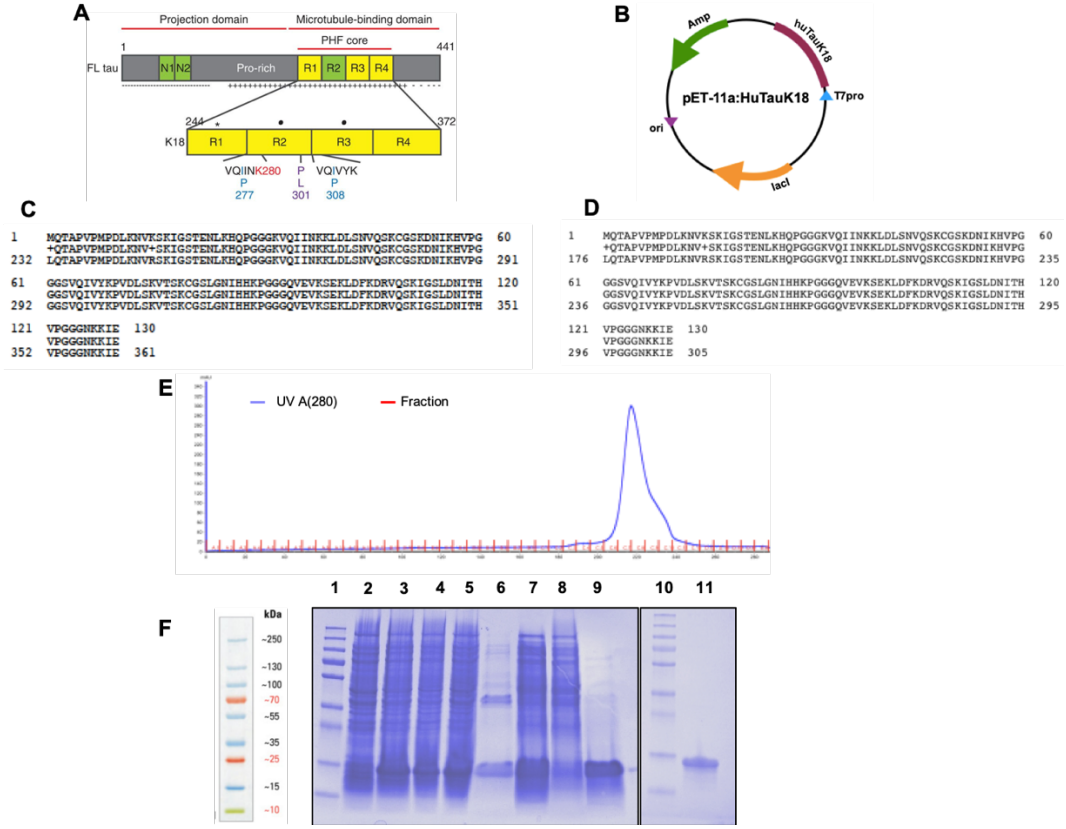

Figure 3.1. Expression and purification of human tau K18 fragment. (A) Tau K18 fragment belongs to the subclass of 4R isoforms and includes only the repeated regions that form the microtubule binding domain (spanning amino acids 244-372). Known pathogenic mutations are indicated underneath the structure, but only the wild-type construct was used in this study. (B) Plasmid used for expressing human tau K18 in *E.coli* BL21(DE3). (C) Homology comparison between the microtubule-binding domain of human tau and mouse tau and (D) human tau and rat tau. (E) Chromatogram obtained from the second purification step of tau K18 by size-exclusion chromatography. (F) Expression of recombinant human tau K18. 15% SDS-PAGE. Lanes 1 and 10: molecular mass marker; lane 2: whole

cell extract before IPTG induction; lanes 3, 4 and 5: whole cell lysate after IPTG induction; lanes 6 and 7: pellet and supernatant after cell lysis by homogenization; lanes 8 and 9: pellet and supernatant after boiling; lane 11: purified tau K18 protein.

The in vitro fibrillization assay allows a rapid and efficient misfolding of the recombinant soluble protein into fibrillar, amyloid-like structures enriched in ß-sheets. The aggregation process is monitored by checking the fluorescence of the dye ThT, which gives a strong fluorescence signal upon binding to amyloid fibrils. Once all the monomeric has been converted into fibrils, the ThT signal reaches the plateau phase and remains flat. In order to better characterise tau K18 propensity to aggregate, we tested the effect of three different concentrations of monomeric protein in terms of lag phase duration and maximum intensity of ThT signal (figure 3.2.)

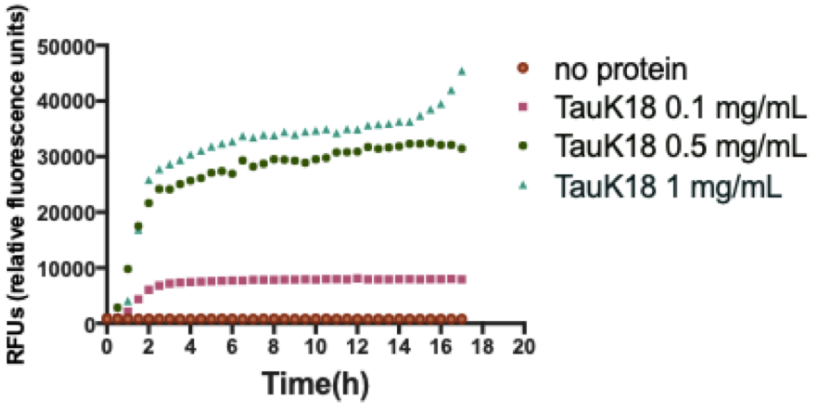

Figure 3.2. *In vitro* auto-aggregation kinetics of human tau K18. Three different concentrations of monomeric tau K18 were tested in the *in vitro* assay: 0.1 mg/mL (pink squares), 0.5 mg/mL (green circles) and 1 mg/mL (light blue triangles). To check for any possible unwanted contribution from the reaction components, a control condition without the recombinant protein was also included (red circles). Each fibrillization curve represents the average of three replicate wells.

Higher concentrations of tau did not significantly alter the duration of the lag phase, which is already very short with the lowest protein concentration (around 1 hour). As expected, the maximum intensity reached by the ThT signal at the plateau was strongly influenced by the protein concentration, with a more consistent production of aggregates when higher amounts of substrate were used. We noticed that while the two lower concentrations of tau K18 converted into fibrils with the typical sigmoid pattern, a further increase of monomeric protein up to 1 mg/mL led to a kinetic curve resembling a double sigmoid, with an early plateau phase followed by a second growth phase and eventually by a definitive saturation.
Given these observations, we chose 0.5 mg/mL as final concentration of tau K18 for further experiments, as it proved to best fit the requirements of both a highly reproducible fibrillization process and a consistent production of amyloid material. We let the reaction go for around 13 hours in order to reach the plateau and to have most of the soluble protein converted into long, mature fibrils (Fig. 3.3, panel A).
The aggregates were then subject to a round of sonication for 5 minutes in order to break them into smaller species. Indeed, in AFM images of non-sonicated fibrils we

could observe that, conversely to synuclein, tau aggregates formed *in vitro* tend to stick one to the other and form big clumps which cannot be easily internalized by cultured cells. Sonication not only disrupts these plaques, but also breaks most of the longer fibrils into small pieces, therefore increasing the homogeneity of the preparation (Fig. 3.3, panels B and C).

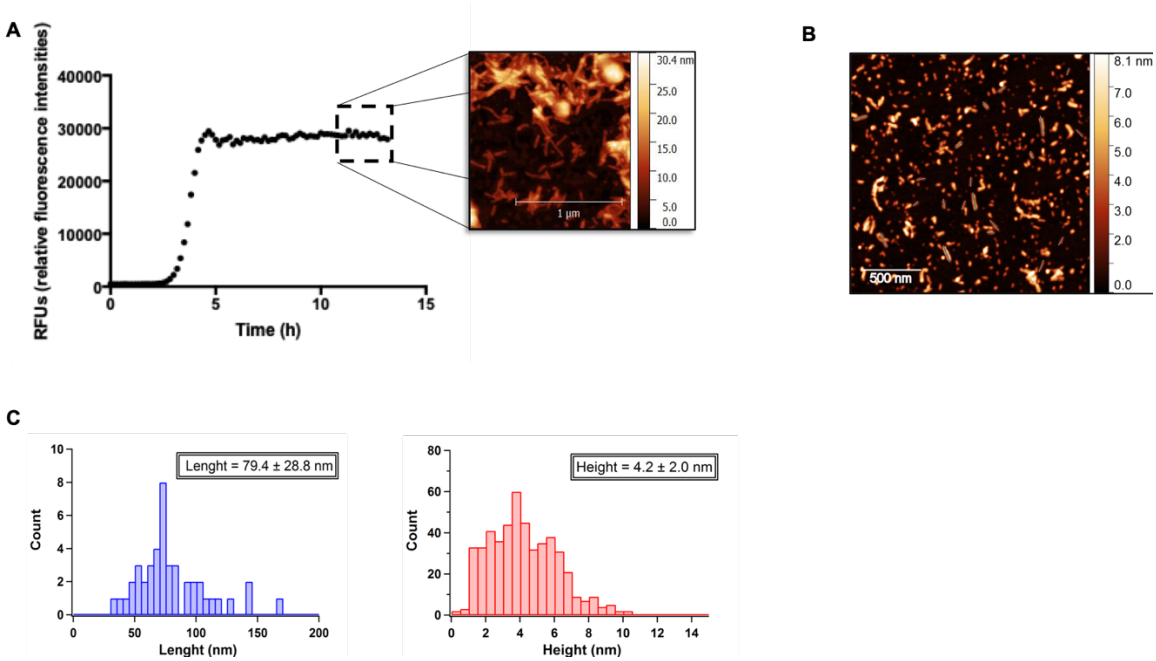

Figure 3.3. Production and characterization of human tau K18 fibrils. (A) Fibrillization curve of human tau K18 0.5 mg/mL, represented as average of three replicate wells. The dashed square indicates the timepoint at which the reaction was stopped and the aggregates collected and analysed by AFM before sonication. (B) AFM analysis of tau aggregates after 5 minutes of sonication and (C) length and height measurements of the fibrils.

Before moving to cell culture studies, we checked the cytotoxicity of the fibril preparation using the 3-(4,5-dimethylthiazol-2-yl)-2,5-diphenyltetrazolium bromide (MTT) assay. This rapid and effective test measures mitochondrial activity, that correlates with cell proliferation. The evaluation of any potential toxic effect of exogenously added material, tau fibrils in this case, is a crucial step in the individuation of the most suitable cell line for further experiments. Three different murine neuroblastoma cell lines (N2a) were exposed for 72 hours to four increasing concentrations of sonicated tau fibrils: 0.5 µM, 1 µM, 2 µM and 5 µM. We used wild-type N2a, that physiologically express the cellular form of the prion protein, and N2a *Prnp*$^{-/-}$ (referred to as N2a KO in this work), in which the expression of PrP^{C} has been ablated using the Crispr/Cas9 system (293S). Finally, we used also N2a cells persistently infected with the RML prion strain (ScN2a), which represent a useful tool to study prion replication. The assay did not reveal any significant reduction of cell viability after the exposure to the different concentrations of tau fibrils compared to control cells (Fig. 3.4), although N2aKO showed a slightly higher sensitivity to tau toxicity compared to their wild-type counterpart in all four cases. However, we cannot attribute the increased mortality rate of N2aKO solely to the toxicity of tau fibrils, as

PrP^C is known to have neuroprotective roles and its ablation might result in a lower cell viability, independently of any exogenous agent.

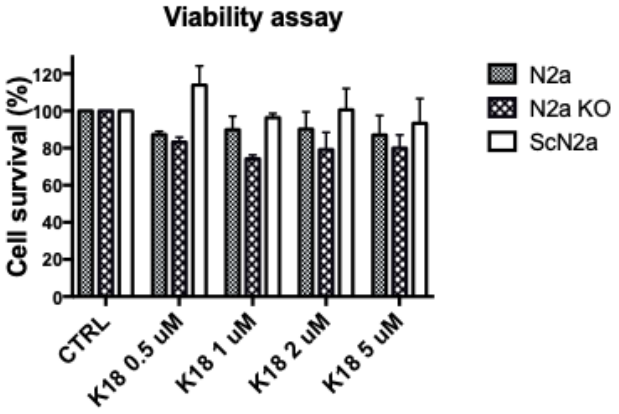

Figure 3.4. Toxicity of tau K18 aggregates in neuroblastoma cell lines. Three different neuroblastoma cell lines were treated with various concentrations of tau K18 fibrils for 72 hours. Results are represented as mean ± standard deviation of three independent experiments performed in six replicates.

3.2. Synthetic tau K18 aggregates induce tau pathology in mouse and rat models

In order to better characterise our synthetic tau aggregates, we performed a unilateral injection of K18 amyloids, both sonicated and non-sonicated, into the hippocampus of mice and rats overexpressing a truncated human 4R tau construct (Fig 3.5, A). This specific brain area was chosen because of its propensity to accumulate tau aggregates in tauopathies. Even though none of the animals showed any clinical sign of pathology after 3 months from injection, they were sacrificed and the brains were analysed immunohistochemically (IHC) with AT8 antibody. We were able to detect some tau pathology in all brain samples, with K18 sonicated fibrils being the most effective in inducing tau aggregation (Fig. 3.5, B-C). Compared to the effect of PHFs isolated from AD brain, synthetic fibrils induced a less robust tau pathology, and mice were more subjected to fibrils-induced aggregation than rats (Table 1). Importantly, all the aggregated tau detected is phosphorylated on Ser202 and Thr205. Tau pathology looked like tiny fibrils concentrated in the space close to the cell membrane but not filling the whole cytoplasm. Thus, our results confirm that K18 fibrils are able to initiate tau pathology *in vivo*. As synthetic fibrils might require more time to trigger aggregation, we did not sacrifice all the animals; specifically, some R4m7 mice injected with K18 fibrils are still alive and will be sacrificed after 6-8 months post-injection to evaluate the extent of the induced tau pathology.

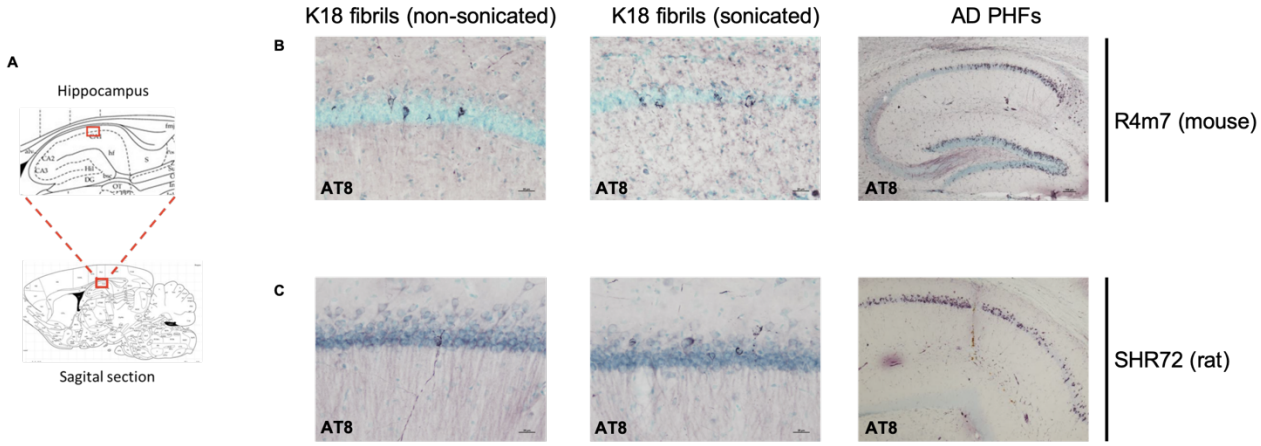

Figure 3.5. Immunohistochemical staining for tau pathology in the hippocampus of R4m7 mice and SHR72 rats. (A) K18 sonicated and non-sonicated fibrils were injected unilaterally in the hippocampus of transgenic mice (R4m7) an rats (SHR72) overexpressing a 4R truncated construct of tau. Tau pathology, consisting of small NFTs and neurophil threads, was detected in the hippocampus of mice (B) and rats (C) after 3 months post-injection. Tau aggregates were stained with AT8 antibody, which recognizes tau phosphorylated on Ser202 and Thr205. PHFs extracted from AD brains were used as positive controls.

Animal	Line	Fibrils	Number of NFTs
Mouse	R4m7	K18 non sonicated	198
Mouse	R4m7	K18 sonicated	245
Rat	SHR72	K18 non sonicated	9
Rat	SHR72	K 18 sonicated	35

Table 3.1. Quantification of NFTs in mice and rats treated with tau K18 fibrils. 12 slides/animal were used for quantification.

3.3. Tau K18 fibrils internalization in neuroblastoma cells is time- and concentration dependent

Tau fibrils have been reported to enter many types of cell lines without the need for any transduction reagent like lipofectamine[301], which is a *conditio sine qua non* when the aim is to characterise the role of a possible receptor protein. Therefore, we directly added tau K18 fibrils to the cell culture medium and studied their uptake at different timepoints.

To confirm the internalization of the exogenously added tau assemblies into cells, we took advantage of confocal microscopy and of an innovative approach first tested on synuclein aggregates by Karpowicz *et al.* [295]. According to this procedure, fibrils produced by *in vitro* aggregation of recombinant proteins are chemically conjugated to the succinimidyl ester of a fluorescent dye, in this case Alexa Fluor® 488, to yield a fluorescently-labelled product. Using this method, the aggregates are sonicated before the conjugation and are all equally labelled.

Non-internalized fibrils tend to deposit on the surface of the coverslip or to adhere to the membrane, making it difficult to discriminate if the aggregates have really entered the cells. To eliminate any contribution from those fibrils, live cells were incubated with a sterile solution of the vital dye Trypan Blue, which quenches green fluorescence through an energy-transfer mechanism [295]. Since Trypan Blue cannot penetrate live cells, only the aggregates outside the cells will be quenched, without affecting the internalized ones. We performed several trials in order to optimize both the concentration of Trypan Blue and the incubation time according to the sensitivity of our cell lines (data not shown).
Figure 3.6. shows the time- and concentration dependency of tau internalization in N2a cells.

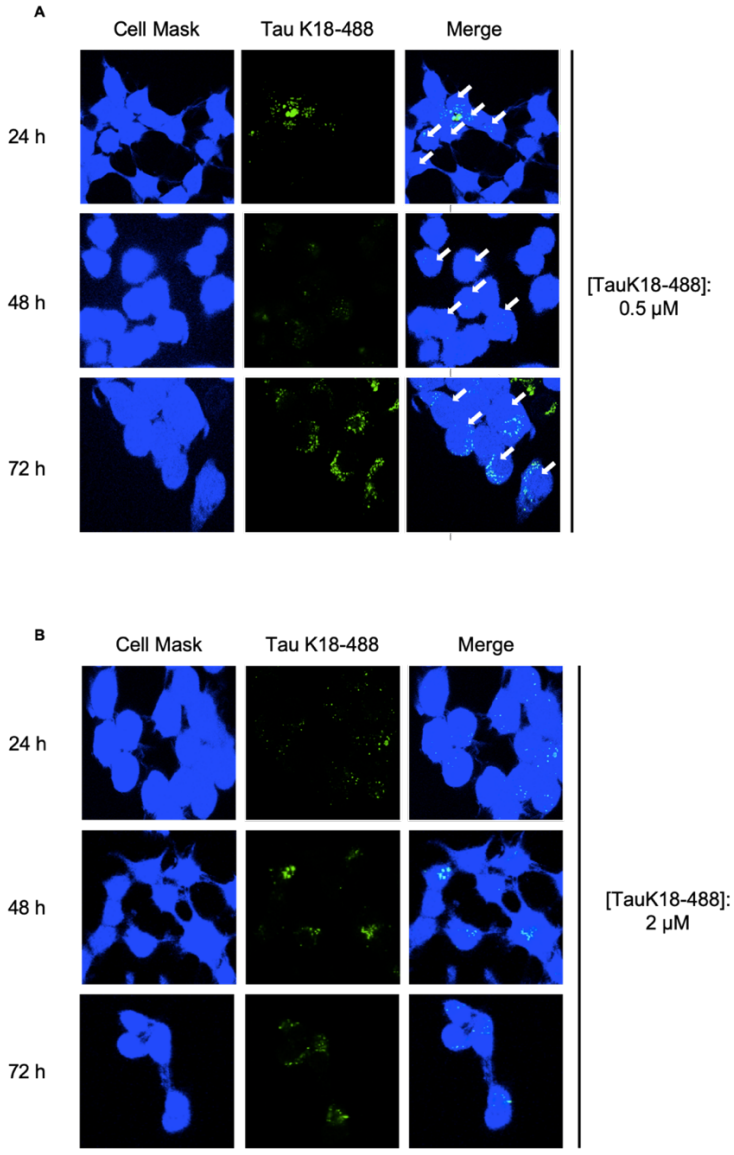

Figure 3.6. Immunofluorescence data of internalized tau K18-488 fibrils in N2a cells at different timepoints. N2a cells were incubated with (A) 0.5 µM or (B) 2 µM of tau K18-488 fibrils for 24, 48 and 72 hours. Images were acquired as series of Z-stacks and the analysis was carried out in 3D. Panels A and B show the XY projection of one of the central sections of the stack. White arrows in panel A indicate the cells positive for tau aggregates.

N2a cell line	*Positive cells (%)*	
	Tau K18 0.5 μM	Tau K18 2 μM
24 hours	~ 55 %	100%
48 hours	~ 80%	100%
72 hours	100%	100%

Table 3.2. Quantification of N2a cells positive for tau K18 aggregates, expressed as a percentage.

Tau fibrils are easily taken up by N2a cells after one day of incubation, and the internalization rate seems to be dependent on the concentration of the exogenous material. Indeed, after 3 days in contact with the fibrils all analysed cells had internalized the aggregates, whereas after 24 hours only cells incubated with the higher concentration of fibrils were 100% positive. When a lower concentration was used, the uptake increased over time both in terms of number of positive cells and of internalized fibrils.

Given these results, we decided to use 2 μM as the final concentration of tau K18 fibrils for all the experiments described in this work.

3.4. The cellular prion protein interacts with tau K18 fibrils and facilitates their internalization

Previous works reported that PrP^C can act as a receptor for ß-sheet enriched structures like amyloid-ß and synuclein, mediating their toxic effect through the activation of signalling cascades and, in the case of intracellular amyloids, also promoting their uptake by recipient cells. Since tau shares key features with the aforementioned amyloids, we hypothesized that PrP^C might be involved also in the internalization and spreading of tau fibrils.
Both for amyloid-ß and synuclein, the first step required for these events to take place is the binding of the extracellular aggregates to PrP^C[205, 274]. Concerning tau, full-length tau was described to bind to PrP^C through the interaction of the microtubule binding domains of tau and the amino acids 23-91 of the prion protein [302]; however, no studies have been conducted using fibrillar forms. In order to verify our hypothesis, we first checked if a direct interaction exists between PrP^C and tau K18 fibrils. We performed a pull-down assay, a variant of the classical co-immunoprecipitation in which one of the two proteins is used as a bait instead of the antibody. Figure 3.7 (panel A) sums up the key steps of this procedure. Before the incubation with cell lysate, tau fibrils were chemically conjugated to the succinimidyl ester of biotin, similarly to what has been previously described for fluorescent labelling. This step is necessary in order to pull them down using streptavidin beads.

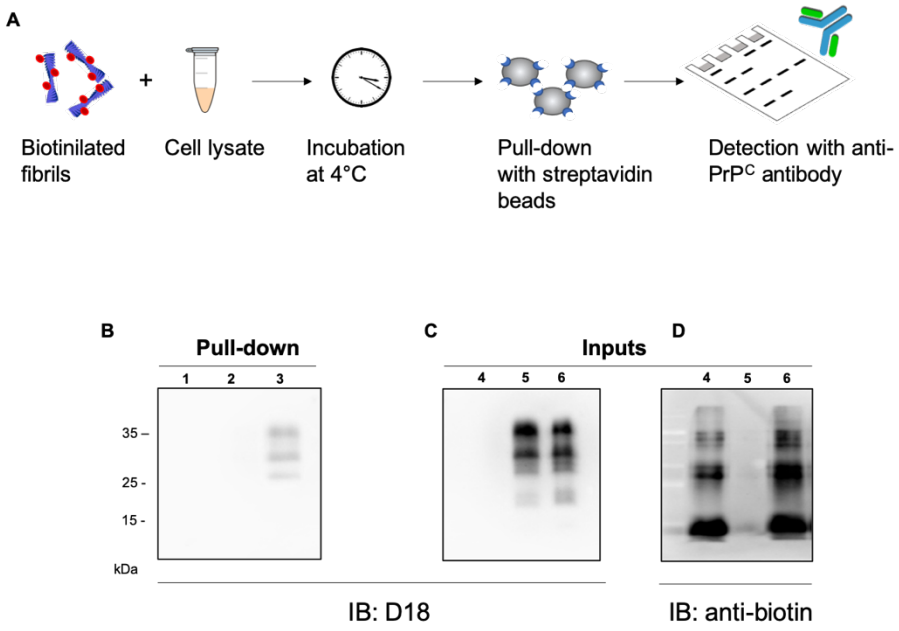

Figure 3.7. Direct interaction between tau K18 fibrils and the endogenous PrP^C from N2a cells visualized by pull-down assay. (A) Sonicated tau K18 fibrils were chemically conjugated to NHS-biotin and subsequently incubated with N2a cell lysate overnight at 4°C to eventually form a complex. The day after, tau K18 fibrils were pulled down using streptavidin beads, and the precipitated samples were run on SDS-PAGE and blotted for PrP^C detection. (B) Western Blot of pulled down samples. Lane 1: K18 fibrils only; lane 2: N2a lysate only; lane 3: K18 fibrils and cell lysate. The membrane was probed with human anti-PrP^C antibody D18. (C) Western Blot of input samples probed with anti-PrP^C D18 and (D) with anti-biotin to visualize tau K18 fibrils. Lane 4: K18 fibrils only; lane 5: N2a cell lysate only; lane 6: K18 fibrils and cell lysate.

When we probed the pulled-down samples for PrP^C by Western Blotting, we observed that the typical three-bands pattern was visible only when both binding partners were present. Although the signal coming from the pulled-down sample was fainter than its corresponding input, meaning that not all the PrP^C binds to the fibrils, it indeed confirmed our hypothesis of a direct interaction taking place between the two proteins. This result was somehow expected, as the binding site on tau had been mapped on the microtubule binding domain.

Afterwards, we moved on to evaluate if any differences in the internalization of the fibrils occurred between N2a and N2aKO. According to the results obtained in the experiments described in 3.2, both N2a and N2aKO were treated with 2 μM of tau K18-488 fibrils for 24 hours, and then processed for confocal microscopy analysis. Figure 3.8 shows two representative images for both cell types. Like in the previous experiments, we collected multiple sections along the z-axis to reconstruct the whole cellular volume, which can be visualized either in 2D, with orthogonal planes (panels A and C) or as compact 3D objects (panels B and C).

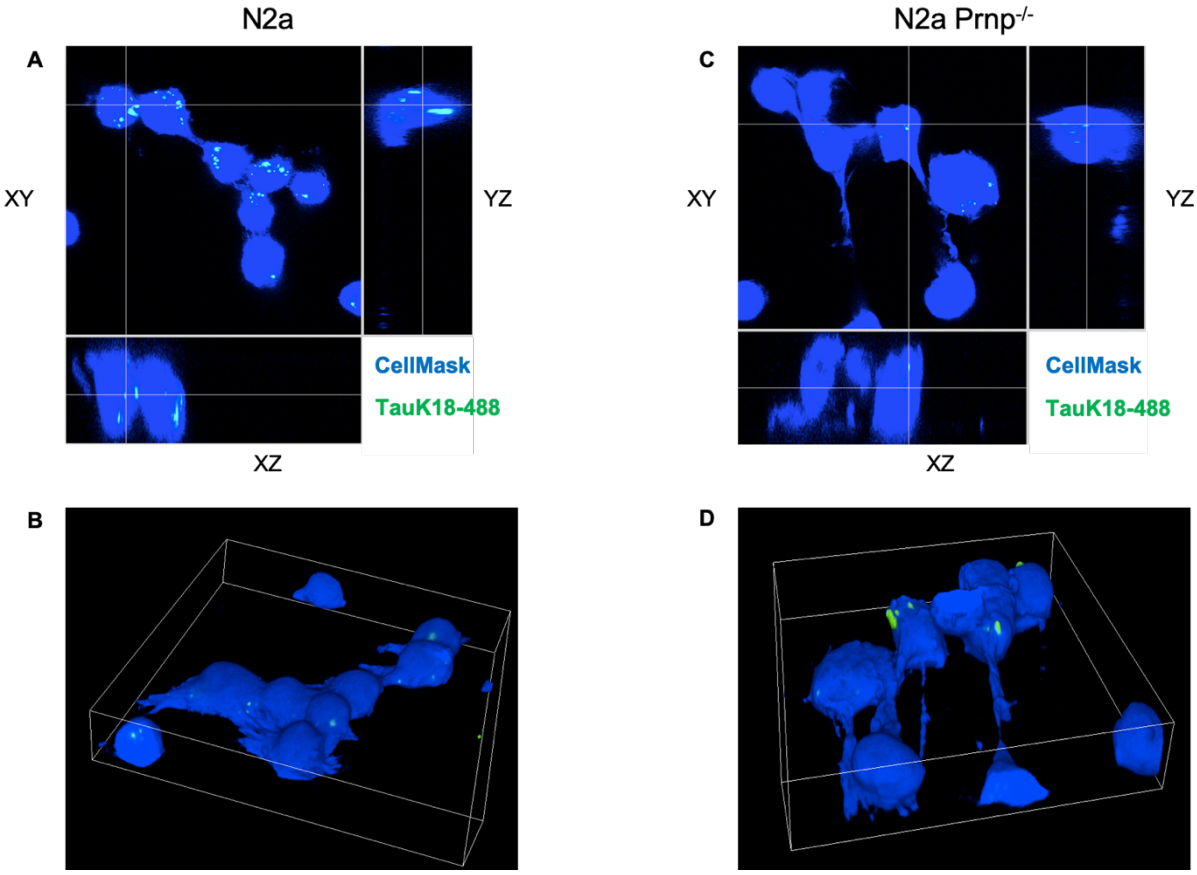

Figure 3.8. Representative images of immunofluorescence data collected to evaluate the uptake of tau K18 fibrils in neuroblastoma cells. (A) and (C) show one of the central sections of the whole Z-stack of N2a and N2aKO, respectively. All the three orthogonal planes (XY, XZ, YZ) are displayed. (B) and (D) show the 3D reconstruction of N2a and N2aKO cells, respectively. 3D volumes are reconstructed by the algorithm of NIS Elements software based on the sections that were collected. Fibrils are represented by green spots; those internalized appear less bright in the 3D representation, and sometimes are not visible due to the density of the cell bodies.

A good degree of internalization was observed for both N2a and N2aKO, with almost 100% of the cells showing green puncta inside their cell bodies. However, when we evaluated the number of internalized aggregates, we noticed that N2a cells expressing PrP^C take up around 60% more fibrils compared to N2aKO (Figure 3.9, panel A). We calculated an average uptake of 73 ± 40 fibrils for N2a cells and 46 ± 27 for N2aKO. We also correlated the number of internalized fibrils with the cell volume, mainly to see if bigger cells actually take up more amyloids (Figure 3.9, panels B and C). There is indeed a direct and moderate correlation between the two parameters, as indicated by the Pearson's coefficients calculated for both cell types. However, the average cell volume calculated is very similar, and the majority of both N2a and N2a KO stay between 500 and 1000 μm^3, ruling out the possibility that different phases of the cell cycle might be responsible for the different internalization.

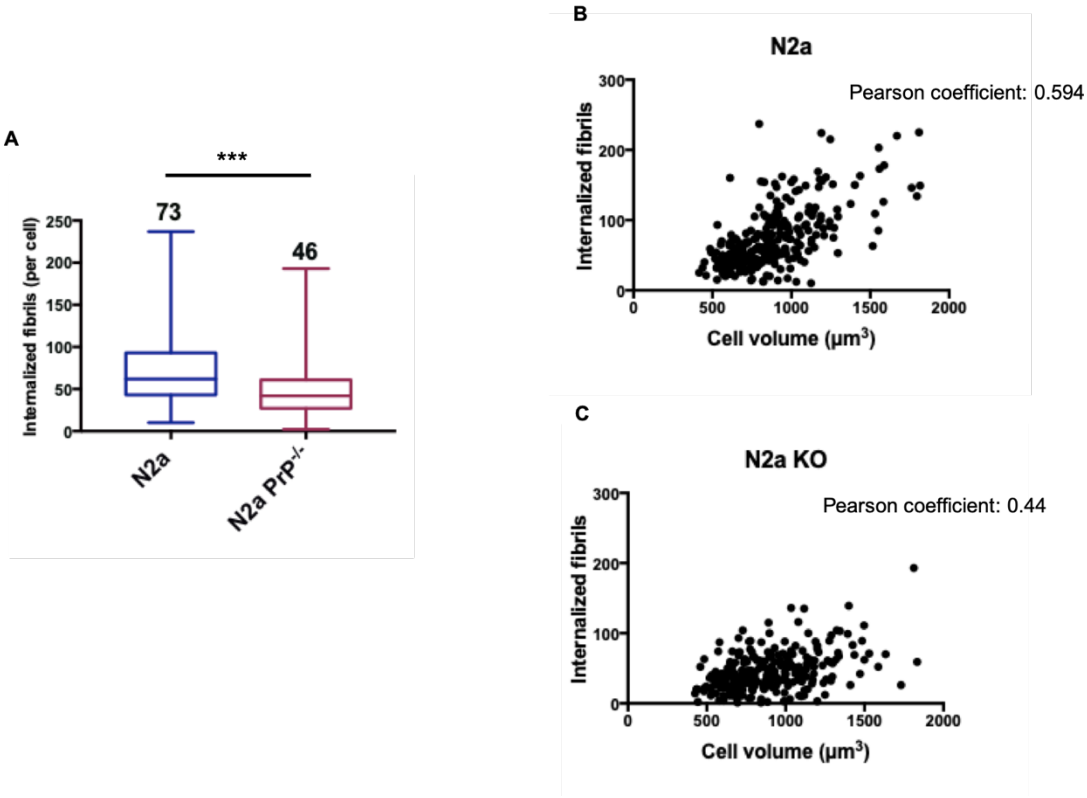

Figure 3.9. Uptake of tau K18 fibrils in neuroblastoma cells. (A) Box and whiskers plot showing the distribution of the number of internalized fibrils in N2a and N2aKO cells. Numbers on top of the whiskers indicate the average number of internalized aggregates. A total of four hundred cells were counted in blind in three independent experiments. Data were evaluated with unpaired T-test with Welch's correction. Statistical analysis is indicated as: * = p <0.05, ** = p< 0.01, *** = p<0.001. (B) and (C) Correlation between cell volume and the number of internalized fibrils per cell in N2a and N2a KO. For both cell types a direct correlation exists, and can be defined as "moderate correlation" according to Pearson's coefficient.

These data clearly indicate that the presence of PrP^C on the cell membrane, although not mandatory for the entrance of tau K18 fibrils, greatly promotes the uptake process. The precise mechanism underpinning this phenomenon is not yet fully understood, but it probably involves a step of energy-dependent endocytosis. To confirm this idea, we compared the internalization rate of tau K18 fibrils in both cell types at two different temperatures: at 37°C, the physiological temperature at which cellular processes occur, and at 4°C, when all energy-dependent processes are inhibited, including endocytosis. While the concentration of the fibrils was the same as before (2 µM), the incubation time was reduced to 6 hours in order to perform the experiment at 4°C without any substantial cell damage (Fig. 3.10).

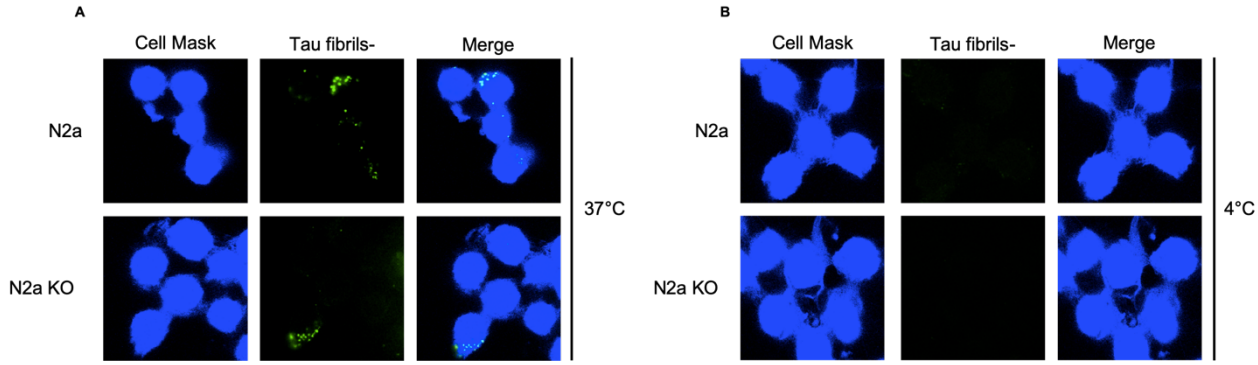

Figure 3.10. Tau K18 internalization is energy-dependent. 2D representative images of immunofluorescence data on tau internalization by N2a and N2aKO at 37°C (A) and 4°C (B). The analysis was carried out in 3D on series of multiple z-sections. The images presented in these panels show only the XY orthogonal projection of one of the central sections of the stack.

Temperature of incubation	**Percentage of cells positive for tau K18 aggregates**	
	N2a	N2a KO
37°C	80%	43%
4°C	Less than 1%	Less than 1%

Table 3.3. Quantification of N2a cells positive for tau K18 aggregates at 37°C and at 4 °C, expressed as a percentage.

The data confirm the aforementioned time-dependency of tau uptake; indeed, after 6 hours of treatment only 80% of N2a cells showed fibrils in their cell bodies, while in the previous experiments where the incubation time had been prolonged to 24 hours, 100% of cells were positive for aggregates. Significantly fewer N2aKO cells had internalized tau fibrils (43%), suggesting that the PrP^C-mediated mechanism plays a role in the early phases of the uptake process. When the incubation temperature was lowered to 4°C, we observed an almost complete inhibition of the uptake in both cell types regardless of their genetic background. Indeed, at this temperature the number of positive cells was comparable between N2a and N2aKO, meaning that whatever internalization pathway is mediated by PrP^C, it is not active when energy-dependent mechanisms are blocked.

We conclude that the cellular prion protein might act as a receptor for tau aggregates and facilitates their entrance into cultured cells through a direct binding and a subsequent endocytosis-mediated pathway.

3.5. Tau K18 fibrils induce an increase of the endogenous prion protein

The discovery of the important role of PrP^C in the internalization of tau amyloids opens the question if this mechanism can be in some way over-activated by the fibrils

themselves, in order to sustain their spreading. To test this, we analysed the effect of the treatment with tau K18 fibrils on the endogenous levels of PrP^C at different timepoints.

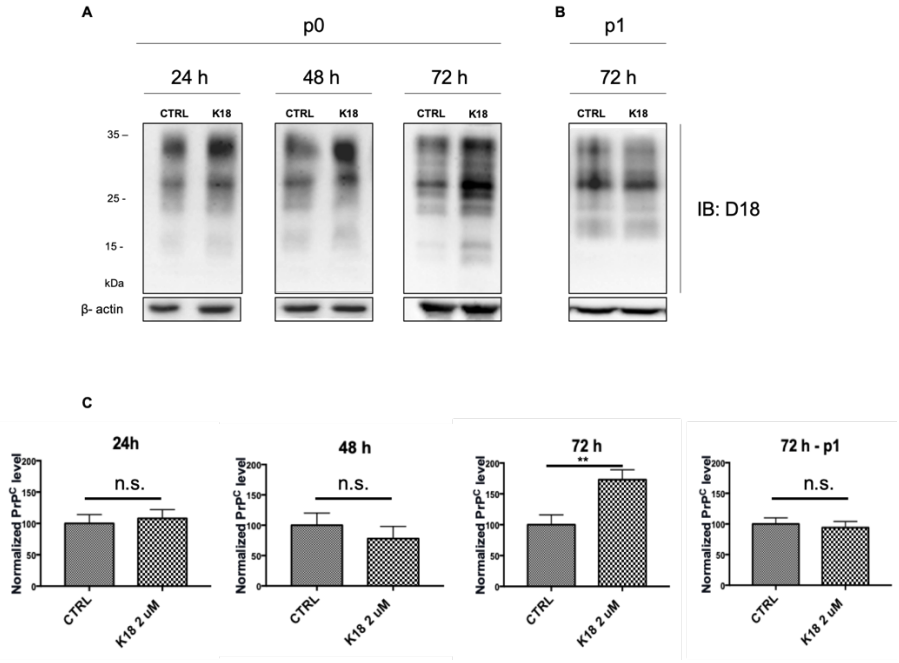

Fig. 3.11. Effect of tau K18 fibrils on PrP^C level in N2a cells at different timepoints. (A) Western blot analysis of N2a cells treated with 2 μM of tau K18 fibrils for 24, 48 and 72 hours and (B) of the first passage of N2a treated for 72 hours. Membranes were probed with human anti-PrP antibody D18. Each lane was loaded with 50 μg of total proteins. (C) The quantification of three independent experiments is shown in the graphs. Data are represented as the percentage of total PrP relative to ß-actin, which is an internal loading control. PrP^C levels of control cells have been normalized to 100. The histograms represent the mean ± SD. Data were evaluated by unpaired T-test. Statistical analysis is indicated as: n.s.= not significant; *= $p<0.05$; **= $p<0.01$; ***= $p<0.001$.

After 72 hours of incubation with tau fibrils, we reported an increase of around 60% of the PrP^C level in N2a cells (Figure 3.11, panels A and C). This effect seems to be dependent on the presence of the aggregates in the culture medium, because as soon as treated cells are passaged and kept in fibrils-free medium, PrP^C level is again equal to that of control cells (Figure 3.11, panel B).
We hypothesize that tau fibrils might act either at the RNA level, by increasing the transcription of the *Prnp* gene, or at the protein level, e.g. impairing the degradation of PrP^C. Therefore, we isolated total RNA from control and treated N2a cells and performed a RT-PCR analysis (Figure 3.12). The results showed that there is no upregulation of *Prnp* transcription following 72 hours of incubation with tau K18 fibrils, thus indicating that the effect must be at a post-transcriptional level.

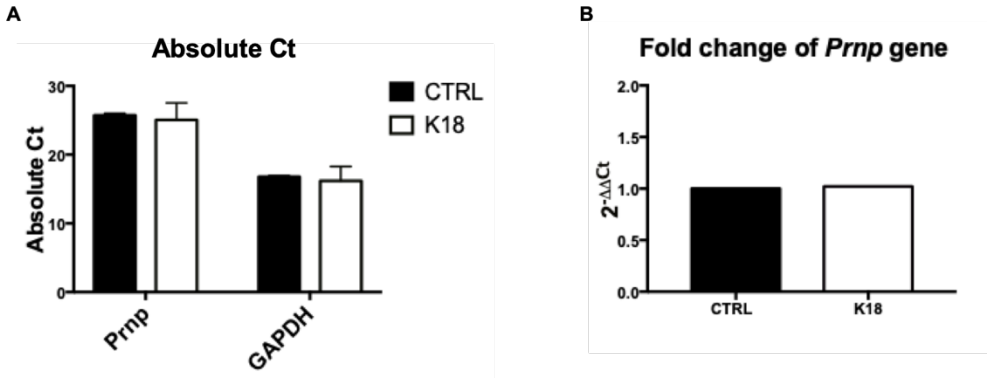

Figure 3.12. RT-PCR analysis of *Prnp* expression levels on control and treated N2a cells. (A) Average values with SD of absolute CT_s among the samples for *Prnp* and GAPDH genes. Every sample was analysed in duplicate. (B) Relative expression levels of *Prnp* gene normalized against GAPDH in control and K18-treated cells. The relative expression in control cells has been normalized to 1.

After having established that the increase in PrP^C level is a consequence of the addition of exogenous tau fibrils, we wondered if this phenomenon might be in some way related to the role of the prion protein in the internalization of the amyloids. Specifically, tau fibrils could exploit the higher amount of PrP^C exposed on the cell surface to increase their internalization rate. To verify this, we used immunofluorescence to evaluate if more PrP^C was transported to the cell membrane as a consequence of the treatment with tau aggregates (Figure 3.13). As a positive control to assess the validity of the experimental method, we used chlorpromazine, a drug that has been shown to reduce the levels of PrP^C on the cell membrane (data not shown) [298].

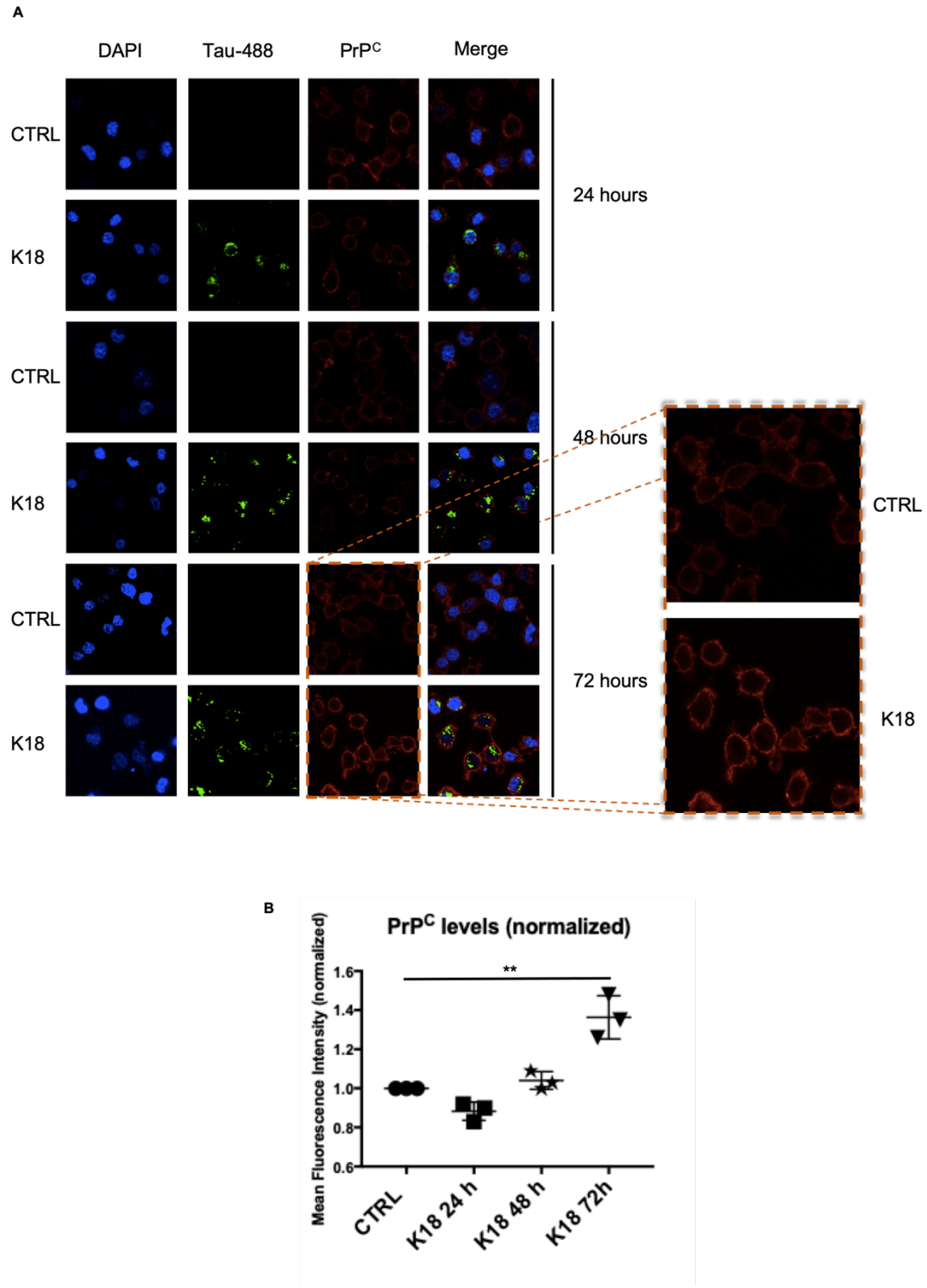

Figure 3.13. A 72 hours exposure to tau K18 fibrils increases the levels of PrP^C on the cell membrane of N2a cells. (A) Representative immunofluorescence images of untreated and treated N2a at three different timepoints. Membrane staining for PrP^C was performed at 4°C on alive cells using the W226 antibody. The magnified sections show a visible difference in the fluorescence intensity associated to PrP^C between control cells and cells treated for 72 hours. (B) Scatter plot of the intensity of the PrP-associated membrane staining of treated N2a compared to control cells. The intensity values, which correlates with the levels of PrP on the membrane, is reported as the ratio between the average intensities of treated and control cells for each timepoint. Controls have been normalized to 1.

The three values represent three independent experiments, in which 700 cells for each condition were analysed. Data have been evaluated with unpaired T-test. Statistical analysis is indicated as: n.s.= not significant; *= p<0.05; **= p<0.01; ***= p<0.001.

As already observed in the immunoblot analysis, PrP^C levels increase after 72 hours of incubation with tau aggregates. The quantification of membrane staining confirms that at least a part of the protein in excess is localized on the cell membrane (Figure 3.13, panel B); however, it is not clear if this is due to an impaired recycling, with the consequent retainment on the membrane, or to the transportation of newly synthesized protein to the surface. Be it as it may, a higher amount of PrP^C exposed outside the cells might result in more extracellular tau fibrils gaining cell entrance. Figure 3.14 shows a comparison of the number of fibrils internalized by both N2a and N2aKO after 24 and 72 hours of treatment.

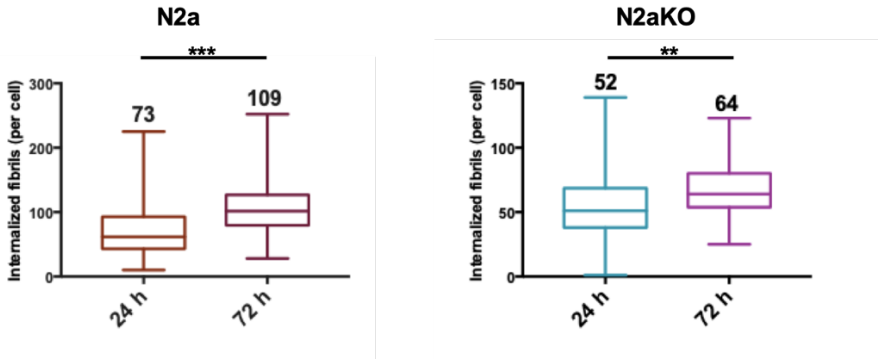

Figure 3.14. Quantification of internalized fibrils after 24 hours and 72 hours of treatment. Numbers on top of the whiskers represent the average number of internalized fibrils. Data were evaluated with unpaired T-test with Welch's correction. Statistical analysis is indicated as: * = p <0.05, ** = p< 0.01, *** = p<0.001.

We observed that the internalization rate in N2a cells increases of around 50% when tau fibrils are left in the culture medium for three days. To rule out the possibility that this difference is due to other uptake mechanisms acting independently of PrP^C, we conducted the same analysis on N2aKO cells. In this case the increase in the uptake was very modest, around 15%. Hence, the stronger effect observed in N2a must be connected with the presence of the prion protein on the membrane, suggesting that our hypothesis of tau fibrils taking advantage of the excess PrP^C to enter the cells might actually prove true.

3.6. Targeting PrP^C reduces the internalization and the spreading of amyloids

All the results reported so far point towards the involvement of PrP^C in a novel receptor-mediated internalization pathway of tau fibrils. Therefore, we investigated if the targeting of specific domains of PrP^C with antibodies might impair this mechanism and reduce the spreading of the pathology. Immunotherapy against the prion protein already proved successful in reducing the tau-mediated inhibition of long-term potentiation in mice inoculated with soluble tau aggregates [303]. To shed light on the molecular mechanisms underlying the phenotypic effects observed *in vivo*, we

quantified the internalized aggregates in N2a cells that had been subjected to pre-treatment with anti-PrP^C antibodies. Three different antibodies were tested: POM12, that targets the octarepeat regions in the N-terminus of PrP^C; POM3, which is directed against the hydrophobic domain and specifically to the non-octarepeat region; and POM4, which recognizes a discontinuous and conformational epitope composed of a very C-terminal part of the protein and a portion spanning amino acids 121-134 (Figure 3.15).

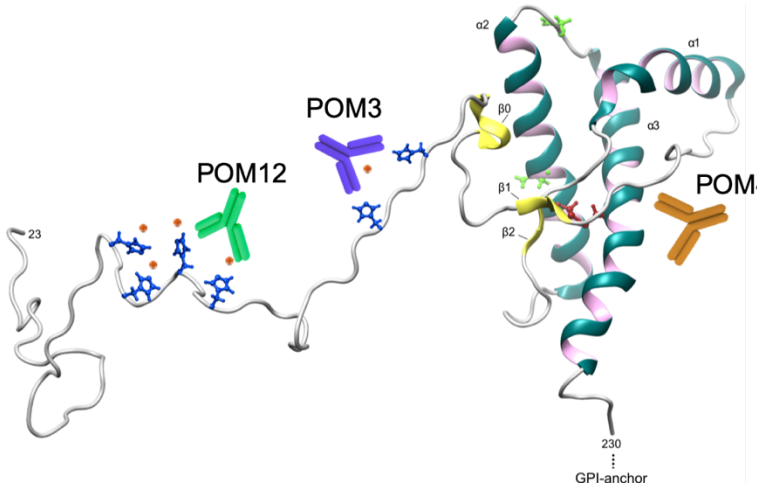

Figure 3.15. Three antibodies of the POMs series target distinct domains on PrP^C. The structure of the prion protein has been modified from [206].

The experiments on tau fibrils internalization and the subsequent quantification were conducted as described in sections 3.2 and 3.3. Before the addition of the fibrils, N2a cells were incubated with each one of the three antibodies for 1 hour, so that the antibody could bind to PrP^C. We checked the binding of the antibody by immunofluorescence prior to perform the actual experiment (data not shown). We chose to use an antibody concentration of 15 µg/mL (80 nM), as it proved to be sufficient to target the majority of PrP^C in N2a cells and inhibit PrP^{Sc} replication [304].

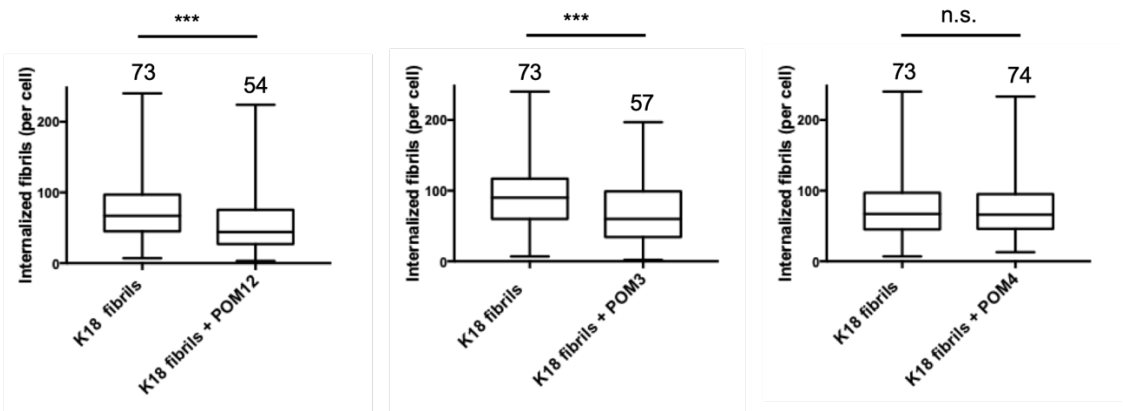

Figure 3.16. Targeting PrP^C reduces the uptake of tau K18 fibrils. Box and whiskers plots representing the distribution of internalized fibrils in N2a cells treated only with tau K18 fibrils and in N2a that were pre-treated with different anti-PrP^C antibodies. Numbers on top of the whiskers indicate

the average number of internalized fibrils. Data were evaluated with unpaired T-test. Statistical analysis is indicated as: n.s.= not significant *= p<0.05; **= p<0.01; ***= p<0.001.

The targeting of different domains on PrP^C produced distinct and specific effects on the internalization rate of tau K18 fibrils (Fig. 3.16). Indeed, POM12 binds to a region that is known to be involved in the interaction with ß sheets-enriched amyloids. By impairing the docking of tau fibrils to PrP^C, POM12 blocks this receptor-mediated endocytic pathway and reduces the uptake of the aggregates. A similar effect is observed upon treatment with POM3, whose epitope (the non octarepeat region spanning amino acids 95-100) was not considered to play a role in tau – PrP^C binding according to previous studies [302]. Yet, it is possible that the hydrophobic domain might actually participate in the binding of fibrillar species of tau but not of the monomers; as its name says, this region of PrP^C is highly hydrophobic and could interact with the ß sheets of the amyloids through non-specific hydrophobic effects. Another hypothesis sees POM3 acting as a steric hindrance that physically renders the binding site on the N-terminus inaccessible to tau fibrils. In both cases, a proper combination of the two antibodies in a single administration might end up in a further lowering of the internalization.
On the other hand, POM4 did not produce any significant effect on tau uptake. However, as the C-terminal domain of PrP^C is structurally very complex, we cannot exclude the hypothesis of its involvement in the internalization pathway, which might occur through a different epitope than the one targeted by POM4. Further experiments with antibodies targeting other regions on the globular domain could identify more sites that take part to this process.

3.7. Exogenous tau K18 fibrils decrease PrP^{Sc} levels in prion infected ScN2a cells

ScN2a are cells persistently infected with prions. In this work, we used two types of ScN2a, propagating either the RML or the 22L prion strains. Both strains have undergone adaptation in murine cells, but are considered to be unrelated, as RML derives from drowsy goat scrapie and 22L from sheep scrapie [305].
First, we focused on ScN2a RML cell lines and we evaluated the effect of tau K18 fibrils on the endogenous levels of PrP^{Sc}. Our group already reported that both non-sonicated and sonicated synuclein fibrils reduce the amount of prions in scrapie-infected cell lines[205]. We therefore wondered if this mechanism can be generalized to other ß sheet-enriched amyloids, independently of the protein identity.
Figure 3.17 (panel A) shows the PrP^{Sc} levels after incubation of ScN2a RML with 2 µM of tau K18 fibrils at three different timepoints (24, 48 and 72 hours). PrP^{Sc} levels were analysed by immunoblotting before and after proteolysis with proteinase K (20 µg/mL, 37°C for 1 hour)

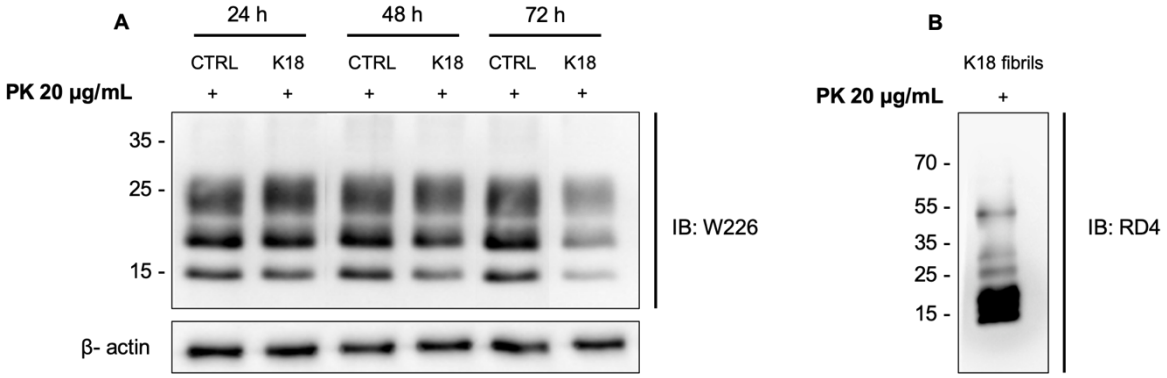

Figure 3.17. Western blot analysis of PrP^{Sc} in ScN2a RML cell lysates after treatment with tau K18 fibrils. (A) Following the treatment with tau K18 aggregates, total PrP and PK-resistant PrP^{Sc} proteins were separated by SDS-PAGE and detected with anti-PrP Ab (W226). β-actin is a loading control. "K18" indicate the treatment with 2 µM of tau fibrils. (B) Tau fibrils present in the cell lysate of ScN2a RML treated for 72 hours were subjected to proteinase K digestion and detected with anti-4 repeat tau antibody RD4.

The results clearly indicate that tau K18 fibrils have the ability to promote the clearance of prion aggregates inside cells, supporting the hypothesis of a mechanism mediated more by the abundance of specific conformational structures rather than by sequence requirements. PrP^{Sc} elimination however seems to be a quite slow process, as the decrease in the signal of proteinase K-resistant material started to be observed only after 72 hours of incubation with the exogenous aggregates. This is consistent with what reported in the previously mentioned work [205], where the exposure of ScN2a RML cells to synuclein aggregates lasts for 96 hours. The addition of fibrils greatly reduced the scrapie load, while in control cells a characteristic pattern of N-terminally truncated fragments of di-, mono- and unglycosylated PrP was observed, with a prevalence of the monoglycosylated band.

Moreover, we found PK-resistant forms of tau K18 fibrils in cell lysates of ScN2a treated for 72 hours (Figure 3.17, panel B). Such observation implies that tau fibrils are not easily degraded by the host cells, and therefore they are free to act on the molecular pathways involved in maintaining the endogenous levels of PrP^{Sc}.

Next, we investigated if the clearance of prions enhanced by tau K18 is dependent on the presence of the aggregates in the culture medium. According to the previous experiment, we chose to use 72 hours as incubation time (Figure 3.18). This time we tested also the effect of monomeric tau on scrapie levels. While fibrils were able to efficiently clear prions, although not completely, monomeric-treated samples showed a pattern of PK-resistant bands very similar to that of control cells both in intensity and number of bands. This further corroborates our hypothesis of the predominant role of ß sheet amyloids in the prion clearance.

The reduction of PrP^{Sc} seems to be affected, at least in part, by the presence of tau K18 fibrils in the culture medium. Indeed, although tau K18 species were removed from the cell culture medium after passage p0, scrapie levels remained low after 2 passages (Figure 3.18 panel A). Control cells and cells treated with tau K18 fibrils

were kept in culture for additional passages to monitor the clearance, but after passage 3 the scrapie levels of treated cells rose again to the initial level (Figure 3.18, panel B).

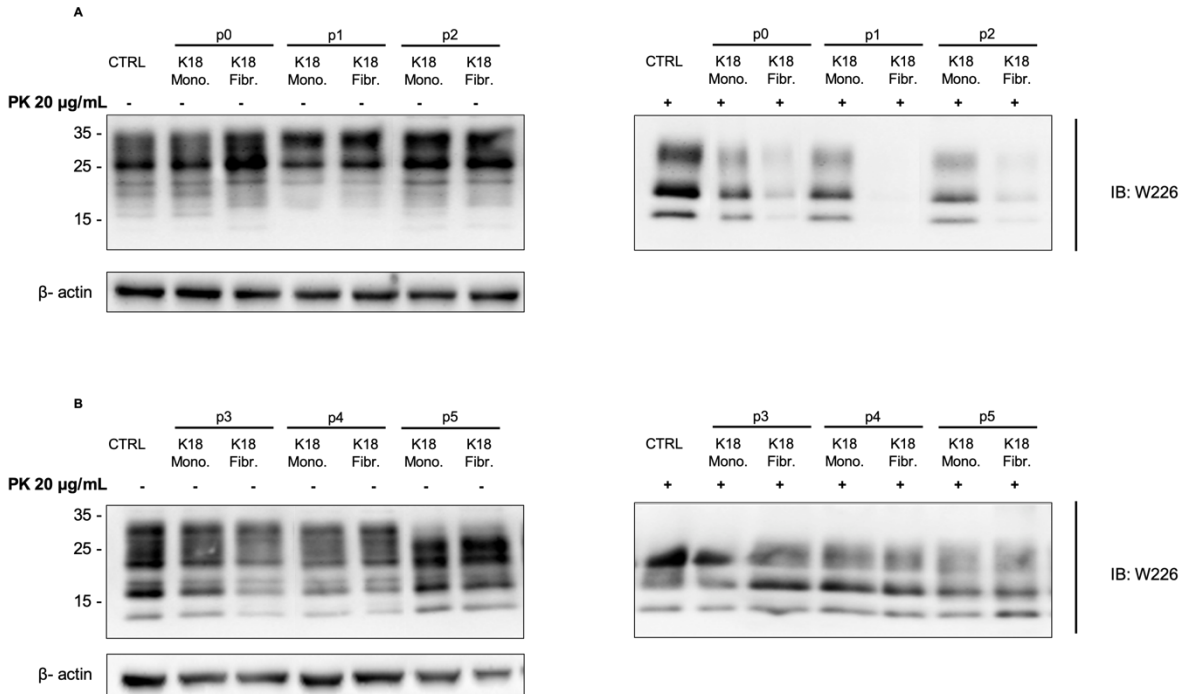

Figure 3.18. Western blot analysis of PrP^{Sc} in ScN2a RML cell lysates after treatment with tau K18 fibrils. Following the treatment with tau K18 aggregates, total PrP and PK-resistant PrP^{Sc} proteins were separated by SDS-PAGE and detected with anti-PrP Ab (W226). β-actin is a loading control. "K18 mono" and "K18 fibr" indicate the treatment with 2 µM of monomeric tau and tau fibrils respectively. (A) Total PrP and PrP^{Sc} of ScN2a from passage 0 to passage 2. (B) Total PrP and PrP^{Sc} of ScN2a from passage 3 to passage 5.

In order to try to achieve a complete clearance of PrP^{Sc}, we prolonged the incubation with tau K18 fibrils at passage 0 up to 6 days; however, a faint but detectable signal remained along all passages, suggesting that an acute treatment is not sufficient to eliminate prions from the cells (Figure 3.19). A chronic administration would probably guarantee a complete clearance of the scrapie in a few passages.

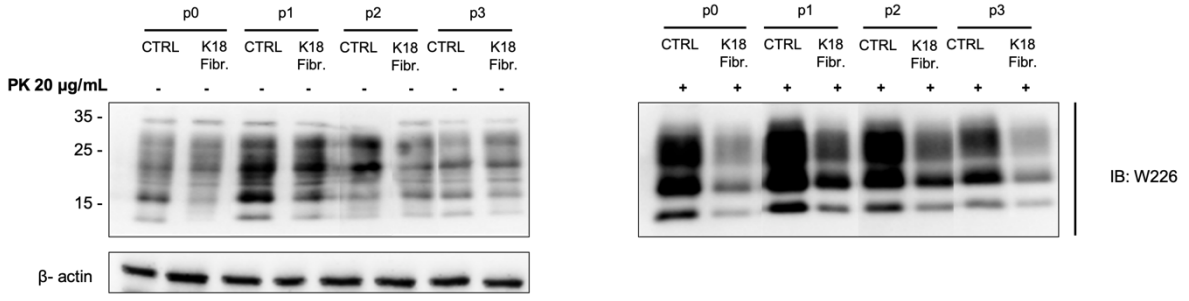

Figure 3.19. Western blot analysis of PrPSc in ScN2a RML cell lysates after treatment with tau K18 fibrils. Following the treatment with tau K18 aggregates for 6 days, total PrP and PK-resistant

PrP^{Sc} proteins were separated by SDS-PAGE and detected with anti-PrP Ab (W226). β-actin is a loading control.

In physiological conditions, PrP^{C} is subjected to proteolytic processing that produces biologically active fragments. The processing of the prion protein is thought to influence not only the course of prion disorders, but also other neurodegenerative diseases (463S). The so-called α-cleavage cuts the mature form of PrP^{C} at residues K110/H111 or H111/M112 (human sequence) upstream of the hydrophobic sequence [306] and generates two fragments: the N-terminal soluble fragment N1, of approximately 11 kDa, and a C-terminal, membrane-attached fragment of around 18 kDa, named C1. The α-cleavage strongly impairs the formation of prions by disrupting the PrP 109-122 region, which is critical for the conformational changes involved in both prion replication and toxicity [307]. The promotion of this specific processing might be a possible mechanism by which the treatment with tau K18 fibrils leads to the decrease of PrP^{Sc}. When ScN2a incubated with tau fibrils for 72 hours were subjected to enzymatic deglycosylation with PNGase F (Figure 3.20), we noticed that the 19 kDa band representing the PK-resistant core is less intense in tau-treated sample compared to the control. The fact that the band does not disappear completely is in agreement with the only partial PrP^{Sc} clearance observed in figure 3.17 (panel A, lane "K18 fibrils", p0). In parallel to decrease of the PK-resistant band, in the K18 treated sample there is the formation of a new band running at around 15 kDa that corresponds to the C1 fragment. We could confirm that this band is indeed the C1 fragment by probing the membranes with two different antibodies that recognize either the C-terminal part of PrP (W226) or the N-terminus (SAF34). As observed in figure 3.20 (panel B), the fragment could not be detected when probing with SAF34 antibody.

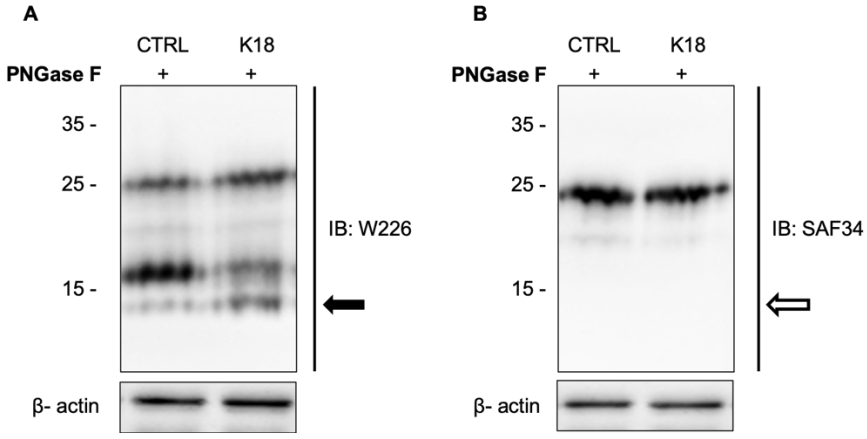

Figure 3.20. Electrophoretic pattern of PNGase F digested PrP in ScN2a control cells and cells treated with tau K18 fibrils. After PNGase F deglycosylation cell lysates were separated by SDS-PAGE and PrP was immunoblotted with two Abs that recognize (A) C-terminal (W226), and (B) N-terminal of the prion protein (SAF34). Solid black arrow shows the presence of C1 fragment recognized with C-terminal Ab, while the broken black arrow indicates the absence of the bands when the membrane was probed with N-terminal Ab. β-actin is a loading control.

Afterwards, we tested the strain specificity of tau K18-induced clearance of PrP^{Sc} by repeating the treatment on ScN2a infected with the 22L prion strain (Figure 3.21). Also, in this case we reported a strong reduction in the scrapie load after the administration of the fibrils, indicating that the mechanism activated by tau K18 is not affected by the different strain conformation.

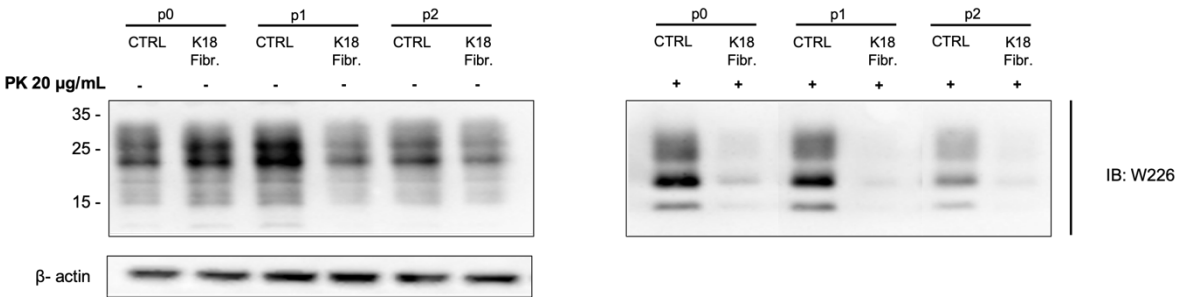

Figure 3.21. Western blot analysis of PrP^{Sc} in ScN2a 22L cell lysates after treatment with tau K18 fibrils. Following the treatment with tau K18 aggregates for 3 days, total PrP and PK-resistant PrP^{Sc} proteins were separated by SDS-PAGE and detected with anti-PrP Ab (W226). β-actin is a loading control.

3.8. Activation of the degradation pathways is not involved in tau-mediated PrP^{Sc} clearance

Our results so far show that the exposition of ScN2a cells propagating distinct prion strains to tau K18 sonicated fibrils results in the almost complete elimination of prions after a single administration; still, the molecular pathways activated by the amyloids to promote the clearance have not been identified.
In general, exogenously added material can clear prions by two main mechanisms, and more often through their combination. Compounds or aggregated proteins can trigger the overactivation of degradation pathways (i.e. autophagolysosomal pathway) that are normally involved in the turnover of prions, or affect the activity of other factors that take part to prion formation. Alternatively, compound and/or aggregated proteins could bind either to PrP^{Sc} and destabilize it, or to PrP^{C} and stabilize its native conformation, therefore inhibiting prion conversion. The observation that the potential differences in conformations characterizing the RML and 22L prion strains do not affect the clearance suggests that K18 fibrils might bind preferentially to the native PrP^{C}.

Nevertheless, we decide to evaluate if the cellular degradative mechanisms play a role in the elimination of PrP^{Sc}. Among these pathways, macroautophagy is known to be involved in the degradation of protein aggregates. ScN2a both untreated and treated with K18 fibrils for 72 hours were incubated with the macroautophagy inhibitor 3-methyladenine (3-MA) for 16 hours and PrP^{Sc} levels were analysed by Western Blot (Figure 3.22).

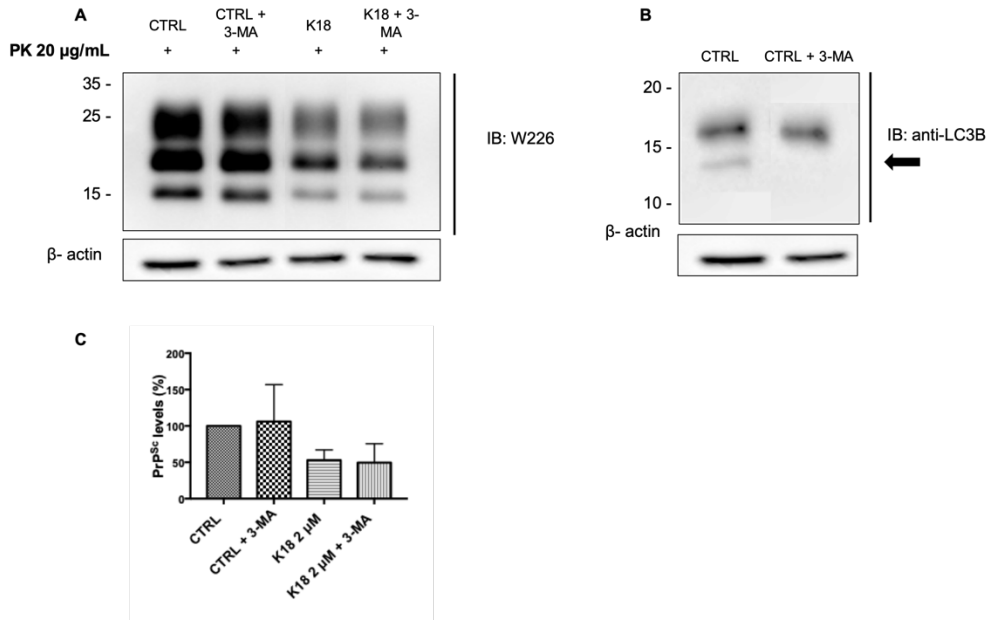

Figure 3.22 Western blot analysis of PrP^{Sc} in ScN2a RML cell lysates after treatment with tau K18 fibrils and macroautophagy inhibitor 3-methyladenine. A) Western Blot analysis of ScN2a RML lysates treated with 10 mM 3-MA, 2 µM K18 fibrils or both. PK-resistant PrP^{Sc} proteins were separated by SDS-PAGE and detected with anti-PrP Ab (W226). β-actin is a loading control. (B)Western Blot analysis of LC3 levels in ScN2a untreated and treated with 10 mM of 3-MA. The black arrow point at the lower band representing the lipidated form of LC3, which is present in control cells and absent in 3-MA treated cells. (C) Quantification of two independent experiments. Data are shown as mean ± SDs.

If autophagy was involved in the clearance of PrP^{Sc}, we would expect to have an increase in PrP^{Sc} levels after the incubation of ScN2a with 3-MA (Figure 3.22, panel A, first and second lanes); however, no difference could be detected after 16 hours of macroautophagy inhibition. As a control to verify the actual blockage of the autophagy, we analysed the conversion of LC3-I into LC3-II, which is recruited on the autophagosomal membrane and is considered to be an autophagic marker[308]. The treatment with 3-MA completely inhibited the conversion of LC3-I into LC3-II, therefore confirming the block of autophagy (Figure 3.22, panel C).
We tested also the effect of 3-MA on K18-treated samples, since the autophagic pathway could be activated to specifically eliminate the exogenous fibrils and result in the simultaneous, unpredicted clearance of prions as a side effect. If this were true, the prion load would be higher after the inhibition of macroautophagy. After PK digestion, we observed that the PrP^{Sc} levels in the samples treated with only K18 and with both K18 and 3-MA were almost the same (Figure 3.22, panel A, third and fourth lanes). We then concluded that the macroautophagic pathway inhibited by 3-MA is not involved in the tau-induced PrP^{Sc} clearance.

Next, we wondered if lysosomes could be responsible for the observed decrease of prions, and so we evaluated this hypothesis by inhibiting the lysosomal function with NH_4Cl. Ammonium chloride is a highly soluble salt that has been reported to inhibit lysosomal activity by increasing the pH, blocking the autophagosome-lysosome

fusion and interfering with the activity of the proteases (253-254Ludo). We compared the PrP^{Sc} levels in control and K18-treated ScN2a both in presence and in absence of 10 mM NH_4Cl (Figure 3.23).

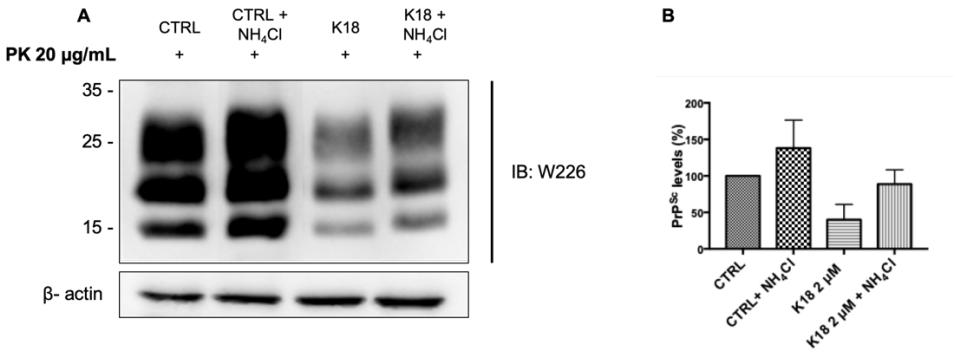

Figure 3.23. PrP^{Sc} clearance mediated by tau fibrils is only partially affected by the inhibition of lysosomal degradation. (A) Western Blot analysis of ScN2a RML lysates treated for 72 hours with 10 mM NH_4Cl, 2 µM K18 fibrils or both. PK-resistant PrP^{Sc} proteins were separated by SDS-PAGE and detected with anti-PrP Ab (W226). β-actin is a loading control. (B) Quantification of three independent experiments. Data are shown as mean ± SDs.

The partial inhibition of lysosomal activity was confirmed by the increase of the prion load in ScN2a treated with NH_4Cl compared to control ScN2a. However, the addition of the inhibitor to the cells treated with tau led only to a modest recover of the initial scrapie levels, which on the contrary should return to the initial state if lysosomes were involved. Although the three experiments performed show a similar trend, the differences between samples treated with NH_4Cl and the control were not statistically significant. Therefore, we concluded that although a contribution of the lysosomal pathway cannot be completely ruled out, it is not the major mechanism by which tau fibrils promote the clearance of PrP^{Sc}.

DISCUSSION AND CONCLUSIONS

The cellular prion protein PrP^C is mostly known for its unique role in the pathogenesis of prion disorders, where it converts into a misfolded, aggregation-prone conformer termed PrP^{Sc} that is the key player of these diseases. A decade ago, Strittmatter and colleagues have reported that PrP^C binds Aβ oligomers and transduces their toxicity [284]. Although that report generated a significant amount of controversy [309], it is now generally accepted that at least in some cases PrP^C may indeed mediate some effects of Aβ oligomers. Moreover, PrP^C is able to promote the internalization of synuclein fibrils in neuroblastoma cell lines [205].
All these studies prove indeed that PrP^C might mediate the neurotoxicity of diverse pathogenic protein aggregates by acting as a membrane receptor for their internalization and/or as a transducer of their associated neurotoxicity through activation of metabotropic glutamate receptors. Indeed, several neurodegeneration-related proteins like amyloid ß, synuclein and tau appear to share key features with the prion protein, such as the propensity to assume aberrant conformations and trigger the aggregation of their physiological counterpart by recruiting the soluble protein and promoting their misfolding through physical monomer-monomer interactions. Proteins that possess these characteristics are referred to as “prion-like proteins”, and their corresponding diseases often show a typical pattern of progression that recalls the diffusion of prion diseases through the brain.
Tauopathies are a group of progressive neurodegeneration disorders caused by the accumulation and spreading of aggregated isoforms of the protein tau. Except for Pick’s disease, the hallmark of all the other tauopathies is the deposition of the tau isoforms with four repeated microtubule binding domains in specific cell types and brain regions. In this work, we took advantage of a truncated 4R construct of tau (called K18) which is often used as a model for the study of this class of tauopathies. K18 fragment readily aggregates *in vitro* to form ß sheet-enriched amyloids that are taken up by cultured cells through many mechanisms. As already shown for synuclein fibrils, the prion protein might be involved in one of the internalization pathways. In this section, our results concerning the role of the prion protein in the uptake of tau fibrils and the effect of the internalized aggregates on both PrP^C and PrP^{Sc} will be discussed.

4.1. PrP^C acts as a receptor to facilitate the entrance of tau fibrils in cultured cells

The cellular prion protein has been shown to interact with various neurodegeneration-related amyloids through a binding between its unstructured N-terminus and the ß sheet-enriched domains of the exogenous fibrils. As this interaction was reported both for synuclein and amyloid-ß, it seems plausible to posit that it might be mediated by the presence of specific secondary structure elements rather than by sequence identities. Therefore, we hypothesized that a similar mechanism might be

underpinning also the spreading of tau fibrils. The use of K18 fragment as a model of AD has been recently questioned due to the different arrangement of the residues in the K18 fibrils compared to brain-purified ones [83]; however, reports indicating that the interaction with PrP^C seems to be dependent on major structure conformations like the amount of ß sheets and not on minor residue arrangements convinced us that K18 fragment might prove useful to shed light on the involvement of the prion protein in the onset of tauopathies.
First, we showed that a direct binding between PrP^C and sonicated tau fibrils is indeed occurring. This is the first mandatory step in the cascade of events that might lead to a PrP^C-dependent internalization, and although there is proof of the interaction of the prion protein with monomeric full-length tau in the literature [302], no experiments had been performed so far using synthetic aggregates. The choice of subjecting tau fibrils to a brief cycle of sonication (5 minutes) is motivated by the fact that during the aggregation, nascent amyloids tend to stick to each other and form sorts of big plaques that are not easily internalized by the cells. Sonication breaks these big aggregates and allows a better interaction of the single fibrils with their potential receptors, including PrP^C.
In order to evaluate the contribution of a putative receptor, exogenous fibrils must be taken up by the chosen cell line without the need for a chemical transducer. Spontaneous uptake of tau fibrils from the cell culture medium has already been shown for some cell lines (HEK293, QBI-293) [247, 254, 310] and for primary neurons [301]. When added to the culture medium of our murine neuroblastoma cell line, tau fibrils were internalized with a rate that depends both on the duration of the incubation and on the initial concentration of the aggregates. Cultures treated with low concentrations of tau fibrils required up to three days in order for all the cells to show aggregates in the cell cytoplasm, while at the higher concentration of 2 µM an incubation of 24 hours proved sufficient. These specific requirements are strictly related to the cell type used, as the time needed for the internalization varied from 3 days in HEK293T to 6 days in primary neurons, and as such they have to be carefully addressed before setting up further experiments.

Afterwards, we evaluated the role of the prion protein in the spreading of tau pathology by comparing the number of internalized tau amyloids between cells that express PrP^C on the cell surface (N2a) and cells from which *Prnp* (the gene encoding PrP^C) was removed (N2a KO). To visualize the internalized fibrils, we chemically conjugated tau amyloids to a fluorophore as described in [295]. Succinimidyl esters bind to all primary amines of proteins and oligonucleotides with no distinction, therefore only pure synthetic fibrils can be conjugated without the risk of undesired signal coming from other material. The use of fluorescently-labelled amyloids allows a direct and precise visualization of the aggregates both in live cell imaging and in classical immunofluorescence experiments on fixed cells, making the use of antibodies unnecessary and thus reducing the background signal usually associated with immunolabelling. Moreover, quantification of internalized fibrils results in a more precise counting, especially when the aggregates have undergone a round of

sonication that by breaking randomly along the length of the fibril, might destroy the epitope recognized by the antibody.

The results obtained suggest that PrP^C plays a role in the endocytosis of tau fibrils, although its presence is not mandatory. N2a KO cells, even if deprived of PrP^C, were able to internalize a discrete number of fibrils, consistently with previous reports of multiple mechanisms going on at the same time and independently from each other. However, when the prion protein was present, the number of internalized fibrils almost doubled, meaning that the PrP^C-mediated pathway gives indeed a strong contribution to this process.
Most intriguingly, we discovered that the interaction between PrP^C and tau fibrils has mutual effects on both partners; while the former acts as a sort of receptor, the presence of tau aggregates leads to an increase of the cellular level of the prion protein, which is re-localized mainly on the plasma membrane where it could perform again its receptor activity. According to our data, the excess PrP^C is probably a result of an impairment in the normal recycling pathway caused by tau fibrils, as no changes in total PrP content of the cells were detected.
Although this phenomenon might be a simple side-effect of the interaction and subsequent internalization of the aggregates, we deem it likely that tau fibrils are boosting their own spreading by increasing the number of receptor molecules on the cell surface. A similar hypothesis has been proved true in the case of intercellular transfer of tau amyloids through tunneling nanotubes, where extracellular tau species (monomers and fibrils) activated the formation of new nanotubes and therefore facilitated fibrillar tau transport between neurons [272]. On the other hand, it has been shown that protein aggregates (tau and synuclein) are trafficked in early endosomes and lysosomes after the internalization [205, 242, 311]. The need of the cell to deal quickly with a big amount of exogenous and potentially dangerous material might lead to a clogging of the whole degradation system, with subsequent impact on the normal turnover of the endogenous proteins. Indeed, a similar effect on PrP levels has been reported also after treatment with synuclein fibrils, although the localization of the excess protein was not investigated. Alternatively, the binding of the amyloids to the PrP^C on the cell membrane might simply impede its internalization and retain the protein in its position, therefore leading to a general increase as the newly synthesized protein follows its normal pathway all the way up to the surface.

The potential function of PrP^C in binding and mediating cell-to-cell spread of tau amyloids points to an intriguing new function of PrP^C and opens a very interesting field of research. Moreover, the identification of such a receptor provides a potentially valuable target for pharmacological intervention.
Immunotherapy has shown promising results against many neurodegenerative diseases [312]. In particular, passive immunization occurred when prion-infected cell lines were exposed to monoclonal anti-PrP antibodies (SAF32, SAF61, 6H4), resulting in a decrease of PrP^{Sc} levels as previously observed also *in vitro* [313]. When applied to animal models of prion disorders, anti-PrP antibodies could block the

spread of prions from the periphery to the central nervous system [314]. Passive immunotherapy configures as the safest option in antibody-based treatments of prion disorders, as an active immunization against the prion protein might elicit a strong inflammatory response in the brain.
Nevertheless, the number of diseases that might possibly benefit from a PrP^C-directed immunotherapy is not limited only to prion disorders. Amyloid ß-induced cognitive deficits in AD, like memory impairment and suppression of synaptic plasticity, are triggered by a signaling cascade that starts with the binding of the oligomers to the prion protein, and thereby they can be rescued by pre-treatments with anti-PrP^C antibodies that impede the docking of Aß oligomers [315-318]. A recent publication pointed out that the targeting of either the mid region or the N-terminus of PrP^C might be effective also in abrogating the impairment of long-term potentiation caused by soluble aggregates of tau protein [303]. While this study focused mainly on the antibody-mediated recovery of normal brain functions in rats injected with synthetic or brain-derived tau fibrils, in this thesis we aimed at unraveling the exact molecular mechanisms underlying this phenomenon. In agreement with the *in vivo* data, we found that the average number of internalized tau fibrils was significantly lower in cells pre-treated with POM antibodies that targeted a portion of the N-terminal domain (POM12) and the hydrophobic domain (POM3). We are currently testing different treatment conditions as well as possible combinations of these two types of antibodies in order to maximize the inhibitory effect.
On the contrary, the POM4 antibody that targets a region of the C-terminal domain did not produce any effect on the uptake of fibrils. Given that the globular domain of PrP^C has a compact, well-defined and inflexible structure, we cannot rule out the possibility that it could also be involved in facilitating the entrance of tau fibrils, maybe through a different epitope that was not blocked by POM4.
Taken together, our data provide the first mechanistic study of the role of the prion protein in the spreading of tau pathology and the molecular details underlying the ability of anti-PrP^C antibodies to rescue tau-induced pathology.

4.2. Tau K18 fibrils reduce PrP^{Sc} levels in prion-infected cell lines

The incubation of ScN2a cell line with tau K18 fibrils for 3 days produced an almost total clearance of PrP^{Sc} after a single administration. Albeit the elimination of prions was not complete and could not be maintained over serial passages in fibrils-free medium, the PrP^{Sc} levels remained lower than those of control conditions for many days, suggesting that a second administration of tau fibrils might be able to fully abolish the prion load. Tau-mediated clearance does not seem to be affected by differences in the PrP^{Sc} conformation, as a similar reduction was observed for both RML and 22L prion strains.
Anti-prion compounds, or aggregated proteins in this case, are able to diminish prion levels in scrapie-infected cell lines by following one of two main mechanisms of action, and sometimes the final result is achieved by a combination of these two pathways working at the same time. In the indirect mechanism, exogenous molecules promote

PrP^{Sc} elimination by over-activating the cellular degradation pathways such as the autophagolysosomal system, that in cells propagating prions are regulated to maintain a basal level of prion load. The activation could involve the organelles themselves, or it could focus on other proteins that take part to the degradation process. Alternatively, compounds can bind directly to either PrP^{C} or PrP^{Sc} and inhibit prion conversion by depleting respectively the pool of the substrate or of the template. Evidence presented in this thesis suggest that this second event might be the most probable way through which the tau-mediated clearance of scrapie prions occurs, with tau fibrils binding preferentially to PrP^{C}. In addition to having shown that K18 fibrils interact with the cellular form of the prion protein, the similar effects observed after the exposition of two different prion strains to tau aggregates led us to believe that PrP^{Sc} might not be the target. As the exact structure of PrP^{Sc} is poorly defined, the structural differences distinguishing the RML and 22L prion strains are not known, and could be so subtle not to impact the binding of K18 fibrils in a detectable manner. However, it comes more straightforward to hypothesize that the partner involved in the interaction is the physiological form PrP^{C}.

Our data, although preliminary, hint at a more complex mechanism of action for tau K18 fibrils than just binding to the PrP^{C}. The analysis of the total PrP of ScN2a after deglycosylation, which allows for unambiguous identification of all products of PrP processing, revealed that K18 amyloids promote the α-cleavage of the PrP^{C} with the formation of the fragment C1.

This type of PrP processing is considered neuroprotective against prions, as the cleavage site is located inside the amyloidogenic sequence 109-122. This portion of the protein that spans the hydrophobic domain is postulated to acquire ß sheet structure and play a critical role in prion formation and toxicity. The α-cleavage occurs between amino acids 110/111 or 111/112 and disrupts this region, therefore preventing prion conversion. Two fragments are originated: the C1 fragment, whose functions are still debated but appear to be linked to the enhancement of apoptotic effects, and the neuroprotective fragment N1, which reduces the p53-dependent cell death. Most importantly, none of these two fragments is a substrate for prion conversion, and therefore the cleavage of PrP into these two peptides prevents prion accumulation.

Despite these observations, we investigated also whether the cellular degradation pathways such as macroautophagy and lysosomal degradation are involved, at least partially, in tau-induced PrP^{Sc} clearance. Macroautophagy proceeds through the formation of a double membrane structure called phagosome which engulfs the cargo that has to be degraded (like organelles or protein aggregates) and delivers it to the lysosomes [319]. Stimulation of autophagy is an efficient way to decrease the prion load in cell cultures [320, 321]. The compound we used to block the pathway, 3-methyladenine, is one of the most commonly employed inhibitors of autophagy [322] and it acts on the phosphoinositide-3 kinases (PI3K) that catalyse the first step in the formation of the phagosome. We could not detect any effect of the treatment with 3-MA on the PrP^{Sc} levels, independently on previous incubation with K18 fibrils. Although 3-MA has been recently questioned as an inhibitor because of its apparent

dual role in the modulation of autophagy [323], our data based on the treatments with this compound seem to exclude a role for macroautophagy in the clearance of prions, at least in our specific cell line. Indeed, several alternative pathways of PrP^{Sc} elimination have been reported, varying according to the cell type used and the forms of misfolded PrP (i.e. newly formed PrP^{Sc}, mature PrP^{Sc}, mutant PrP) [324]. Moreover, Goold et al. [325] proposed a new and interesting role for the UPS in PrP^{Sc} degradation, which might be a valid alternative to the pathways analysed in this thesis. Since both tau and synuclein fibrils have been reported to colocalize with lysosomes once they have been internalized, tau-induced clearance of prions might occur as an effect of the overactivation of the lysosomal system. As a first preliminary experiment, we performed an inhibition of the whole lysosomal environment by the treatment with NH_4Cl, that increases the pH of the vesicles and impairs the activity of the enzymes. What we observed was just a mild recovery of normal prion levels in ScN2a treated with both K18 fibrils and NH_4Cl, which made us think that the stimulation of the lysosomal activity is not the primary mechanism by which tau amyloids promote the decrease in PrP^{Sc} levels. We are currently assessing the effect of tau fibrils on the activity of the cathepsins known to have a role in prion degradation (cathepsins B, S and L).

In conclusion, in this study we provided significant evidence of an important role for PrP^{C} in mediating the internalization of exogenous tau fibrils, therefore contributing to the cell-to-cell spreading of the aggregates and to the onset of the pathology. Moreover, we successfully evaluated the potentiality of PrP^{C} as a therapeutic target to inhibit the uptake of tau amyloids. The interaction between tau fibrils and the cellular prion protein seems to affect also the process of prion replication in prion-infected cell lines. This occurs probably through the inhibition of the mechanism of PrP^{C} conversion into PrP^{Sc}, due to an increased rate α-cleavage of PrP^{C} stimulated by the binding to tau fibrils. The role of endogenous degradation mechanisms could not be ruled out, although they play only a marginal role. These findings open new avenues in tauopathies and prion research, as well as potentially valuable targets for therapeutic intervention.

REFERENCES

1. Recchia, A., et al., *Alpha-synuclein and Parkinson's disease.* Faseb j, 2004. **18**(6): p. 617-26.
2. O'Sullivan, S.S., et al., *Nonmotor symptoms as presenting complaints in Parkinson's disease: a clinicopathological study.* Mov Disord, 2008. **23**(1): p. 101-6.
3. Polymeropoulos, M.H., et al., *Mutation in the alpha-synuclein gene identified in families with Parkinson's disease.* Science, 1997. **276**(5321): p. 2045-7.
4. Kruger, R., et al., *Ala30Pro mutation in the gene encoding alpha-synuclein in Parkinson's disease.* Nat Genet, 1998. **18**(2): p. 106-8.
5. Zarranz, J.J., et al., *The new mutation, E46K, of alpha-synuclein causes Parkinson and Lewy body dementia.* Ann Neurol, 2004. **55**(2): p. 164-73.
6. Appel-Cresswell, S., et al., *Alpha-synuclein p.H50Q, a novel pathogenic mutation for Parkinson's disease.* Mov Disord, 2013. **28**(6): p. 811-3.
7. Olanow, C.W. and W.G. Tatton, *Etiology and pathogenesis of Parkinson's disease.* Annu Rev Neurosci, 1999. **22**: p. 123-44.
8. Langston, J.W. and P.A. Ballard, Jr., *Parkinson's disease in a chemist working with 1-methyl-4-phenyl-1,2,5,6-tetrahydropyridine.* N Engl J Med, 1983. **309**(5): p. 310.
9. Spillantini, M.G., et al., *Alpha-synuclein in Lewy bodies.* Nature, 1997. **388**(6645): p. 839-40.
10. Spillantini, M.G., et al., *alpha-Synuclein in filamentous inclusions of Lewy bodies from Parkinson's disease and dementia with lewy bodies.* Proc Natl Acad Sci U S A, 1998. **95**(11): p. 6469-73.
11. Borroni, B., A. Alberici, and E. Buratti, *Review: Molecular pathology of frontotemporal lobar degenerations.* Neuropathol Appl Neurobiol, 2019. **45**(1): p. 41-57.
12. Neumann, M. and I.R.A. Mackenzie, *Review: Neuropathology of non-tau frontotemporal lobar degeneration.* Neuropathology and Applied Neurobiology, 2019. **45**(1): p. 19-40.
13. Ahmed, Z., et al., *Globular glial tauopathies (GGT): consensus recommendations.* Acta Neuropathol, 2013. **126**(4): p. 537-544.
14. Hutton, M., et al., *Association of missense and 5'-splice-site mutations in tau with the inherited dementia FTDP-17.* Nature, 1998. **393**(6686): p. 702-5.
15. Goedert, M. and R. Jakes, *Mutations causing neurodegenerative tauopathies.* Biochim Biophys Acta, 2005. **1739**(2-3): p. 240-50.
16. Lee, V.M., M. Goedert, and J.Q. Trojanowski, *Neurodegenerative tauopathies.* Annu Rev Neurosci, 2001. **24**: p. 1121-59.
17. Stefansson, H., et al., *A common inversion under selection in Europeans.* Nat Genet, 2005. **37**(2): p. 129-37.
18. Caffrey, T.M., et al., *Haplotype-specific expression of exon 10 at the human MAPT locus.* Hum Mol Genet, 2006. **15**(24): p. 3529-37.
19. Hayashi, S., et al., *Late-onset frontotemporal dementia with a novel exon 1 (Arg5His) tau gene mutation.* Ann Neurol, 2002. **51**(4): p. 525-30.
20. Poorkaj, P., et al., *An R5L tau mutation in a subject with a progressive supranuclear palsy phenotype.* Ann Neurol, 2002. **52**(4): p. 511-6.

21. Grover, A., et al., *Effects on splicing and protein function of three mutations in codon N296 of tau in vitro.* Neurosci Lett, 2002. **323**(1): p. 33-6.
22. D'Souza, I. and G.D. Schellenberg, *Regulation of tau isoform expression and dementia.* Biochim Biophys Acta, 2005. **1739**(2-3): p. 104-15.
23. Buee, L., et al., *Tau protein isoforms, phosphorylation and role in neurodegenerative disorders.* Brain Res Brain Res Rev, 2000. **33**(1): p. 95-130.
24. Gotz, J., G. Halliday, and R.M. Nisbet, *Molecular Pathogenesis of the Tauopathies.* Annu Rev Pathol, 2019. **14**: p. 239-261.
25. Probst, A., et al., *Pick's disease: hyperphosphorylated tau protein segregates to the somatoaxonal compartment.* Acta Neuropathol, 1996. **92**(6): p. 588-96.
26. Ferrer, I., et al., *Glial and neuronal tau pathology in tauopathies: characterization of disease-specific phenotypes and tau pathology progression.* J Neuropathol Exp Neurol, 2014. **73**(1): p. 81-97.
27. Kato, S. and H. Nakamura, *Presence of two different fibril subtypes in the Pick body: an immunoelectron microscopic study.* Acta Neuropathol, 1990. **81**(2): p. 125-9.
28. Murayama, S., et al., *Immunocytochemical and ultrastructural studies of Pick's disease.* Ann Neurol, 1990. **27**(4): p. 394-405.
29. Perry, G., et al., *Filaments of Pick's bodies contain altered cytoskeletal elements.* Am J Pathol, 1987. **127**(3): p. 559-68.
30. Odawara, T., et al., *Degeneration of Pick bodies visualized by methenamine-silver staining and immunohistochemistry.* Neuropathology, 2002. **22**(3): p. 180-5.
31. Hodges, J.R., *Frontotemporal dementia (Pick's disease): clinical features and assessment.* Neurology, 2001. **56**(11 Suppl 4): p. S6-10.
32. Steele, J.C., J.C. Richardson, and J. Olszewski, *Progressive supranuclear palsy: a heterogeneous degeneration involving the brain stem, Basal Ganglia and cerebellum with vertical gaze and pseudobulbar palsy, nuchal dystonia and dementia.* Semin Neurol, 2014. **34**(2): p. 129-50.
33. Coyle-Gilchrist, I.T., et al., *Prevalence, characteristics, and survival of frontotemporal lobar degeneration syndromes.* Neurology, 2016. **86**(18): p. 1736-43.
34. Probst, A., et al., *Progressive supranuclear palsy: extensive neuropil threads in addition to neurofibrillary tangles. Very similar antigenicity of subcortical neuronal pathology in progressive supranuclear palsy and Alzheimer's disease.* Acta Neuropathol, 1988. **77**(1): p. 61-8.
35. Yamada, T., P.L. McGeer, and E.G. McGeer, *Appearance of paired nucleated, Tau-positive glia in patients with progressive supranuclear palsy brain tissue.* Neurosci Lett, 1992. **135**(1): p. 99-102.
36. Armstrong, M.J., *Progressive Supranuclear Palsy: an Update.* Curr Neurol Neurosci Rep, 2018. **18**(3): p. 12.
37. Boxer, A.L., et al., *Advances in progressive supranuclear palsy: new diagnostic criteria, biomarkers, and therapeutic approaches.* Lancet Neurol, 2017. **16**(7): p. 552-563.
38. Rebeiz, J.J., E.H. Kolodny, and E.P. Richardson, Jr., *Corticodentatonigral degeneration with neuronal achromasia.* Arch Neurol, 1968. **18**(1): p. 20-33.
39. Mahapatra, R.K., et al., *Corticobasal degeneration.* Lancet Neurol, 2004. **3**(12): p. 736-43.
40. Graham, N.L., T.H. Bak, and J.R. Hodges, *Corticobasal degeneration as a cognitive disorder.* Mov Disord, 2003. **18**(11): p. 1224-32.

41. Dickson, D.W., et al., *Ballooned neurons in select neurodegenerative diseases contain phosphorylated neurofilament epitopes.* Acta Neuropathol, 1986. **71**(3-4): p. 216-23.
42. Uchihara, T., et al., *Abnormal cytoskeletal pathology peculiar to corticobasal degeneration is different from that of Alzheimer's disease or progressive supranuclear palsy.* Acta Neuropathol, 1994. **88**(4): p. 379-83.
43. Dickson, D.W., *Neuropathologic differentiation of progressive supranuclear palsy and corticobasal degeneration.* J Neurol, 1999. **246 Suppl 2**: p. Ii6-15.
44. Bigio, E.H., et al., *Frontal lobe dementia with novel tauopathy: sporadic multiple system tauopathy with dementia.* J Neuropathol Exp Neurol, 2001. **60**(4): p. 328-41.
45. Kovacs, G.G., et al., *White matter tauopathy with globular glial inclusions: a distinct sporadic frontotemporal lobar degeneration.* J Neuropathol Exp Neurol, 2008. **67**(10): p. 963-75.
46. Ahmed, Z., et al., *Globular glial tauopathies (GGT) presenting with motor neuron disease or frontotemporal dementia: an emerging group of 4-repeat tauopathies.* Acta Neuropathol, 2011. **122**(4): p. 415-28.
47. Chung, D.C., et al., *Tau exhibits unique seeding properties in globular glial tauopathy.* Acta Neuropathol Commun, 2019. **7**(1): p. 36.
48. Tolnay, M. and F. Clavaguera, *Argyrophilic grain disease: a late-onset dementia with distinctive features among tauopathies.* Neuropathology, 2004. **24**(4): p. 269-83.
49. Braak, H. and E. Braak, *Argyrophilic grain disease: frequency of occurrence in different age categories and neuropathological diagnostic criteria.* J Neural Transm (Vienna), 1998. **105**(8-9): p. 801-19.
50. Ding, Z.T., et al., *Argyrophilic grain disease: frequency and neuropathology in centenarians.* Acta Neuropathol, 2006. **111**(4): p. 320-8.
51. Yokota, O., et al., *Coexistence of amyotrophic lateral sclerosis and argyrophilic grain disease: a non-demented autopsy case showing circumscribed temporal atrophy and involvement of the amygdala.* Neuropathology, 2007. **27**(6): p. 539-50.
52. Tatsumi, S., et al., *Argyrophilic grains are reliable disease-specific features of corticobasal degeneration.* J Neuropathol Exp Neurol, 2014. **73**(1): p. 30-8.
53. Martinez-Lage, P. and D.G. Munoz, *Prevalence and disease associations of argyrophilic grains of Braak.* J Neuropathol Exp Neurol, 1997. **56**(2): p. 157-64.
54. Saito, Y. and S. Murayama, *Neuropathology of mild cognitive impairment.* Neuropathology, 2007. **27**(6): p. 578-84.
55. Saito, Y., et al., *Staging of argyrophilic grains: an age-associated tauopathy.* J Neuropathol Exp Neurol, 2004. **63**(9): p. 911-8.
56. Saito, Y., et al., *Severe involvement of ambient gyrus in dementia with grains.* J Neuropathol Exp Neurol, 2002. **61**(9): p. 789-96.
57. Knopman, D.S., et al., *Neuropathology of cognitively normal elderly.* J Neuropathol Exp Neurol, 2003. **62**(11): p. 1087-95.
58. Ikeda, K., et al., *A study of dementia with argyrophilic grains. Possible cytoskeletal abnormality in dendrospinal portion of neurons and oligodendroglia.* Acta Neuropathol, 1995. **89**(5): p. 409-14.
59. Tolnay, M., et al., *Argyrophilic grain disease: widespread hyperphosphorylation of tau protein in limbic neurons.* Acta Neuropathol, 1997. **93**(5): p. 477-84.
60. Braak, H. and E. Braak, *Neuropathological stageing of Alzheimer-related changes.* Acta Neuropathol, 1991. **82**(4): p. 239-59.

61. Dubois, B., et al., *Preclinical Alzheimer's disease: Definition, natural history, and diagnostic criteria.* Alzheimers Dement, 2016. **12**(3): p. 292-323.
62. Kawas, C., et al., *Age-specific incidence rates of Alzheimer's disease: the Baltimore Longitudinal Study of Aging.* Neurology, 2000. **54**(11): p. 2072-7.
63. Jouanne, M., S. Rault, and A.S. Voisin-Chiret, *Tau protein aggregation in Alzheimer's disease: An attractive target for the development of novel therapeutic agents.* Eur J Med Chem, 2017. **139**: p. 153-167.
64. Thal, D.R., et al., *Phases of A beta-deposition in the human brain and its relevance for the development of AD.* Neurology, 2002. **58**(12): p. 1791-800.
65. Masters, C.L., et al., *Alzheimer's disease.* Nat Rev Dis Primers, 2015. **1**: p. 15056.
66. Scheuner, D., et al., *Secreted amyloid beta-protein similar to that in the senile plaques of Alzheimer's disease is increased in vivo by the presenilin 1 and 2 and APP mutations linked to familial Alzheimer's disease.* Nat Med, 1996. **2**(8): p. 864-70.
67. Hecimovic, S., et al., *Mutations in APP have independent effects on Abeta and CTFgamma generation.* Neurobiol Dis, 2004. **17**(2): p. 205-18.
68. Kumar-Singh, S., et al., *Mean age-of-onset of familial alzheimer disease caused by presenilin mutations correlates with both increased Abeta42 and decreased Abeta40.* Hum Mutat, 2006. **27**(7): p. 686-95.
69. Blanco, J.A., et al., *Novel presenilin 1 mutation (p.Thr-Pro116-117Ser-Thr) in a Spanish family with early-onset Alzheimer's disease.* Neurobiol Aging, 2019.
70. Rossor, M.N., et al., *Alzheimer's disease families with amyloid precursor protein mutations.* Ann N Y Acad Sci, 1993. **695**: p. 198-202.
71. Zhang, S., et al., *Association between variant amyloid deposits and motor deficits in FAD-associated presenilin-1 mutations: A systematic review.* Neurosci Biobehav Rev, 2015. **56**: p. 180-92.
72. Norton, S., et al., *Potential for primary prevention of Alzheimer's disease: an analysis of population-based data.* Lancet Neurol, 2014. **13**(8): p. 788-94.
73. Artiga, M.J., et al., *Allelic polymorphisms in the transcriptional regulatory region of apolipoprotein E gene.* FEBS Lett, 1998. **421**(2): p. 105-8.
74. Saunders, A.M., et al., *Association of apolipoprotein E allele epsilon 4 with late-onset familial and sporadic Alzheimer's disease.* Neurology, 1993. **43**(8): p. 1467-72.
75. Farrer, L.A., et al., *Effects of age, sex, and ethnicity on the association between apolipoprotein E genotype and Alzheimer disease. A meta-analysis. APOE and Alzheimer Disease Meta Analysis Consortium.* Jama, 1997. **278**(16): p. 1349-56.
76. Holtzman, D.M., et al., *Apolipoprotein E isoform-dependent amyloid deposition and neuritic degeneration in a mouse model of Alzheimer's disease.* Proc Natl Acad Sci U S A, 2000. **97**(6): p. 2892-7.
77. Strittmatter, W.J., et al., *Apolipoprotein E: high-avidity binding to beta-amyloid and increased frequency of type 4 allele in late-onset familial Alzheimer disease.* Proc Natl Acad Sci U S A, 1993. **90**(5): p. 1977-81.
78. Goedert, M., et al., *Tau proteins of Alzheimer paired helical filaments: abnormal phosphorylation of all six brain isoforms.* Neuron, 1992. **8**(1): p. 159-68.
79. Goedert, M., et al., *Multiple isoforms of human microtubule-associated protein tau: sequences and localization in neurofibrillary tangles of Alzheimer's disease.* Neuron, 1989. **3**(4): p. 519-26.
80. Kidd, M., *Paired helical filaments in electron microscopy of Alzheimer's disease.* Nature, 1963. **197**: p. 192-3.

81. Terry, R.D., *THE FINE STRUCTURE OF NEUROFIBRILLARY TANGLES IN ALZHEIMER'S DISEASE.* J Neuropathol Exp Neurol, 1963. **22**: p. 629-42.
82. Yagishita, S., et al., *Reappraisal of the fine structure of Alzheimer's neurofibrillary tangles.* Acta Neuropathol, 1981. **54**(3): p. 239-46.
83. Fitzpatrick, A.W.P., et al., *Cryo-EM structures of tau filaments from Alzheimer's disease.* Nature, 2017. **547**(7662): p. 185-190.
84. Karran, E., M. Mercken, and B. De Strooper, *The amyloid cascade hypothesis for Alzheimer's disease: an appraisal for the development of therapeutics.* Nat Rev Drug Discov, 2011. **10**(9): p. 698-712.
85. Hardy, J. and D. Allsop, *Amyloid deposition as the central event in the aetiology of Alzheimer's disease.* Trends Pharmacol Sci, 1991. **12**(10): p. 383-8.
86. Hardy, J.A. and G.A. Higgins, *Alzheimer's disease: the amyloid cascade hypothesis.* Science, 1992. **256**(5054): p. 184-5.
87. Small, S.A. and K. Duff, *Linking Abeta and tau in late-onset Alzheimer's disease: a dual pathway hypothesis.* Neuron, 2008. **60**(4): p. 534-42.
88. Baker, H.F., et al., *Evidence for the experimental transmission of cerebral beta-amyloidosis to primates.* Int J Exp Pathol, 1993. **74**(5): p. 441-54.
89. Stohr, J., et al., *Purified and synthetic Alzheimer's amyloid beta (Abeta) prions.* Proc Natl Acad Sci U S A, 2012. **109**(27): p. 11025-30.
90. Stohr, J., et al., *Distinct synthetic Abeta prion strains producing different amyloid deposits in bigenic mice.* Proc Natl Acad Sci U S A, 2014. **111**(28): p. 10329-34.
91. Wood, J.L., L.J. Lund, and S.H. Done, *The natural occurrence of scrapie in moufflon.* Vet Rec, 1992. **130**(2): p. 25-7.
92. Wells, G.A., et al., *A novel progressive spongiform encephalopathy in cattle.* Vet Rec, 1987. **121**(18): p. 419-20.
93. Barlow, R.M., *Transmissible mink encephalopathy: pathogenesis and nature of the aetiological agent.* J Clin Pathol Suppl (R Coll Pathol), 1972. **6**: p. 102-9.
94. Wyatt, J.M., et al., *Naturally occurring scrapie-like spongiform encephalopathy in five domestic cats.* Vet Rec, 1991. **129**(11): p. 233-6.
95. Williams, E.S. and S. Young, *Spongiform encephalopathy of Rocky Mountain elk.* J Wildl Dis, 1982. **18**(4): p. 465-71.
96. Casalone, C., et al., *Identification of a second bovine amyloidotic spongiform encephalopathy: molecular similarities with sporadic Creutzfeldt-Jakob disease.* Proc Natl Acad Sci U S A, 2004. **101**(9): p. 3065-70.
97. Comoy, E.E., et al., *Atypical BSE (BASE) Transmitted from Asymptomatic Aging Cattle to a Primate.* PLOS ONE, 2008. **3**(8): p. e3017.
98. Wilson, R., et al., *Presence of subclinical infection in gene-targeted human prion protein transgenic mice exposed to atypical bovine spongiform encephalopathy.* J Gen Virol, 2013. **94**(Pt 12): p. 2819-27.
99. Greenlee, J.J., J.D. Smith, and R.A. Kunkle, *White-tailed deer are susceptible to the agent of sheep scrapie by intracerebral inoculation.* Vet Res, 2011. **42**: p. 107.
100. Peggion, C., M.C. Sorgato, and A. Bertoli, *Prions and prion-like pathogens in neurodegenerative disorders.* Pathogens, 2014. **3**(1): p. 149-63.
101. Gambetti, P., et al., *Sporadic and familial CJD: classification and characterisation.* Br Med Bull, 2003. **66**: p. 213-39.
102. Kovacs, G.G., et al., *Mutations of the prion protein gene phenotypic spectrum.* J Neurol, 2002. **249**(11): p. 1567-82.

103. Safar, J.G., et al., *Structural determinants of phenotypic diversity and replication rate of human prions.* PLoS Pathog, 2015. **11**(4): p. e1004832.
104. Perez, M., et al., *Prion peptide induces neuronal cell death through a pathway involving glycogen synthase kinase 3.* Biochem J, 2003. **372**(Pt 1): p. 129-36.
105. Lopes, J.P., C.R. Oliveira, and P. Agostinho, *Role of cyclin-dependent kinase 5 in the neurodegenerative process triggered by amyloid-Beta and prion peptides: implications for Alzheimer's disease and prion-related encephalopathies.* Cell Mol Neurobiol, 2007. **27**(7): p. 943-57.
106. Brown, D.R., *Altered toxicity of the prion protein peptide PrP106-126 carrying the Ala(117)-->Val mutation.* Biochem J, 2000. **346 Pt 3**: p. 785-91.
107. Giaccone, G., et al., *Tauopathy in human and experimental variant Creutzfeldt-Jakob disease.* Neurobiol Aging, 2008. **29**(12): p. 1864-73.
108. Sikorska, B., et al., *Ultrastructural study of florid plaques in variant Creutzfeldt-Jakob disease: a comparison with amyloid plaques in kuru, sporadic Creutzfeldt-Jakob disease and Gerstmann-Straussler-Scheinker disease.* Neuropathol Appl Neurobiol, 2009. **35**(1): p. 46-59.
109. Reiniger, L., et al., *Tau, prions and Abeta: the triad of neurodegeneration.* Acta Neuropathol, 2011. **121**(1): p. 5-20.
110. Ghetti, B., et al., *Vascular variant of prion protein cerebral amyloidosis with tau-positive neurofibrillary tangles: the phenotype of the stop codon 145 mutation in PRNP.* Proc Natl Acad Sci U S A, 1996. **93**(2): p. 744-8.
111. Cleveland, D.W. and J.D. Rothstein, *From Charcot to Lou Gehrig: deciphering selective motor neuron death in ALS.* Nat Rev Neurosci, 2001. **2**(11): p. 806-19.
112. Elden, A.C., et al., *Ataxin-2 intermediate-length polyglutamine expansions are associated with increased risk for ALS.* Nature, 2010. **466**(7310): p. 1069-75.
113. Wu, C.H., et al., *Mutations in the profilin 1 gene cause familial amyotrophic lateral sclerosis.* Nature, 2012. **488**(7412): p. 499-503.
114. Polymenidou, M., et al., *Long pre-mRNA depletion and RNA missplicing contribute to neuronal vulnerability from loss of TDP-43.* Nat Neurosci, 2011. **14**(4): p. 459-68.
115. Furukawa, Y., et al., *A seeding reaction recapitulates intracellular formation of Sarkosyl-insoluble transactivation response element (TAR) DNA-binding protein-43 inclusions.* J Biol Chem, 2011. **286**(21): p. 18664-72.
116. Binder, L.I., A. Frankfurter, and L.I. Rebhun, *The distribution of tau in the mammalian central nervous system.* J Cell Biol, 1985. **101**(4): p. 1371-8.
117. Dugger, B.N., et al., *The Presence of Select Tau Species in Human Peripheral Tissues and Their Relation to Alzheimer's Disease.* J Alzheimers Dis, 2016. **51**(2): p. 345-56.
118. Kahlson, M.A. and K.J. Colodner, *Glial Tau Pathology in Tauopathies: Functional Consequences.* J Exp Neurosci, 2015. **9**(Suppl 2): p. 43-50.
119. Andreadis, A., W.M. Brown, and K.S. Kosik, *Structure and novel exons of the human tau gene.* Biochemistry, 1992. **31**(43): p. 10626-33.
120. Liu, F. and C.X. Gong, *Tau exon 10 alternative splicing and tauopathies.* Mol Neurodegener, 2008. **3**: p. 8.
121. Wang, Y. and E. Mandelkow, *Tau in physiology and pathology.* Nat Rev Neurosci, 2016. **17**(1): p. 5-21.
122. Avila, J., et al., *Tau Structures.* Front Aging Neurosci, 2016. **8**: p. 262.
123. Leterrier, J.F., R.K. Liem, and M.L. Shelanski, *Interactions between neurofilaments and microtubule-associated proteins: a possible mechanism for intraorganellar bridging.* J Cell Biol, 1982. **95**(3): p. 982-6.

124. Rendon, A., D. Jung, and V. Jancsik, *Interaction of microtubules and microtubule-associated proteins (MAPs) with rat brain mitochondria.* Biochem J, 1990. **269**(2): p. 555-6.
125. Chen, J., et al., *Projection domains of MAP2 and tau determine spacings between microtubules in dendrites and axons.* Nature, 1992. **360**(6405): p. 674-7.
126. Georgieff, I.S., et al., *Expression of high molecular weight tau in the central and peripheral nervous systems.* J Cell Sci, 1993. **105 (Pt 3)**: p. 729-37.
127. Carlier, M.F., et al., *Interaction between microtubule-associated protein tau and spectrin.* Biochimie, 1984. **66**(4): p. 305-11.
128. Griffith, L.M. and T.D. Pollard, *The interaction of actin filaments with microtubules and microtubule-associated proteins.* J Biol Chem, 1982. **257**(15): p. 9143-51.
129. Lee, G., et al., *Tau interacts with src-family non-receptor tyrosine kinases.* J Cell Sci, 1998. **111 (Pt 21)**: p. 3167-77.
130. Hwang, S.C., et al., *Activation of phospholipase C-gamma by the concerted action of tau proteins and arachidonic acid.* J Biol Chem, 1996. **271**(31): p. 18342-9.
131. Drechsel, D.N., et al., *Modulation of the dynamic instability of tubulin assembly by the microtubule-associated protein tau.* Mol Biol Cell, 1992. **3**(10): p. 1141-54.
132. Correas, I., R. Padilla, and J. Avila, *The tubulin-binding sequence of brain microtubule-associated proteins, tau and MAP-2, is also involved in actin binding.* Biochem J, 1990. **269**(1): p. 61-4.
133. Panda, D., et al., *Kinetic stabilization of microtubule dynamics at steady state by tau and microtubule-binding domains of tau.* Biochemistry, 1995. **34**(35): p. 11117-27.
134. Goode, B.L. and S.C. Feinstein, *Identification of a novel microtubule binding and assembly domain in the developmentally regulated inter-repeat region of tau.* J Cell Biol, 1994. **124**(5): p. 769-82.
135. Kampers, T., et al., *RNA stimulates aggregation of microtubule-associated protein tau into Alzheimer-like paired helical filaments.* FEBS Lett, 1996. **399**(3): p. 344-9.
136. Brady, R.M., R.P. Zinkowski, and L.I. Binder, *Presence of tau in isolated nuclei from human brain.* Neurobiol Aging, 1995. **16**(3): p. 479-86.
137. Greenwood, J.A. and G.V. Johnson, *Localization and in situ phosphorylation state of nuclear tau.* Exp Cell Res, 1995. **220**(2): p. 332-7.
138. Drewes, G., et al., *Microtubule-associated protein/microtubule affinity-regulating kinase (p110mark). A novel protein kinase that regulates tau-microtubule interactions and dynamic instability by phosphorylation at the Alzheimer-specific site serine 262.* J Biol Chem, 1995. **270**(13): p. 7679-88.
139. Dickey, C.A., et al., *The high-affinity HSP90-CHIP complex recognizes and selectively degrades phosphorylated tau client proteins.* J Clin Invest, 2007. **117**(3): p. 648-58.
140. Simic, G., et al., *Tau Protein Hyperphosphorylation and Aggregation in Alzheimer's Disease and Other Tauopathies, and Possible Neuroprotective Strategies.* Biomolecules, 2016. **6**(1): p. 6.
141. Eidenmuller, J., et al., *Phosphorylation-mimicking glutamate clusters in the proline-rich region are sufficient to simulate the functional deficiencies of hyperphosphorylated tau protein.* Biochem J, 2001. **357**(Pt 3): p. 759-67.
142. Liu, F., et al., *Site-specific effects of tau phosphorylation on its microtubule assembly activity and self-aggregation.* Eur J Neurosci, 2007. **26**(12): p. 3429-36.
143. Hoover, B.R., et al., *Tau mislocalization to dendritic spines mediates synaptic dysfunction independently of neurodegeneration.* Neuron, 2010. **68**(6): p. 1067-81.

144. De-Paula, V.J., et al., *Inhibition of phospholipase A2 increases tau phosphorylation at Ser214 in embryonic rat hippocampal neurons.* Prostaglandins Leukot Essent Fatty Acids, 2010. **82**(1): p. 57-60.
145. Yu, Y., et al., *Developmental regulation of tau phosphorylation, tau kinases, and tau phosphatases.* J Neurochem, 2009. **108**(6): p. 1480-94.
146. Hanger, D.P., et al., *Novel phosphorylation sites in tau from Alzheimer brain support a role for casein kinase 1 in disease pathogenesis.* J Biol Chem, 2007. **282**(32): p. 23645-54.
147. Hye, A., et al., *Glycogen synthase kinase-3 is increased in white cells early in Alzheimer's disease.* Neurosci Lett, 2005. **373**(1): p. 1-4.
148. Leroy, K., Z. Yilmaz, and J.P. Brion, *Increased level of active GSK-3beta in Alzheimer's disease and accumulation in argyrophilic grains and in neurones at different stages of neurofibrillary degeneration.* Neuropathol Appl Neurobiol, 2007. **33**(1): p. 43-55.
149. Pei, J.J., et al., *Distribution, levels, and activity of glycogen synthase kinase-3 in the Alzheimer disease brain.* J Neuropathol Exp Neurol, 1997. **56**(1): p. 70-8.
150. Gong, C.X., et al., *Phosphorylation of microtubule-associated protein tau is regulated by protein phosphatase 2A in mammalian brain. Implications for neurofibrillary degeneration in Alzheimer's disease.* J Biol Chem, 2000. **275**(8): p. 5535-44.
151. Liu, F., et al., *Contributions of protein phosphatases PP1, PP2A, PP2B and PP5 to the regulation of tau phosphorylation.* Eur J Neurosci, 2005. **22**(8): p. 1942-50.
152. Caccamo, A., et al., *Lithium reduces tau phosphorylation but not A beta or working memory deficits in a transgenic model with both plaques and tangles.* Am J Pathol, 2007. **170**(5): p. 1669-75.
153. Engel, T., et al., *Chronic lithium administration to FTDP-17 tau and GSK-3beta overexpressing mice prevents tau hyperphosphorylation and neurofibrillary tangle formation, but pre-formed neurofibrillary tangles do not revert.* J Neurochem, 2006. **99**(6): p. 1445-55.
154. Gandini, A., et al., *Tau-Centric Multitarget Approach for Alzheimer's Disease: Development of First-in-Class Dual Glycogen Synthase Kinase 3beta and Tau-Aggregation Inhibitors.* J Med Chem, 2018. **61**(17): p. 7640-7656.
155. Takahashi, M., et al., *Glycosylation of microtubule-associated protein tau in Alzheimer's disease brain.* Acta Neuropathol, 1999. **97**(6): p. 635-41.
156. Wang, J.Z., I. Grundke-Iqbal, and K. Iqbal, *Glycosylation of microtubule-associated protein tau: an abnormal posttranslational modification in Alzheimer's disease.* Nat Med, 1996. **2**(8): p. 871-5.
157. Liu, F., et al., *Involvement of aberrant glycosylation in phosphorylation of tau by cdk5 and GSK-3beta.* FEBS Lett, 2002. **530**(1-3): p. 209-14.
158. Yu, C.H., et al., *O-GlcNAcylation modulates the self-aggregation ability of the fourth microtubule-binding repeat of tau.* Biochem Biophys Res Commun, 2008. **375**(1): p. 59-62.
159. Gong, C.X., et al., *Impaired brain glucose metabolism leads to Alzheimer neurofibrillary degeneration through a decrease in tau O-GlcNAcylation.* J Alzheimers Dis, 2006. **9**(1): p. 1-12.
160. Basurto-Islas, G., et al., *Accumulation of aspartic acid421- and glutamic acid391-cleaved tau in neurofibrillary tangles correlates with progression in Alzheimer disease.* J Neuropathol Exp Neurol, 2008. **67**(5): p. 470-83.
161. Horowitz, P.M., et al., *Early N-terminal changes and caspase-6 cleavage of tau in Alzheimer's disease.* J Neurosci, 2004. **24**(36): p. 7895-902.

162. Park, S.Y. and A. Ferreira, *The generation of a 17 kDa neurotoxic fragment: an alternative mechanism by which tau mediates beta-amyloid-induced neurodegeneration.* J Neurosci, 2005. **25**(22): p. 5365-75.
163. Chung, C.W., et al., *Proapoptotic effects of tau cleavage product generated by caspase-3.* Neurobiol Dis, 2001. **8**(1): p. 162-72.
164. Mondragon-Rodriguez, S., et al., *Cleavage and conformational changes of tau protein follow phosphorylation during Alzheimer's disease.* Int J Exp Pathol, 2008. **89**(2): p. 81-90.
165. Rohn, T.T., et al., *Caspase-9 activation and caspase cleavage of tau in the Alzheimer's disease brain.* Neurobiol Dis, 2002. **11**(2): p. 341-54.
166. Saito, M., et al., *Tau phosphorylation and cleavage in ethanol-induced neurodegeneration in the developing mouse brain.* Neurochem Res, 2010. **35**(4): p. 651-9.
167. Guillozet-Bongaarts, A.L., et al., *Pseudophosphorylation of tau at serine 422 inhibits caspase cleavage: in vitro evidence and implications for tangle formation in vivo.* J Neurochem, 2006. **97**(4): p. 1005-14.
168. Cappelletti, G., et al., *The nitration of tau protein in neurone-like PC12 cells.* FEBS Lett, 2004. **562**(1-3): p. 35-9.
169. Reynolds, M.R., et al., *Tau nitration occurs at tyrosine 29 in the fibrillar lesions of Alzheimer's disease and other tauopathies.* J Neurosci, 2006. **26**(42): p. 10636-45.
170. Reyes, J.F., et al., *A possible link between astrocyte activation and tau nitration in Alzheimer's disease.* Neurobiol Dis, 2008. **31**(2): p. 198-208.
171. Reynolds, M.R., R.W. Berry, and L.I. Binder, *Site-specific nitration and oxidative dityrosine bridging of the tau protein by peroxynitrite: implications for Alzheimer's disease.* Biochemistry, 2005. **44**(5): p. 1690-700.
172. Arnaud, L.T., N. Myeku, and M.E. Figueiredo-Pereira, *Proteasome-caspase-cathepsin sequence leading to tau pathology induced by prostaglandin J2 in neuronal cells.* J Neurochem, 2009. **110**(1): p. 328-42.
173. Cripps, D., et al., *Alzheimer disease-specific conformation of hyperphosphorylated paired helical filament-Tau is polyubiquitinated through Lys-48, Lys-11, and Lys-6 ubiquitin conjugation.* J Biol Chem, 2006. **281**(16): p. 10825-38.
174. Nakashima, H., et al., *Chronic lithium treatment decreases tau lesions by promoting ubiquitination in a mouse model of tauopathies.* Acta Neuropathol, 2005. **110**(6): p. 547-56.
175. Dorval, V. and P.E. Fraser, *Small ubiquitin-like modifier (SUMO) modification of natively unfolded proteins tau and alpha-synuclein.* J Biol Chem, 2006. **281**(15): p. 9919-24.
176. Takahashi, K., et al., *SUMO-1 immunoreactivity co-localizes with phospho-Tau in APP transgenic mice but not in mutant Tau transgenic mice.* Neurosci Lett, 2008. **441**(1): p. 90-3.
177. Daebel, V., et al., *beta-Sheet core of tau paired helical filaments revealed by solid-state NMR.* J Am Chem Soc, 2012. **134**(34): p. 13982-9.
178. Bibow, S., et al., *The dynamic structure of filamentous tau.* Angew Chem Int Ed Engl, 2011. **50**(48): p. 11520-4.
179. Lim, S., et al., *Cell-based Models To Investigate Tau Aggregation.* Comput Struct Biotechnol J, 2014. **12**(20-21): p. 7-13.
180. Gustke, N., et al., *Domains of tau protein and interactions with microtubules.* Biochemistry, 1994. **33**(32): p. 9511-22.

181. McKinley, M.P., et al., *Developmental expression of prion protein gene in brain.* Dev Biol, 1987. **121**(1): p. 105-10.
182. Lieberburg, I., *Developmental expression and regional distribution of the scrapie-associated protein mRNA in the rat central nervous system.* Brain Res, 1987. **417**(2): p. 363-6.
183. Kretzschmar, H.A., et al., *Scrapie prion proteins are synthesized in neurons.* Am J Pathol, 1986. **122**(1): p. 1-5.
184. Basler, K., et al., *Scrapie and cellular PrP isoforms are encoded by the same chromosomal gene.* Cell, 1986. **46**(3): p. 417-28.
185. Hsiao, K., et al., *Linkage of a prion protein missense variant to Gerstmann-Straussler syndrome.* Nature, 1989. **338**(6213): p. 342-5.
186. Prusiner, S.B., et al., *Prion protein biology.* Cell, 1998. **93**(3): p. 337-48.
187. Qin, Z., et al., *Effect of 4-hydroxy-2-nonenal modification on alpha-synuclein aggregation.* J Biol Chem, 2007. **282**(8): p. 5862-70.
188. Dudek, S.M. and G.V. Johnson, *Transglutaminase catalyzes the formation of sodium dodecyl sulfate-insoluble, Alz-50-reactive polymers of tau.* J Neurochem, 1993. **61**(3): p. 1159-62.
189. Rapoport, T.A., *Protein translocation across the eukaryotic endoplasmic reticulum and bacterial plasma membranes.* Nature, 2007. **450**(7170): p. 663-9.
190. Hebert, D.N. and M. Molinari, *In and out of the ER: protein folding, quality control, degradation, and related human diseases.* Physiol Rev, 2007. **87**(4): p. 1377-408.
191. Stahl, N., et al., *Scrapie prion protein contains a phosphatidylinositol glycolipid.* Cell, 1987. **51**(2): p. 229-40.
192. Lawson, V.A., et al., *Prion protein glycosylation.* J Neurochem, 2005. **93**(4): p. 793-801.
193. Hegde, R.S., et al., *A transmembrane form of the prion protein in neurodegenerative disease.* Science, 1998. **279**(5352): p. 827-34.
194. Stewart, R.S., B. Drisaldi, and D.A. Harris, *A transmembrane form of the prion protein contains an uncleaved signal peptide and is retained in the endoplasmic Reticulum.* Mol Biol Cell, 2001. **12**(4): p. 881-9.
195. Stahl, N., et al., *Glycosylinositol phospholipid anchors of the scrapie and cellular prion proteins contain sialic acid.* Biochemistry, 1992. **31**(21): p. 5043-53.
196. Sarnataro, D., et al., *PrP(C) association with lipid rafts in the early secretory pathway stabilizes its cellular conformation.* Mol Biol Cell, 2004. **15**(9): p. 4031-42.
197. Ballmer, B.A., et al., *Modifiers of prion protein biogenesis and recycling identified by a highly parallel endocytosis kinetics assay.* J Biol Chem, 2017. **292**(20): p. 8356-8368.
198. Shyng, S.L., M.T. Huber, and D.A. Harris, *A prion protein cycles between the cell surface and an endocytic compartment in cultured neuroblastoma cells.* J Biol Chem, 1993. **268**(21): p. 15922-8.
199. Sunyach, C., et al., *The mechanism of internalization of glycosylphosphatidylinositol-anchored prion protein.* Embo j, 2003. **22**(14): p. 3591-601.
200. Zahn, R., et al., *NMR solution structure of the human prion protein.* Proc Natl Acad Sci U S A, 2000. **97**(1): p. 145-50.
201. Surewicz, W.K. and M.I. Apostol, *Prion protein and its conformational conversion: a structural perspective.* Top Curr Chem, 2011. **305**: p. 135-67.
202. Rossetti, G. and P. Carloni, *Structural Modeling of Human Prion Protein's Point Mutations.* Prog Mol Biol Transl Sci, 2017. **150**: p. 105-122.

203. Beland, M. and X. Roucou, *The prion protein unstructured N-terminal region is a broad-spectrum molecular sensor with diverse and contrasting potential functions.* J Neurochem, 2012. **120**(6): p. 853-68.
204. Fluharty, B.R., et al., *An N-terminal fragment of the prion protein binds to amyloid-beta oligomers and inhibits their neurotoxicity in vivo.* J Biol Chem, 2013. **288**(11): p. 7857-66.
205. Aulic, S., et al., *alpha-Synuclein Amyloids Hijack Prion Protein to Gain Cell Entry, Facilitate Cell-to-Cell Spreading and Block Prion Replication.* Sci Rep, 2017. **7**(1): p. 10050.
206. Legname, G., *Elucidating the function of the prion protein.* PLoS Pathog, 2017. **13**(8): p. e1006458.
207. Abskharon, R.N., et al., *Probing the N-terminal beta-sheet conversion in the crystal structure of the human prion protein bound to a nanobody.* J Am Chem Soc, 2014. **136**(3): p. 937-44.
208. Bueler, H., et al., *Normal development and behaviour of mice lacking the neuronal cell-surface PrP protein.* Nature, 1992. **356**(6370): p. 577-82.
209. Manson, J.C., et al., *129/Ola mice carrying a null mutation in PrP that abolishes mRNA production are developmentally normal.* Mol Neurobiol, 1994. **8**(2-3): p. 121-7.
210. Nishida, N., et al., *A mouse prion protein transgene rescues mice deficient for the prion protein gene from purkinje cell degeneration and demyelination.* Lab Invest, 1999. **79**(6): p. 689-97.
211. Sakaguchi, S., et al., *Loss of cerebellar Purkinje cells in aged mice homozygous for a disrupted PrP gene.* Nature, 1996. **380**(6574): p. 528-31.
212. Mehrabian, M., et al., *CRISPR-Cas9-based knockout of the prion protein and its effect on the proteome.* PLoS One, 2014. **9**(12): p. e114594.
213. Kanaani, J., et al., *Recombinant prion protein induces rapid polarization and development of synapses in embryonic rat hippocampal neurons in vitro.* Journal of Neurochemistry, 2005. **95**(5): p. 1373-1386.
214. Amin, L., et al., *Characterization of prion protein function by focal neurite stimulation.* J Cell Sci, 2016. **129**(20): p. 3878-3891.
215. Nguyen, X.T.A., et al., *Copper Binding Regulates Cellular Prion Protein Function.* Mol Neurobiol, 2019.
216. Santuccione, A., et al., *Prion protein recruits its neuronal receptor NCAM to lipid rafts to activate p59fyn and to enhance neurite outgrowth.* J Cell Biol, 2005. **169**(2): p. 341-54.
217. Niethammer, P., et al., *Cosignaling of NCAM via lipid rafts and the FGF receptor is required for neuritogenesis.* J Cell Biol, 2002. **157**(3): p. 521-32.
218. Kuffer, A., et al., *The prion protein is an agonistic ligand of the G protein-coupled receptor Adgrg6.* Nature, 2016. **536**(7617): p. 464-8.
219. Bartlett, T.E. and Y.T. Wang, *The intersections of NMDAR-dependent synaptic plasticity and cell survival.* Neuropharmacology, 2013. **74**: p. 59-68.
220. Parsons, M.P. and L.A. Raymond, *Extrasynaptic NMDA receptor involvement in central nervous system disorders.* Neuron, 2014. **82**(2): p. 279-93.
221. Khosravani, H., et al., *Prion protein attenuates excitotoxicity by inhibiting NMDA receptors.* J Cell Biol, 2008. **181**(3): p. 551-65.

222. Gasperini, L., et al., *Prion protein and copper cooperatively protect neurons by modulating NMDA receptor through S-nitrosylation.* Antioxid Redox Signal, 2015. **22**(9): p. 772-84.
223. You, H., et al., *Abeta neurotoxicity depends on interactions between copper ions, prion protein, and N-methyl-D-aspartate receptors.* Proc Natl Acad Sci U S A, 2012. **109**(5): p. 1737-42.
224. Griffith, J.S., *Self-replication and scrapie.* Nature, 1967. **215**(5105): p. 1043-4.
225. Prusiner, S.B., *Novel proteinaceous infectious particles cause scrapie.* Science, 1982. **216**(4542): p. 136-44.
226. Prusiner, S.B., *Prions.* Proc Natl Acad Sci U S A, 1998. **95**(23): p. 13363-83.
227. Legname, G., et al., *Synthetic mammalian prions.* Science, 2004. **305**(5684): p. 673-6.
228. Castilla, J., et al., *In vitro generation of infectious scrapie prions.* Cell, 2005. **121**(2): p. 195-206.
229. Deleault, N.R., et al., *Formation of native prions from minimal components in vitro.* Proc Natl Acad Sci U S A, 2007. **104**(23): p. 9741-6.
230. Wang, F., et al., *Generating a prion with bacterially expressed recombinant prion protein.* Science, 2010. **327**(5969): p. 1132-5.
231. Zhou, Z., et al., *Crowded cell-like environment accelerates the nucleation step of amyloidogenic protein misfolding.* J Biol Chem, 2009. **284**(44): p. 30148-58.
232. Silveira, J.R., et al., *The most infectious prion protein particles.* Nature, 2005. **437**(7056): p. 257-61.
233. Govaerts, C., et al., *Evidence for assembly of prions with left-handed beta-helices into trimers.* Proc Natl Acad Sci U S A, 2004. **101**(22): p. 8342-7.
234. Vazquez-Fernandez, E., et al., *The Structural Architecture of an Infectious Mammalian Prion Using Electron Cryomicroscopy.* PLoS Pathog, 2016. **12**(9): p. e1005835.
235. Wille, H. and J.R. Requena, *The Structure of PrP(Sc) Prions.* Pathogens, 2018. **7**(1).
236. Pan, K.M., et al., *Conversion of alpha-helices into beta-sheets features in the formation of the scrapie prion proteins.* Proc Natl Acad Sci U S A, 1993. **90**(23): p. 10962-6.
237. Prusiner, S.B., *Biology and genetics of prions causing neurodegeneration.* Annu Rev Genet, 2013. **47**: p. 601-23.
238. Goedert, M., *NEURODEGENERATION. Alzheimer's and Parkinson's diseases: The prion concept in relation to assembled Abeta, tau, and alpha-synuclein.* Science, 2015. **349**(6248): p. 1255555.
239. Holmes, B.B., et al., *Heparan sulfate proteoglycans mediate internalization and propagation of specific proteopathic seeds.* Proc Natl Acad Sci U S A, 2013. **110**(33): p. E3138-47.
240. Frost, B., et al., *Conformational diversity of wild-type Tau fibrils specified by templated conformation change.* J Biol Chem, 2009. **284**(6): p. 3546-51.
241. Wu, J.W., et al., *Small misfolded Tau species are internalized via bulk endocytosis and anterogradely and retrogradely transported in neurons.* J Biol Chem, 2013. **288**(3): p. 1856-70.
242. Evans, L.D., et al., *Extracellular Monomeric and Aggregated Tau Efficiently Enter Human Neurons through Overlapping but Distinct Pathways.* Cell Rep, 2018. **22**(13): p. 3612-3624.
243. Mudher, A., et al., *What is the evidence that tau pathology spreads through prion-like propagation?* Acta Neuropathol Commun, 2017. **5**(1): p. 99.

244. Guillozet-Bongaarts, A.L., et al., *Tau truncation during neurofibrillary tangle evolution in Alzheimer's disease.* Neurobiol Aging, 2005. **26**(7): p. 1015-22.
245. Pouplana, S., et al., *Thioflavin-S staining of bacterial inclusion bodies for the fast, simple, and inexpensive screening of amyloid aggregation inhibitors.* Curr Med Chem, 2014. **21**(9): p. 1152-9.
246. Khlistunova, I., et al., *Inducible expression of Tau repeat domain in cell models of tauopathy: aggregation is toxic to cells but can be reversed by inhibitor drugs.* J Biol Chem, 2006. **281**(2): p. 1205-14.
247. Mirbaha, H., et al., *Tau Trimers Are the Minimal Propagation Unit Spontaneously Internalized to Seed Intracellular Aggregation.* J Biol Chem, 2015. **290**(24): p. 14893-903.
248. Mukrasch, M.D., et al., *The "jaws" of the tau-microtubule interaction.* J Biol Chem, 2007. **282**(16): p. 12230-9.
249. Sanders, D.W., et al., *Distinct tau prion strains propagate in cells and mice and define different tauopathies.* Neuron, 2014. **82**(6): p. 1271-88.
250. Falcon, B., et al., *Conformation determines the seeding potencies of native and recombinant Tau aggregates.* J Biol Chem, 2015. **290**(2): p. 1049-65.
251. Clavaguera, F., et al., *Transmission and spreading of tauopathy in transgenic mouse brain.* Nat Cell Biol, 2009. **11**(7): p. 909-13.
252. Clavaguera, F., et al., *Brain homogenates from human tauopathies induce tau inclusions in mouse brain.* Proc Natl Acad Sci U S A, 2013. **110**(23): p. 9535-40.
253. Iba, M., et al., *Tau pathology spread in PS19 tau transgenic mice following locus coeruleus (LC) injections of synthetic tau fibrils is determined by the LC's afferent and efferent connections.* Acta Neuropathol, 2015. **130**(3): p. 349-62.
254. Guo, J.L. and V.M. Lee, *Seeding of normal Tau by pathological Tau conformers drives pathogenesis of Alzheimer-like tangles.* J Biol Chem, 2011. **286**(17): p. 15317-31.
255. Nonaka, T., et al., *Seeded aggregation and toxicity of {alpha}-synuclein and tau: cellular models of neurodegenerative diseases.* J Biol Chem, 2010. **285**(45): p. 34885-98.
256. Kumar, H. and J.B. Udgaonkar, *Mechanistic and Structural Origins of the Asymmetric Barrier to Prion-like Cross-Seeding between Tau-3R and Tau-4R.* J Mol Biol, 2018. **430**(24): p. 5304-5312.
257. Weismiller, H.A., et al., *Structural disorder in four-repeat Tau fibrils reveals a new mechanism for barriers to cross-seeding of Tau isoforms.* J Biol Chem, 2018. **293**(45): p. 17336-17348.
258. de Calignon, A., et al., *Propagation of tau pathology in a model of early Alzheimer's disease.* Neuron, 2012. **73**(4): p. 685-97.
259. Liu, L., et al., *Trans-synaptic spread of tau pathology in vivo.* PLoS One, 2012. **7**(2): p. e31302.
260. Yetman, M.J., et al., *Transgene expression in the Nop-tTA driver line is not inherently restricted to the entorhinal cortex.* Brain Struct Funct, 2016. **221**(4): p. 2231-49.
261. Chakrabarty, P., et al., *Inefficient induction and spread of seeded tau pathology in P301L mouse model of tauopathy suggests inherent physiological barriers to transmission.* Acta Neuropathol, 2015. **130**(2): p. 303-5.
262. Guo, J.L., et al., *Unique pathological tau conformers from Alzheimer's brains transmit tau pathology in nontransgenic mice.* J Exp Med, 2016. **213**(12): p. 2635-2654.

263. Falcon, B., et al., *Structures of filaments from Pick's disease reveal a novel tau protein fold.* Nature, 2018. **561**(7721): p. 137-140.
264. Falcon, B., et al., *Novel tau filament fold in chronic traumatic encephalopathy encloses hydrophobic molecules.* Nature, 2019. **568**(7752): p. 420-423.
265. Falcon, B., et al., *Tau filaments from multiple cases of sporadic and inherited Alzheimer's disease adopt a common fold.* Acta Neuropathologica, 2018. **136**(5): p. 699-708.
266. Zhang, W., et al., *Heparin-induced tau filaments are polymorphic and differ from those in Alzheimer's and Pick's diseases.* Elife, 2019. **8**.
267. Mohamed, N.V., A. Desjardins, and N. Leclerc, *Tau secretion is correlated to an increase of Golgi dynamics.* PLoS One, 2017. **12**(5): p. e0178288.
268. Wang, Y., et al., *The release and trans-synaptic transmission of Tau via exosomes.* Mol Neurodegener, 2017. **12**(1): p. 5.
269. Polanco, J.C., et al., *Extracellular Vesicles Isolated from the Brains of rTg4510 Mice Seed Tau Protein Aggregation in a Threshold-dependent Manner.* J Biol Chem, 2016. **291**(24): p. 12445-66.
270. Dujardin, S., et al., *Ectosomes: a new mechanism for non-exosomal secretion of tau protein.* PLoS One, 2014. **9**(6): p. e100760.
271. Baker, S., J.C. Polanco, and J. Gotz, *Extracellular Vesicles Containing P301L Mutant Tau Accelerate Pathological Tau Phosphorylation and Oligomer Formation but Do Not Seed Mature Neurofibrillary Tangles in ALZ17 Mice.* J Alzheimers Dis, 2016. **54**(3): p. 1207-1217.
272. Tardivel, M., et al., *Tunneling nanotube (TNT)-mediated neuron-to neuron transfer of pathological Tau protein assemblies.* Acta Neuropathol Commun, 2016. **4**(1): p. 117.
273. Abounit, S., et al., *Tunneling nanotubes spread fibrillar alpha-synuclein by intercellular trafficking of lysosomes.* Embo j, 2016. **35**(19): p. 2120-2138.
274. Resenberger, U.K., et al., *The cellular prion protein mediates neurotoxic signalling of beta-sheet-rich conformers independent of prion replication.* Embo j, 2011. **30**(10): p. 2057-70.
275. Resenberger, U.K., K.F. Winklhofer, and J. Tatzelt, *Cellular prion protein mediates toxic signaling of amyloid beta.* Neurodegener Dis, 2012. **10**(1-4): p. 298-300.
276. Biasini, E. and D.A. Harris, *Targeting the cellular prion protein to treat neurodegeneration.* Future Med Chem, 2012. **4**(13): p. 1655-8.
277. Chen, S., S.P. Yadav, and W.K. Surewicz, *Interaction between human prion protein and amyloid-beta (Abeta) oligomers: role OF N-terminal residues.* J Biol Chem, 2010. **285**(34): p. 26377-83.
278. Moroncini, G., et al., *Motif-grafted antibodies containing the replicative interface of cellular PrP are specific for PrPSc.* Proc Natl Acad Sci U S A, 2004. **101**(28): p. 10404-9.
279. Solforosi, L., et al., *Toward molecular dissection of PrPC-PrPSc interactions.* J Biol Chem, 2007. **282**(10): p. 7465-71.
280. Iraci, N., et al., *Decoding the function of the N-terminal tail of the cellular prion protein to inspire novel therapeutic avenues for neurodegenerative diseases.* Virus Res, 2015. **207**: p. 62-8.
281. Um, J.W., et al., *Alzheimer amyloid-beta oligomer bound to postsynaptic prion protein activates Fyn to impair neurons.* Nat Neurosci, 2012. **15**(9): p. 1227-35.

282. Wadia, J.S., et al., *Pathologic prion protein infects cells by lipid-raft dependent macropinocytosis.* PLoS One, 2008. **3**(10): p. e3314.
283. Pasupuleti, M., et al., *Antimicrobial activity of human prion protein is mediated by its N-terminal region.* PLoS One, 2009. **4**(10): p. e7358.
284. Lauren, J., et al., *Cellular prion protein mediates impairment of synaptic plasticity by amyloid-beta oligomers.* Nature, 2009. **457**(7233): p. 1128-32.
285. Balducci, C., et al., *Synthetic amyloid-beta oligomers impair long-term memory independently of cellular prion protein.* Proc Natl Acad Sci U S A, 2010. **107**(5): p. 2295-300.
286. Finder, V.H. and R. Glockshuber, *Amyloid-beta aggregation.* Neurodegener Dis, 2007. **4**(1): p. 13-27.
287. Kostylev, M.A., et al., *Prion-Protein-interacting Amyloid-beta Oligomers of High Molecular Weight Are Tightly Correlated with Memory Impairment in Multiple Alzheimer Mouse Models.* J Biol Chem, 2015. **290**(28): p. 17415-38.
288. Mao, X., et al., *Pathological alpha-synuclein transmission initiated by binding lymphocyte-activation gene 3.* Science, 2016. **353**(6307).
289. Bieri, G., A.D. Gitler, and M. Brahic, *Internalization, axonal transport and release of fibrillar forms of alpha-synuclein.* Neurobiol Dis, 2018. **109**(Pt B): p. 219-225.
290. Nygaard, H.B., C.H. van Dyck, and S.M. Strittmatter, *Fyn kinase inhibition as a novel therapy for Alzheimer's disease.* Alzheimers Res Ther, 2014. **6**(1): p. 8.
291. La Vitola, P., et al., *Cellular prion protein neither binds to alpha-synuclein oligomers nor mediates their detrimental effects.* Brain, 2019. **142**(2): p. 249-254.
292. Urrea, L., et al., *Involvement of Cellular Prion Protein in alpha-Synuclein Transport in Neurons.* Mol Neurobiol, 2017.
293. Ferreira, D.G., et al., *alpha-synuclein interacts with PrPC to induce cognitive impairment through mGluR5 and NMDAR2B.* Nat Neurosci, 2017. **20**(11): p. 1569-1579.
294. De Cecco, E. and G. Legname, *The role of the prion protein in the internalization of alpha-synuclein amyloids.* Prion, 2018. **12**(1): p. 23-27.
295. Karpowicz, R.J., Jr., et al., *Selective imaging of internalized proteopathic alpha-synuclein seeds in primary neurons reveals mechanistic insight into transmission of synucleinopathies.* J Biol Chem, 2017. **292**(32): p. 13482-13497.
296. Polymenidou, M., et al., *The POM monoclonals: a comprehensive set of antibodies to non-overlapping prion protein epitopes.* PLoS One, 2008. **3**(12): p. e3872.
297. Zhang, Y., et al., *High-speed atomic force microscopy reveals structural dynamics of alpha-synuclein monomers and dimers.* J Chem Phys, 2018. **148**(12): p. 123322.
298. Stincardini, C., et al., *An antipsychotic drug exerts anti-prion effects by altering the localization of the cellular prion protein.* PLoS One, 2017. **12**(8): p. e0182589.
299. Livak, K.J. and T.D. Schmittgen, *Analysis of relative gene expression data using real-time quantitative PCR and the 2(-Delta Delta C(T)) Method.* Methods, 2001. **25**(4): p. 402-8.
300. Barghorn, S., J. Biernat, and E. Mandelkow, *Purification of recombinant tau protein and preparation of Alzheimer-paired helical filaments in vitro.* Methods Mol Biol, 2005. **299**: p. 35-51.
301. Guo, J.L. and V.M. Lee, *Neurofibrillary tangle-like tau pathology induced by synthetic tau fibrils in primary neurons over-expressing mutant tau.* FEBS Lett, 2013. **587**(6): p. 717-23.

302. Han, J., et al., *Study on interaction between microtubule associated protein tau and prion protein.* Sci China C Life Sci, 2006. **49**(5): p. 473-9.
303. Ondrejcak, T., et al., *Cellular Prion Protein Mediates the Disruption of Hippocampal Synaptic Plasticity by Soluble Tau In Vivo.* J Neurosci, 2018. **38**(50): p. 10595-10606.
304. Perrier, V., et al., *Anti-PrP antibodies block PrPSc replication in prion-infected cell cultures by accelerating PrPC degradation.* J Neurochem, 2004. **89**(2): p. 454-63.
305. Mahal, S.P., et al., *Propagation of RML prions in mice expressing PrP devoid of GPI anchor leads to formation of a novel, stable prion strain.* PLoS Pathog, 2012. **8**(6): p. e1002746.
306. Mange, A., et al., *Alpha- and beta- cleavages of the amino-terminus of the cellular prion protein.* Biol Cell, 2004. **96**(2): p. 125-32.
307. Westergard, L., J.A. Turnbaugh, and D.A. Harris, *A naturally occurring C-terminal fragment of the prion protein (PrP) delays disease and acts as a dominant-negative inhibitor of PrPSc formation.* J Biol Chem, 2011. **286**(51): p. 44234-42.
308. Tanida, I., T. Ueno, and E. Kominami, *LC3 and Autophagy.* Methods Mol Biol, 2008. **445**: p. 77-88.
309. Calella, A.M., et al., *Prion protein and Abeta-related synaptic toxicity impairment.* EMBO Mol Med, 2010. **2**(8): p. 306-14.
310. Holmes, B.B., et al., *Proteopathic tau seeding predicts tauopathy in vivo.* Proc Natl Acad Sci U S A, 2014. **111**(41): p. E4376-85.
311. Masaracchia, C., et al., *Membrane binding, internalization, and sorting of alpha-synuclein in the cell.* Acta Neuropathol Commun, 2018. **6**(1): p. 79.
312. Aguzzi, A. and C.J. Sigurdson, *Antiprion immunotherapy: to suppress or to stimulate?* Nature Reviews Immunology, 2004. **4**(9): p. 725-736.
313. Aguzzi, A., A.K.K. Lakkaraju, and K. Frontzek, *Toward Therapy of Human Prion Diseases.* Annu Rev Pharmacol Toxicol, 2018. **58**: p. 331-351.
314. Heppner, F.L., et al., *Prevention of scrapie pathogenesis by transgenic expression of anti-prion protein antibodies.* Science, 2001. **294**(5540): p. 178-82.
315. Chung, E., et al., *Anti-PrPC monoclonal antibody infusion as a novel treatment for cognitive deficits in an Alzheimer's disease model mouse.* BMC Neurosci, 2010. **11**: p. 130.
316. Gunther, E.C., et al., *Rescue of Transgenic Alzheimer's Pathophysiology by Polymeric Cellular Prion Protein Antagonists.* Cell Rep, 2019. **26**(1): p. 145-158.e8.
317. Cox, T.O., et al., *Anti-PrP(C) antibody rescues cognition and synapses in transgenic alzheimer mice.* Ann Clin Transl Neurol, 2019. **6**(3): p. 554-574.
318. Klyubin, I., et al., *Peripheral administration of a humanized anti-PrP antibody blocks Alzheimer's disease Aβ synaptotoxicity.* J Neurosci, 2014. **34**(18): p. 6140-5.
319. Johnson, C.W., T.J. Melia, and A. Yamamoto, *Modulating macroautophagy: a neuronal perspective.* Future Med Chem, 2012. **4**(13): p. 1715-31.
320. Aguib, Y., et al., *Autophagy induction by trehalose counter-acts cellular prion-infection.* Autophagy, 2009. **5**(3): p. 361-369.
321. Heiseke, A., et al., *Lithium induces clearance of protease resistant prion protein in prion-infected cells by induction of autophagy.* Journal of Neurochemistry, 2009. **109**(1): p. 25-34.
322. Seglen, P.O. and P.B. Gordon, *3-Methyladenine: specific inhibitor of autophagic/lysosomal protein degradation in isolated rat hepatocytes.* Proc Natl Acad Sci U S A, 1982. **79**(6): p. 1889-92.

323. Wu, Y.T., et al., *Dual role of 3-methyladenine in modulation of autophagy via different temporal patterns of inhibition on class I and III phosphoinositide 3-kinase.* J Biol Chem, 2010. **285**(14): p. 10850-61.
324. Goold, R., C. McKinnon, and S.J. Tabrizi, *Prion degradation pathways: Potential for therapeutic intervention.* Molecular and Cellular Neuroscience, 2015. **66**: p. 12-20.
325. Goold, R., et al., *Alternative fates of newly formed PrP^{Sc} upon prion conversion on the plasma membrane.* Journal of Cell Science, 2013. **126**(16): p. 3552.